AD-A106 223 PENNSYLVANIA STATE UNIV UNIVERSITY PARK APPLIED RESE--ETC F/G 20/1
NOISE GENERATION BY GAS JETS IN A TURBULENT WAKE.(U)
APR 81 J J GAVIGAN N00024-79-C-6043
UNCLASSIFIED ARL/PSU/TM-81-99 NL

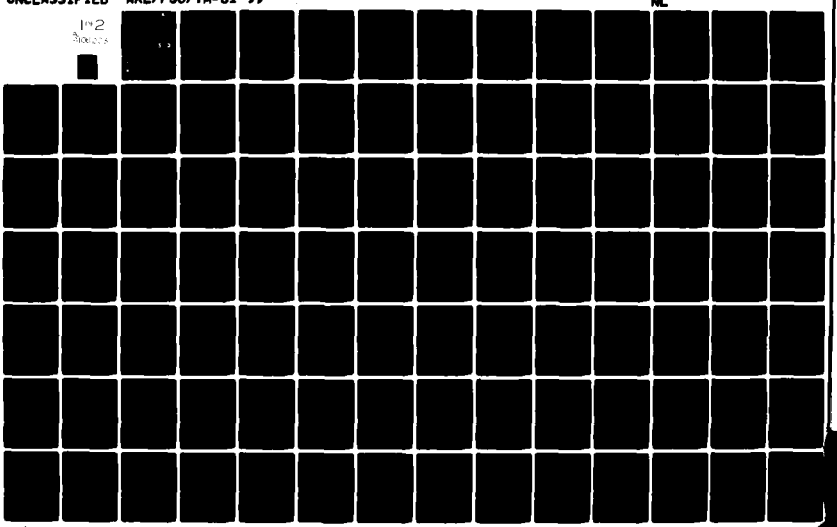

(6) LEVEL II

AD A106223

NOISE GENERATION BY GAS JETS IN A TURBULENT WAKE

John J. Gavigan

Technical Memorandum
File No. TM 81-99
April 9, 1981
Contract No. N00024-79-C-6043

Copy No. 10

The Pennsylvania State University
Intercollege Research Programs and Facilities
APPLIED RESEARCH LABORATORY
Post Office Box 30
State College, PA 16801

NAVY DEPARTMENT

NAVAL SEA SYSTEMS COMMAND

81 10 23

(14) ARL/PSU

UNCLASSIFIED
SECURITY CLASSIFICATION OF THIS PAGE (When Data Entered)

REPORT DOCUMENTATION PAGE

READ INSTRUCTIONS BEFORE COMPLETING FORM

1. REPORT NUMBER: TM-81-99	2. GOVT ACCESSION NO.: AD-A106 223
3. RECIPIENT'S CATALOG NUMBER	
4. TITLE (and Subtitle): NOISE GENERATION BY GAS JETS IN A TURBULENT WAKE	5. TYPE OF REPORT & PERIOD COVERED: Ph.D Thesis
6. PERFORMING ORG. REPORT NUMBER: TM 81-99	
7. AUTHOR(s): John J. Gavigan	8. CONTRACT OR GRANT NUMBER(s): N00024-79-C-6043
9. PERFORMING ORGANIZATION NAME AND ADDRESS: The Pennsylvania State University, Applied Research Laboratory, P.O. Box 30, State College, PA 16801	10. PROGRAM ELEMENT, PROJECT, TASK AREA & WORK UNIT NUMBERS
11. CONTROLLING OFFICE NAME AND ADDRESS: Naval Sea Systems Command, Department of the Navy, Washington, DC 20362	12. REPORT DATE: April 9, 1981
	13. NUMBER OF PAGES: 109 pages & figures
14. MONITORING AGENCY NAME & ADDRESS (if different from Controlling Office)	15. SECURITY CLASS. (of this report): Unclassified, Unlimited
	15a. DECLASSIFICATION/DOWNGRADING SCHEDULE

16. DISTRIBUTION STATEMENT (of this Report)

Approved for public release, distribution unlimited,

17. DISTRIBUTION STATEMENT (of the abstract entered in Block 20, if different from Report)

18. SUPPLEMENTARY NOTES

19. KEY WORDS (Continue on reverse side if necessary and identify by block number)

thesis, noise, generation, gas, jets, turbulent, wake

20. ABSTRACT (Continue on reverse side if necessary and identify by block number)

Radiation noise is generated by the interaction of gas jets with turbulent liquid. Although this phenomenon has long been known, the mechanism of noise generation and its functional relationship to important parameters are not well understood. No experimental studies of gas jet-turbulence interaction noise under controlled conditions can be found in the literature. To remedy this paucity of experimental data, measurements of this phenomenon were made in the 1.22 m diameter test section of the Garfield Thomas Water Tunnel. Gas was exhausted from the aft end of the strut-mounted test body into the turbulent

DD FORM 1 JAN 73 1473 EDITION OF 1 NOV 65 IS OBSOLETE

UNCLASSIFIED
SECURITY CLASSIFICATION OF THIS PAGE (When Data Entered)

wake. A directional hydrophone, mounted outside the flow in a water-filled tank on one side of the test section, was used to make one-third-octave-band acoustic measurements in the frequency range 5 - 50 kHz. By varying the gas exhaust orifice diameters, gas flow rates, and water speeds, the interdependence of the important parameters to radiated noise was determined. For the range of variables used in these experiments, the radiated noise is primarily a function of the ratio of orifice diameter to turbulence length scale, and only secondarily, a function of gas flow rates. Analysis of the results indicate that noise generated by the formation, division, coalescence, and collapse of bubbles can be related to the critical Weber number of the flow.

ABSTRACT

Radiated noise is generated by the interaction of gas jets with turbulent liquid. Although this phenomenon has long been known, the mechanism of noise generation and its functional relationship to important parameters are not well understood. No experimental studies of gas jet-turbulence interaction noise under controlled conditions can be found in the literature. To remedy this paucity of experimental data, measurements of this phenomenon were made in the 1.22 cm diameter test section of the Garfield Thomas Water Tunnel. Gas was exhausted from the aft end of the strut-mounted test body into the turbulent wake. A directional hydrophone mounted outside the flow in a water-filled tank on one side of the test section was used to make one-third-octave-band acoustic measurements in the frequency range 5 - 50 kHz. By varying the gas exhaust orifice diameters, gas flow rates, and water speeds, the interdependence of the important parameters to radiated noise was determined. For the range of variables used in these experiments, the radiated noise is primarily a function of the ratio of orifice diameter to turbulence length scale, and only secondarily, a function of gas flow rates. Analyses of the results indicate that noise generated by the formation, division, coalescence, and collapse of bubbles can be related to the critical Weber number of the flows.

TABLE OF CONTENTS

LIST OF TABLES

LIST OF TABLES (continued)

LIST OF FIGURES

LIST OF FIGURES (continued)

LIST OF FIGURES (continued)

LIST OF FIGURES (continued)

NOMENCLATURE

C, C_l	phase velocity of sound in water
C_g	phase velocity of sound in gas
C_m	complex phase velocity of sound in two-phase mixture of gas and water at low gas concentrations
dB_{sens}	sensitivity level of receiving hydrophone in dB re 1 volt/μbar
dB_v	output voltage of receiving hydrophone in dB re 1 volt
dB_{cal}	calibration level of sound projector in dB re $\frac{1\ \mu bar - 1\ meter}{1\ volt}$
dB_x	input voltage level of sound projector in dB re 1 volt
dB_d	separation distance level in dB re 1 meter
D	mean gas jet diameter
f_o	resonance frequency of bubble
F^2	square of relative Froude Number $[\frac{\text{inertial forces}}{\text{gravitational forces}}]$
g	gravitational constant
L	turbulence length scale
P_o	static pressure
$\dot{Q}$	gas flow rate per orifice
$\dot{Q}_T$	gas flow rate per nozzle
r_o, r_B	radius of gas bubble
r_s	radius of orifice
SPL	one-third-octave sound-pressure level in dB re 1 μbar
u	turbulence velocity scale
U	liquid speed relative to the orifice
v_ℓ	velocity of liquid
v_g	velocity of gas
$\overline{v^2}$	spatial average of the square of the velocity differences over a distance equal to twice the bubble radius

NOMENCLATURE (continued)

W^2	square of relative Weber number $[\frac{\text{inertial forces}}{\text{surface tension forces}}]$
W_c	critical Weber number
β	void fraction $[\frac{\text{gas volume}}{\text{mixture volume}}]$
γ	ratio of specific heats
δ	damping constant; difference between a typical bubble radius and critical bubble radius
Δ	magnitude of difference between gas and water velocities $v_g \quad v_\ell$
ε	local rate of energy dissipation
κ	compressibility of water
ω	applied circular frequency
ω_o	resonant circular frequency
ρ, ρ_ℓ	density of liquid
ρ_g	density of gas
σ	surface tension
d	distance from center of bubble to receiving hydrophone
f_n	frequency for the n^{th} mode
n	mode number
N_n	numerical constant
p_n	radiated sound pressure at distance d from center of bubble
r_n	amplitude of oscillation associated with the n^{th} order

ACKNOWLEDGMENTS

The author wishes to acknowledge the guidance of his advisors, Drs. Walter F. King III and Dr. Norman Davids. Dr. King suggested the problem and, along with Dr. Davids, assisted greatly in the completion of the work.

Advice and assistance by the members of the doctoral committee, Drs. Sabih I. Hayek, Vernon H. Neubert, and the late John C. Snowdon, are particularly acknowledged.

The author wishes to acknowledge the financial support received from the Applied Research Laboratory at The Pennsylvania State University, under contract with the Naval Ordnance Systems Command.

CHAPTER I

INTRODUCTION AND STATEMENT OF THE PROBLEM

Introduction

Many investigators have studied the interaction of two-phase mixtures in turbulent fluids [5,8,11,19,22,23,25]. The two phases usually involved in these investigations are water droplets in air and gas bubbles in water. In all cases, these authors were primarily interested in determining the important parameters governing the formation and collapse of either the drops or bubbles when subjected to turbulence. The study of two-phase mixtures in turbulent flows has many important practical applications. Among these are the atomization of jets in liquids, the generation of emulsions and froths, and the separation of by-products of chemical reactions.

One aspect of two-phase turbulent flows scarcely discussed in the literature is the generation of noise. Although this process has important marine applications, the interdependence of flow parameters and acoustic radiation is not well understood. Of particular importance is the noise generated by the emission of gas through submerged orifices into turbulent water. If the functional dependence of the important parameters on noise generation can be established, practical techniques could be developed to minimize the radiated noise.

Although it has long been known that gas discharging under water produces noise, very few quantitative measurements of the acoustic radiation under controlled conditions are available in the literature. One of the few published acoustical studies of this phenomenon is due

to Mühle and Heckl [18]. They measured the radiated noise generated by air discharging through a submerged tube into quiescent water. One of their major conclusions is that intensity of the noise radiated under these conditions is primarily a function of gas flow rate. Since these measurements were made in quiescent, it is unlikely that the same simple relationship is valid in turbulent water.

The experimental studies described in this dissertation represent the first controlled investigation of noise generation by submerged gas jets exhausting into turbulent water. By an analysis of measurements made under a variety of known conditions, an attempt will be made to determine the influence of the experimental parameters on radiated noise.

Statement of the Problem

The problem is to determine the effect of various physical parameters on radiated noise generated by the interaction of submerged gas jets with a turbulent wake. The relation of the following parameters to radiated noise will be analyzed:

1. Gas flow rate.
2. Water speed.
3. Turbulence length scale.
4. Weber number of bubble-water mixture.
5. Orifice and bubble diameters.

After the role of these parameters on radiated noise has been determined, an attempt will be made to gain insight into the actual mechanism of the noise generated by gas bubble-turbulence interactions.

To ensure the best possible control of all adjustable parameters, these experiments were conducted in the Garfield Thomas Water Tunnel in The Applied Research Laboratory at The Pennsylvania State University. The staff at the facility operated the water tunnel and assisted with the many measurements. Gas at known flow rates was exhausted through specially prepared nozzle plates attached to the aft end of a streamlined body. This body was strut-mounted in the 1.22 m diameter test section of the water tunnel. Acoustic measurements of the radiated noise were made with a directional hydrophone mounted outside of the flow in a water-filled tank attached to one side of the tunnel test section. Plexiglass windows, with an acoustic impedance nearly the same as that of water, ensured a minimal noise attenuation between the exhausting gas and hydrophone. Based on the length of the streamlined body, the Reynolds number of the flow for the water speeds used in these studies is always greater than 10^6. This ensures that the exhausting gas will always be ejected into a turbulent wake behind the body.

The effect of gas bubbles on sound is discussed in Chapter II, while gas jets and bubble generation in stationary and turbulent flows are analyzed in Chapter III. Chapter IV contains a discussion of the experimental procedure along with a detailed description of the water tunnel facility. Results of the measurements are given in Chapter V, and a summary and conclusions are presented in Chapter VI.

CHAPTER II

EFFECT OF BUBBLES ON SOUND

Sound Radiation from Bubbles

Gas bubbles can radiate sound by a variety of mechanisms. One of the first reported scientific studies of the relation between bubbles and sound appears in Bragg's [2] work in which he attributes the murmuring of streams to entrained air bubbles. Minnaert [17] looked at sound generated by the formation of air bubbles at a nozzle and derived an expression for the frequency of volume pulsations. For adiabatic bubbles with radii greater than 10^{-3} cm, Minnaert's expression for the resonance frequency is

$$f_o = \frac{1}{2\pi r_o}\left[\frac{3\gamma p_o}{\rho}\right]^{1/2} , \qquad (2.1)$$

where γ is the ratio of specific heats, p_o is the static pressure at which the bubble radius is r_o, and ρ is the liquid density. Equation (2.1) is plotted in Figure 1. Following the investigations by Minnaert, Meyer and Tamm [16] demonstrated experimentally that bubble sounds are associated with volume pulsations of the bubble. These pulsations behaved like a simple oscillating system with damping. Somewhat later, Strasberg [27] calculated the amplitudes of sound pressures radiated by bubbles excited by various means. These methods of excitation included (1) bubble formation, (2) bubble coalescence or division, (3) the flow of a free stream of liquid containing entrained bubbles past an obstacle, and (4) the flow of bubbles through a pipe

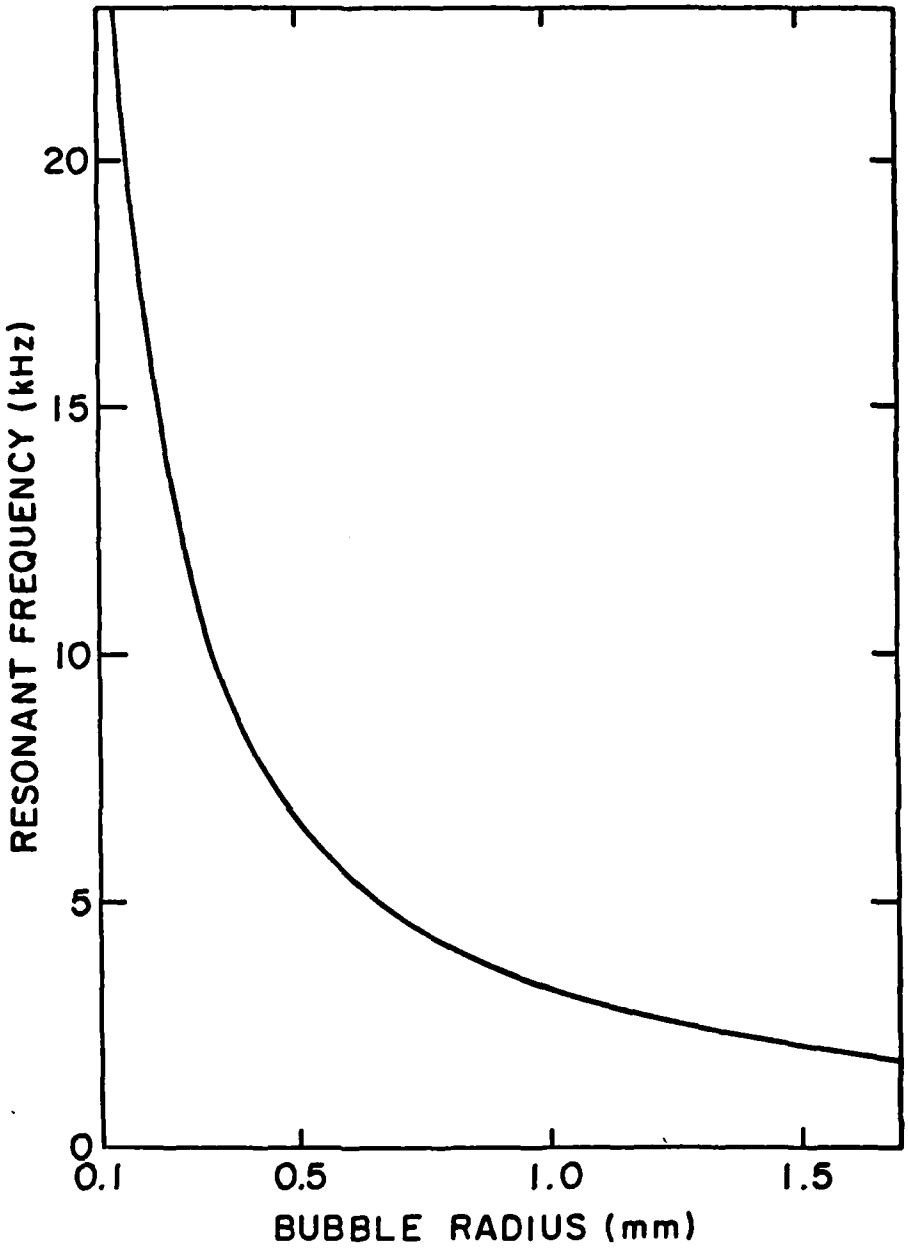

Figure 1. Resonant Frequency of Bubbles with Radii Greater Than 0.001 cm as a Function of Bubble Radius (After Minnaert)

past a constriction. He also verified his predictions by measurements of sound radiated by bubbles formed at an orifice.

At low gas flow rates, when bubbles are formed at the orifice or nozzle, sound is generated as the bubble separates and begins its independent existence. Strasberg shows that the bubble emits a short pulse which has the character of a damped sinusoidal oscillation at the natural frequency of volume pulsation. When bubbles divide or coalesce, a short pulse of sound is generated, as in the case of bubble formation, with, however, a much lower peak sound pressure. Strasberg also found that if the bubble pulsation amplitude was large, nonlinear effects modify the radiated sound in such a way that it becomes similar to noise radiated by cavitation.

At slightly higher gas flow rates, individual bubbles no longer form at the orifice but, rather, streams of bubbles, usually called periodic bubbles, issue from the orifice. When the gas flow rate is increased still more, gas leaves the orifice as a jet and breaks up into bubbles downstream. Smith [24] studied noise generated by gas jets on underwater vehicles and ascribes most of the radiated noise to two sources. One is the volume fluctuations of individual bubbles, and the other is the volume fluctuations associated with the jet collapse and subsequent formation of bubbles. More recently, Mühle and and Heckl [18] reported on experiments designed to study noise generated by stationary submerged gas exhaust pipes. Their results show a strong correlation between gas flow rates and noise, with little influence exerted by the diameter of pipes. The Mühle and Heckl study was carried out in quiescent water, and could not, of course, include any effects due to turbulence.

Speed of Sound in Bubbly Water

In any investigation of noise generated by submerged gas jets, the behavior of sound in two-phase mixtures must be taken into account. It has been known for many years that the phase velocity of sound in water is a function of compressibility κ and density ρ,

$$C = (\rho\kappa)^{-1/2} \quad .$$

For a two-phase mixture of gas and water, the compressibility and, hence, the velocity is a function of the void fraction β (defined as the gas volume divided by the mixture volume). By considering the results of compressibility changes in two-phase mixtures, Meyer and Skudrzyk (15) derived an expression for the complex phase velocity of sound in the mixture at low gas concentrations. Their result can be written as

$$C_m = C_\ell \, \Gamma(\beta,\omega)^{-1/2} \quad ,$$

where

$$\Gamma(\beta,\omega) = 1 + \frac{\beta}{1-\beta} \, \frac{\left(\frac{C_\ell}{C_g}\right)^2 \left(\frac{\rho_\ell}{\rho_g}\right)}{1 - \left(\frac{\omega}{\omega_o}\right)^2 + i\delta \frac{\omega}{\omega_o}} \quad .$$

C_ℓ and C_g are the sound velocities in the liquid and gas, respectively, ρ_ℓ and ρ_g are the densities of the liquid and gas, ω is the applied circular frequency, ω_o is the resonant circular frequency, and δ is the damping constant. This equation was derived for low gas concentrations and is valid for $\beta < 0.003$. The real part of C_m yields the phase velocity of the mixture.

In a similar derivation, Welle et al. [31] extended this work to obtain an expression for the phase velocity that would be valid at higher void fractions. Their result is

$$C_m = C_\ell[(1 - \beta)(1 - \beta + \beta \frac{\rho_g}{\rho_\ell})\Gamma(\beta,\omega)]^{-1/2} \quad . \qquad (2.2)$$

To illustrate this strong dependence of phase velocity on β, Equation (2.2) is plotted in Figure 2 for the applied frequency well below resonance. As can be seen, even a very small fraction of gas bubbles in water can cause the local sound speed to fall substantially below the pure liquid value. Recent calculations for sound sources in bubbly wakes [9] indicate that even very low void fractions, on the order of 10^{-6}, create acoustic channels which act as wave guides for sound. Any noise source caused by gas exhaust behind a moving vehicle would, therefore, probably radiate much of its energy downstream in the wake. This is true, of course, only for sound frequencies below the average resonant frequency of the bubble distribution.

The frequency dependence of the two-phase mixture has been demonstrated by a number of investigators. Spitzer [26], Carstensen and Foldy [4], Laird and Kendig [13], Meyer and Skudrzyk [15], and others have shown that acoustic waves suffer a large attenuation as the sound frequency approaches the resonant frequency of the bubbles. This effect can be seen by considering a two-phase mixture where all bubbles have the same radius. If the applied sound frequency is velow the resonance frequency f_o, the bubbles oscillate in phase with the sound wave, thereby increasing the compressibility of the mixture and decreasing the phase velocity of the sound. On the other hand, for a

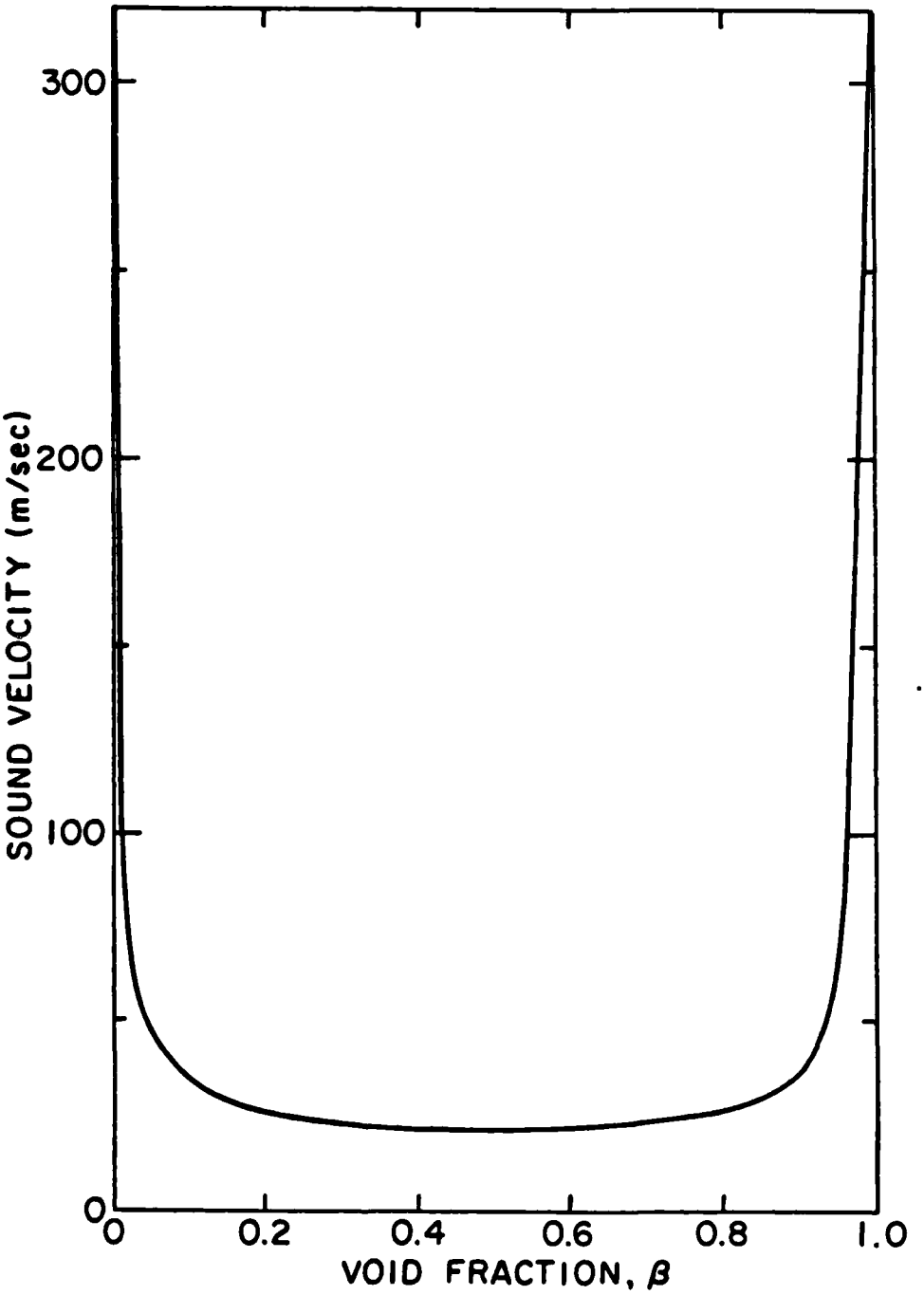

Figure 2. Sound Velocity in Bubbly Water as a Function of Void Fraction

sound wave with frequency above f_o , the bubble displacements are 180° out of phase with the sound pressure, thereby decreasing the compressibility and increasing the phase velocity. In one of the few published experimental studies at these high frequencies, Card et al. [3] show that, at frequencies above resonance, the group and signal velocities are lower than the phase velocity in the pure liquid and decrease with increasing void fraction. From Equation (2.2), the frequency dependence of sound speed in bubbly water is plotted in Figure 3 for two different low values of β . As can be seen, the effect of the two-phase mixture on sound speed is drastic, even for quite small values of β .

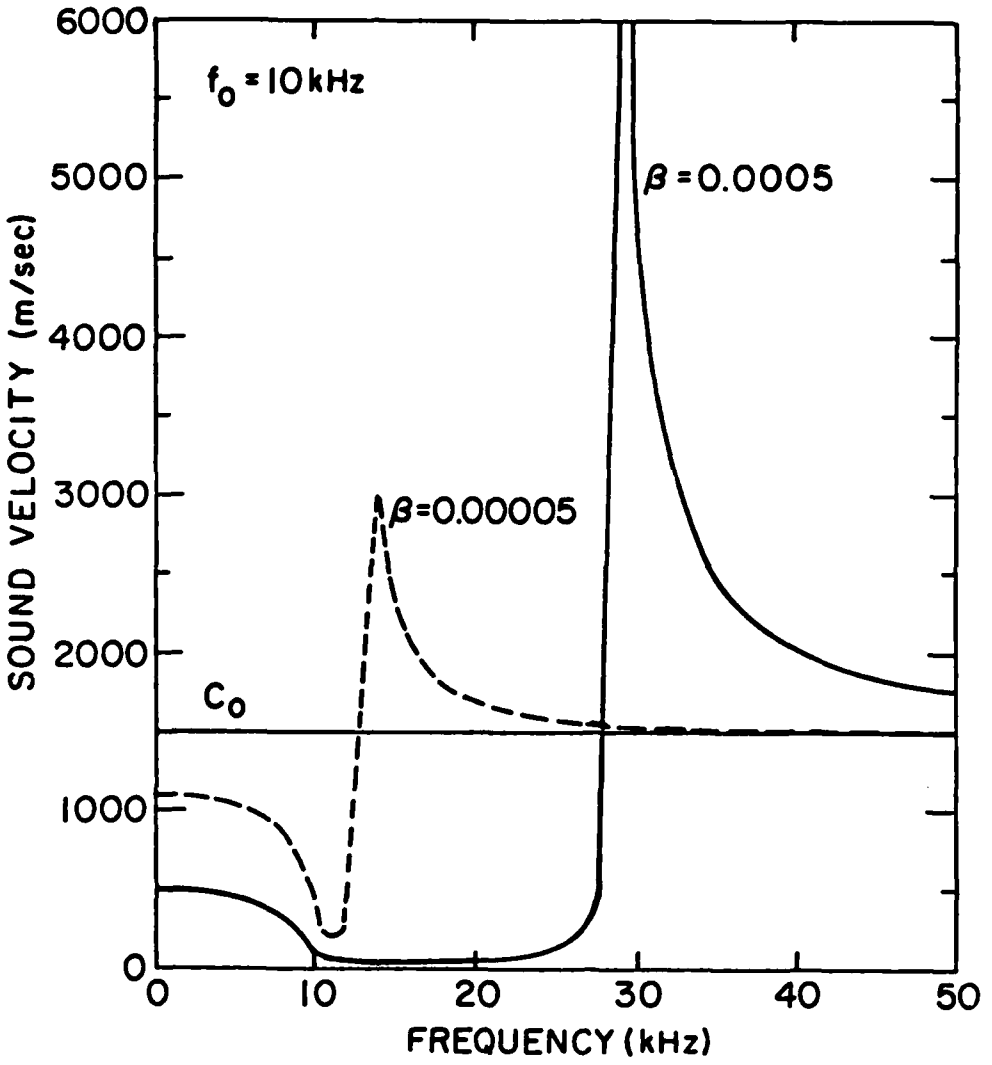

Figure 3. Sound Velocity in Bubbly Water as a Function of Applied Frequency for Two Void Fractions

CHAPTER III

BUBBLES AND JET GENERATION

Bubbles Emitted Into a Stationary Liquid

When gas is exhausted steadily through an orifice submerged in a liquid, it emerges as bubbles. Depending upon the relative flow rates of the fluids involved, the bubbles will be formed either at the orifice or downstream. Although much work has been done on bubble formation at low gas flow rates in a stationary liquid, the literature contains few studies made at higher flow rates.

At low gas flow rates, dynamic effects are negligible and bubble shapes correspond to predictions made on the basis of surface tension forces. In a study of aeration of liquids, Pattle [20] derived an expression for the radius of a bubble blown slowly from a circular orifice. Pattle's expression is

$$r_B = \left[\frac{3\, r_s \sigma\, f(r_s/a)}{2\rho_\ell g} \right]^{1/3} . \qquad (3.1)$$

where r_B is the radius of the bubble, r_s is the radius of the orifice, σ is the surface tension of the liquid, ρ_ℓ is the density of the liquid, g is the gravitational constant, and $f(r_s/a) \cong 1$.

As the gas flow rate is increased, bubbles form periodically at the orifice and the dominant forces become buoyancy and fluid inertia. Several investigators [6,7,12,23] developed expressions for the size of the bubbles in this flow region. Park [19] analyzed and combined the

results of these investigators and determined that an expression which best fits the bubble sizes is

$$r_B = \left[\frac{v_g^2 r_s}{g} \right]^{1/2} , \qquad (3.2)$$

where v_g is the gas velocity.

At some critical gas flow rate, typically large, individual bubbles are no longer formed and the gas leaves the orifice in the form of a jet which breaks up into bubbles downstream of the orifice.

Bubbles Emitted Into a Moving Liquid

Silberman [23] examined the behavior of high gas flow rates that produce jets in moving water. An approximate expression for the mean gas jet diameter a short distance downstream is given by Silberman as

$$D = (4\dot{Q}/\pi U)^{1/2} , \qquad (3.3)$$

where D is the mean gas jet diameter, $\dot{Q}$ is the gas flow rate per orifice, and U is the liquid speed relative to the orifice. If orifices in a nozzle plate are more closely spaced than D, more than one orifice may contribute to each jet. Silberman's result for the size of the bubble produced by any given (high) gas flow rate is

$$r_B = 0.76(\dot{Q}^2/g)^{1/5} . \qquad (3.4)$$

This result is independent of orifice size or liquid flow speed.

A more complete description of gas jet and bubble behavior in flowing water is given by Park [19]. Much of the following description of bubble behavior is summarized from Park's results. The formation and subsequent motion of gas bubbles are affected by surface tension,

viscosity, inertia, and buoyancy. These parameters can be conveniently expressed as the non-dimensional Weber and Froude numbers. The Weber number, a ratio of inertial to surface tension forces, is given for gas in a moving liquid as

$$W = \frac{\rho_g v_g^2}{\sigma/r_s}\left(1 - \frac{v_\ell}{v_g}\right)^2 \quad , \tag{3.5}$$

where v_ℓ is the liquid velocity. The factor $(1 - v_\ell/v_g)^2$ accounts for relative motion between the orifice and the liquid. The gas velocity v_g versus gas flow rate for each orifice is plotted in Figure 4.

The Froude number F relates the inertial to the gravitational force. For a submerged gas jet in moving water, F^2 is given by

$$F^2 = \frac{\rho_g v_g^2}{g(\rho_\ell - \rho_g)r_s}\left(1 - \frac{v_\ell}{v_g}\right)^2 \quad . \tag{3.6}$$

Bubble formation by gas flow through a submerged orifice can be characterized by the Weber and Froude numbers and a ratio of the two $W/F^{2/3}$. This ratio is plotted in Figures 5 through 9 as a function of gas flow rate per orifice for orifice radii of 0.025 cm, 0.063 cm, 0.127 cm, and 0.191 cm, respectively. The gas velocity v_g versus $W/F^{2/3}$ for all nozzle radii is plotted in Figures 10 through 14. When the Weber number lies in the range $0 \leq W \leq 1.2$, inertial and capillary forces are the important factors. The Froude number and relative speed between the orifice and liquid area are of little significance in this range. Average bubble radii in this flow range are given by

$$r_B/r_s \simeq 3 \quad , \tag{3.7}$$

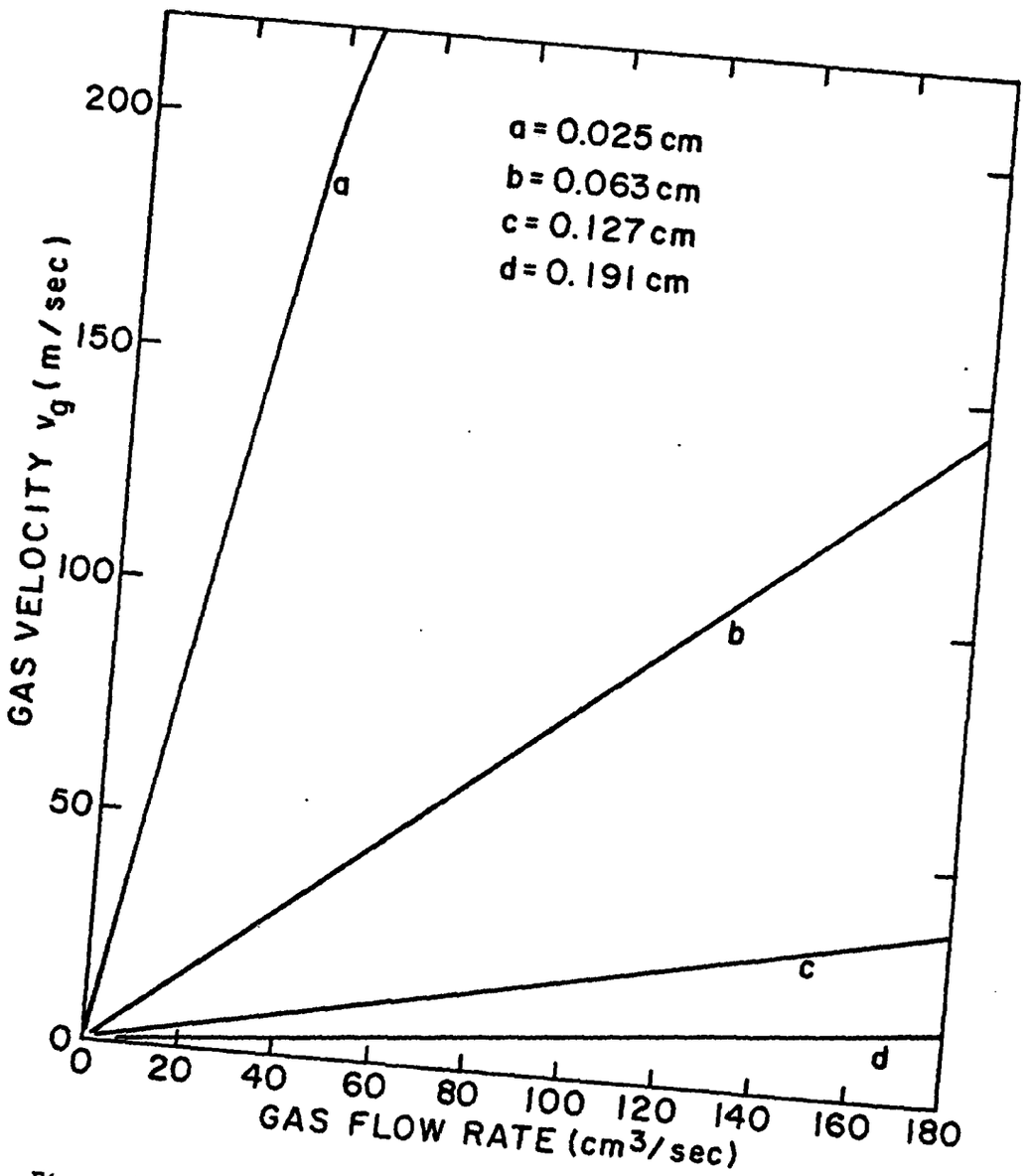

Figure 4. Velocity of Gas as it Leaves the Orifice as a Function of Gas Flow Rate. Gas Flow Rates Are for Each Orifice

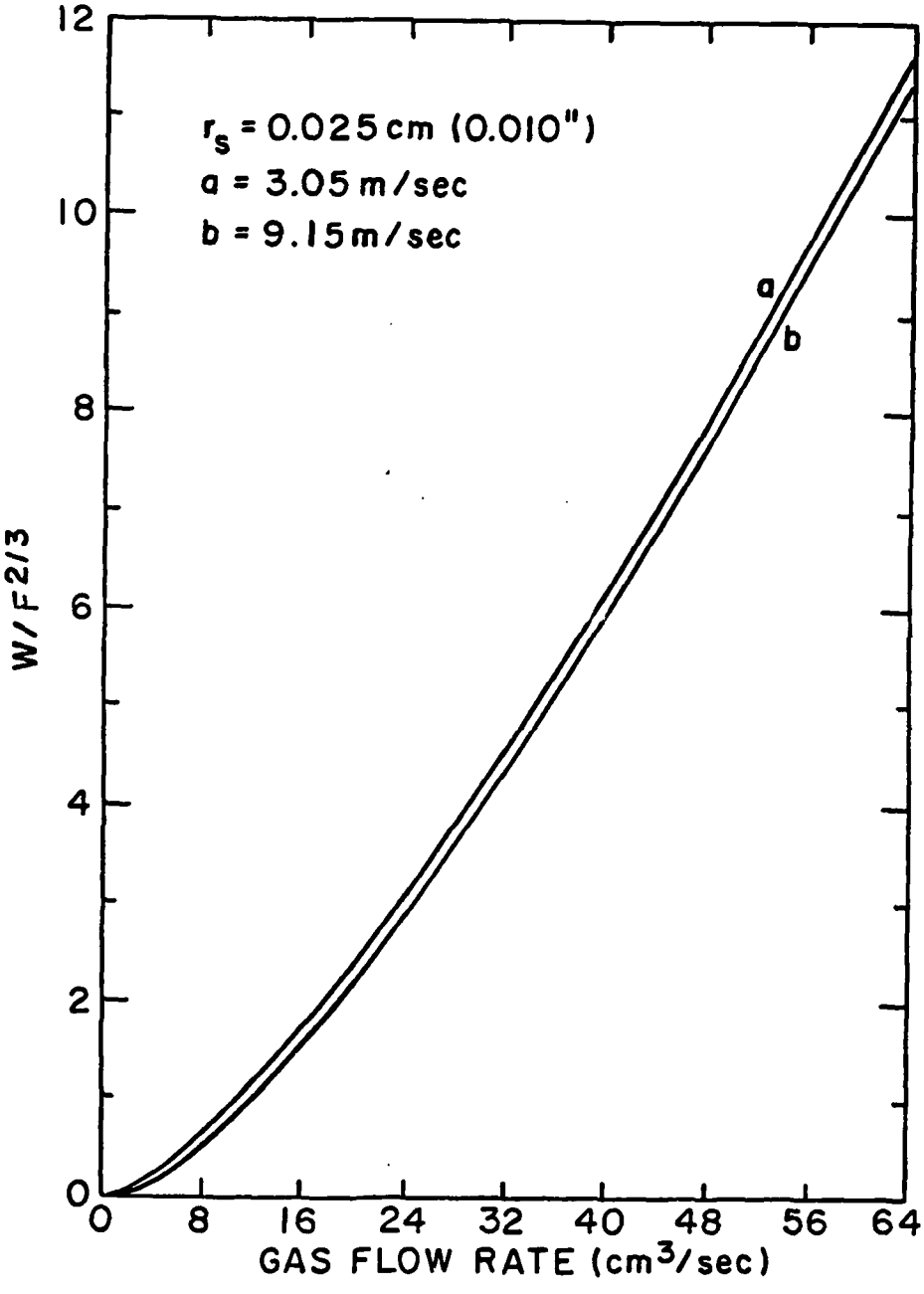

Figure 5. $W/F^{2/3}$ as a Function of Gas Flow Rate for an Orifice with Radius 0.025 cm

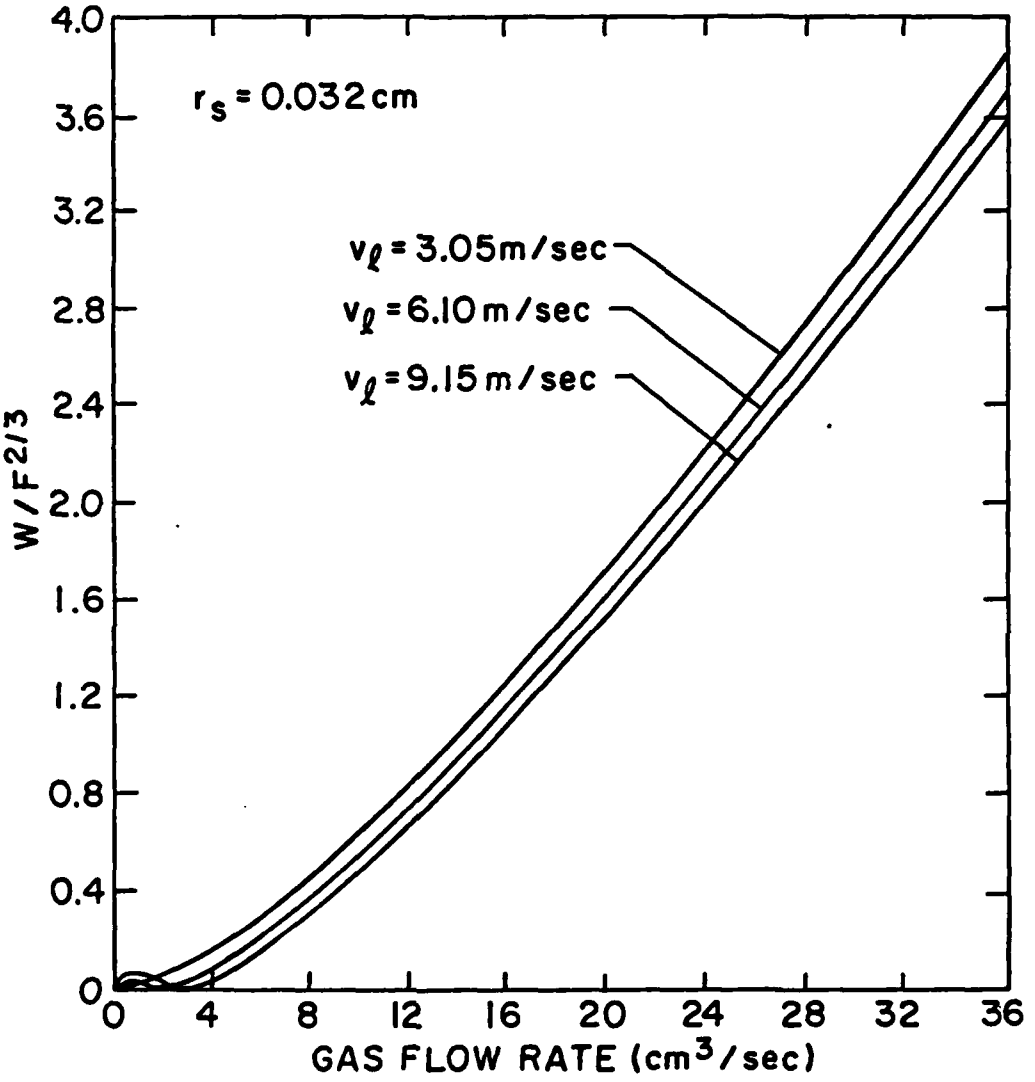

Figure 6. $W/F^{2/3}$ as a Function of Gas Flow Rate for an Orifice with Radius 0.032 cm

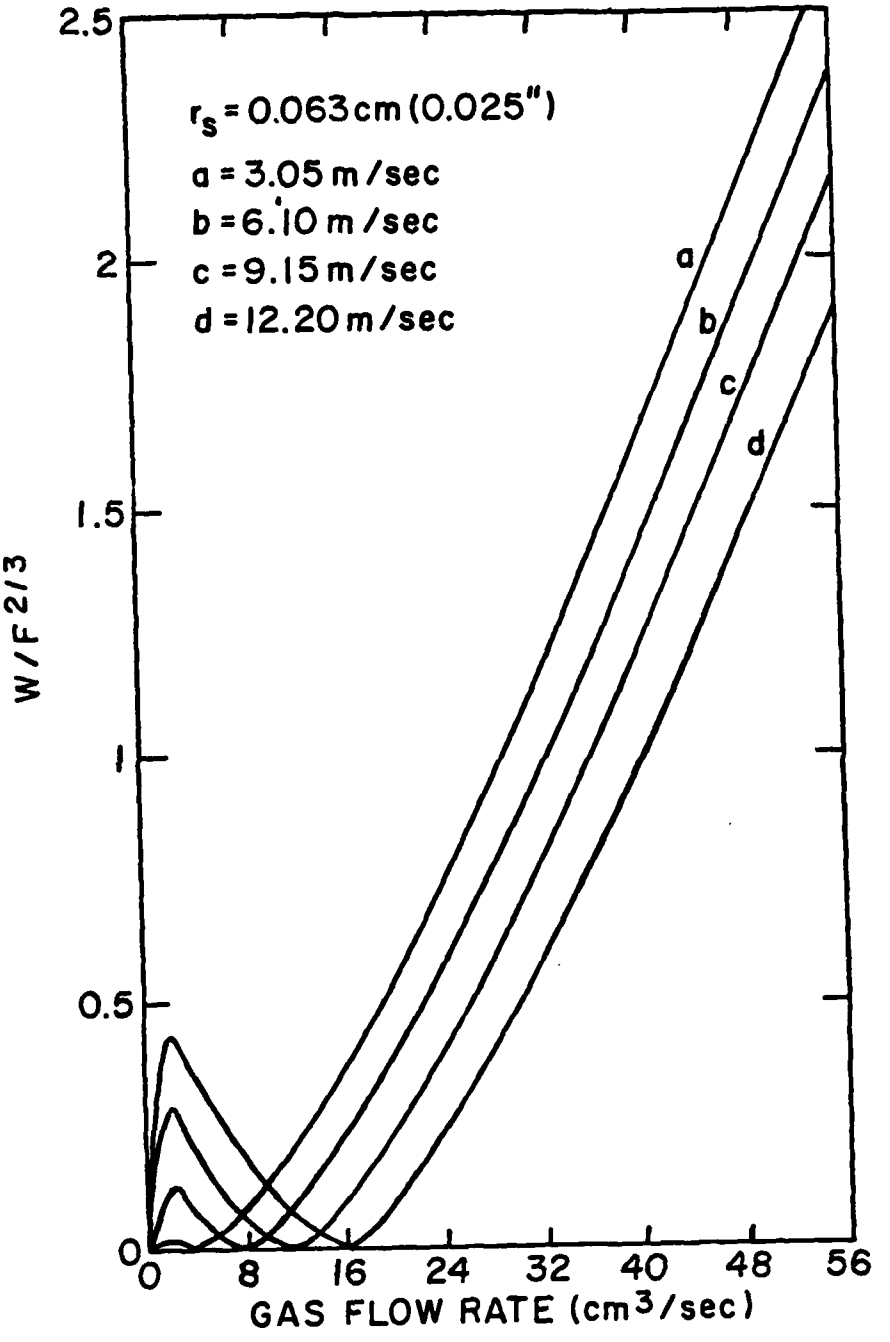

Figure 7. $W/F^{2/3}$ as a Function of Gas Flow Rate for an Orifice with Radius 0.063 cm

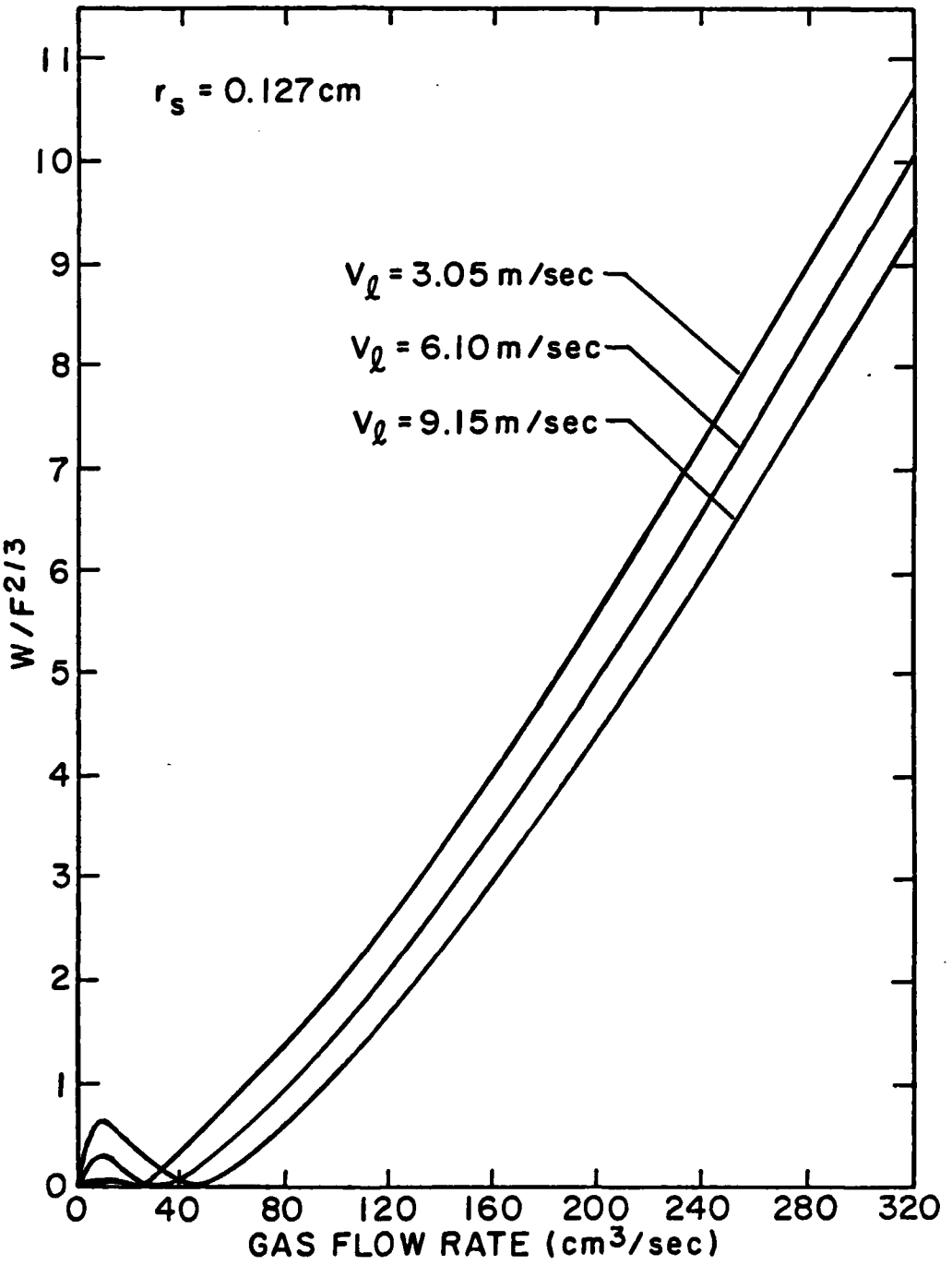

Figure 8. $W/F^{2/3}$ as a Function of Gas Flow Rate for an Orifice with Radius 0.127 cm

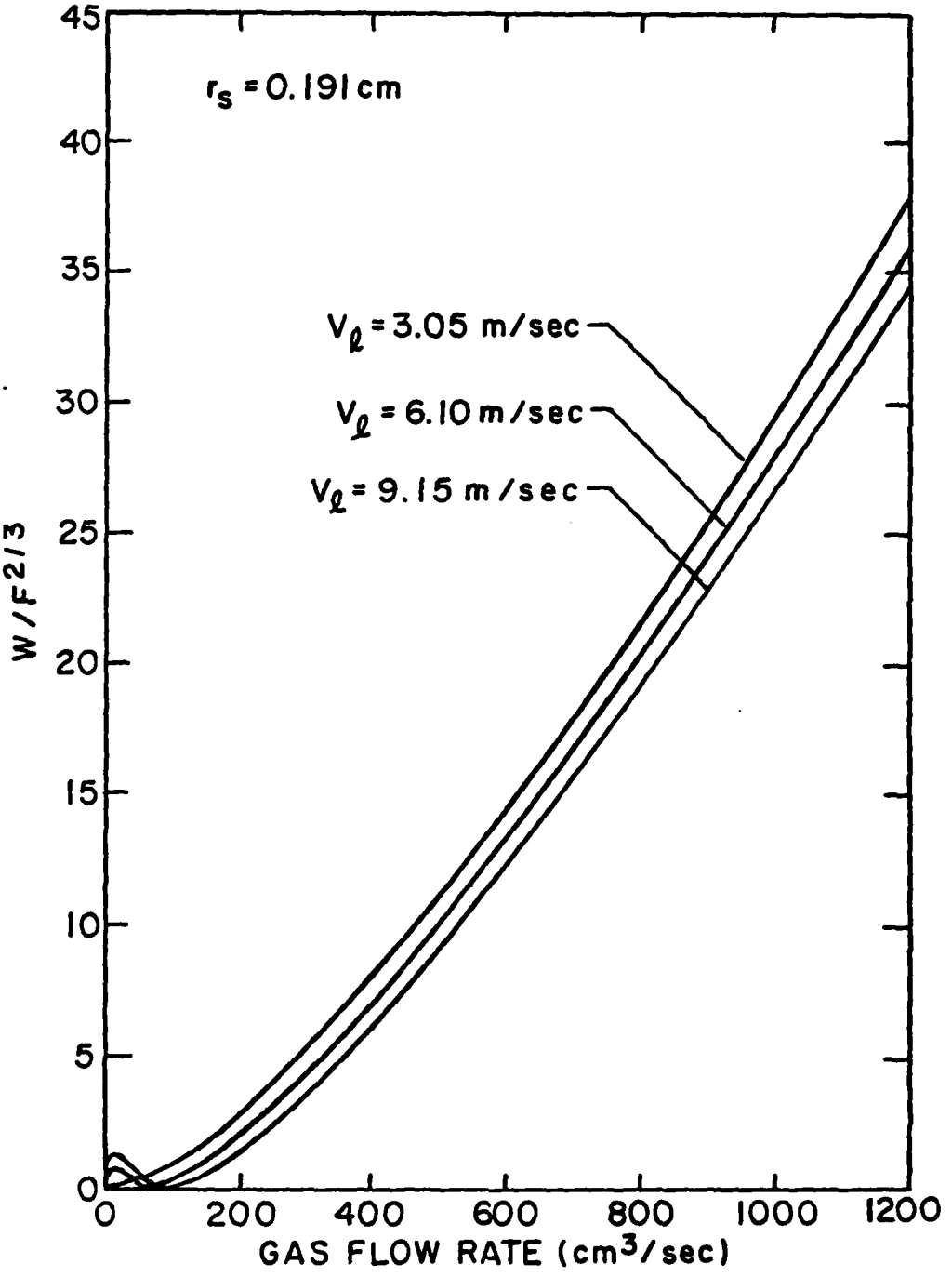

Figure 9. $W/F^{2/3}$ as a Function of Gas Flow Rate for an Orifice with Radius 0.191 cm

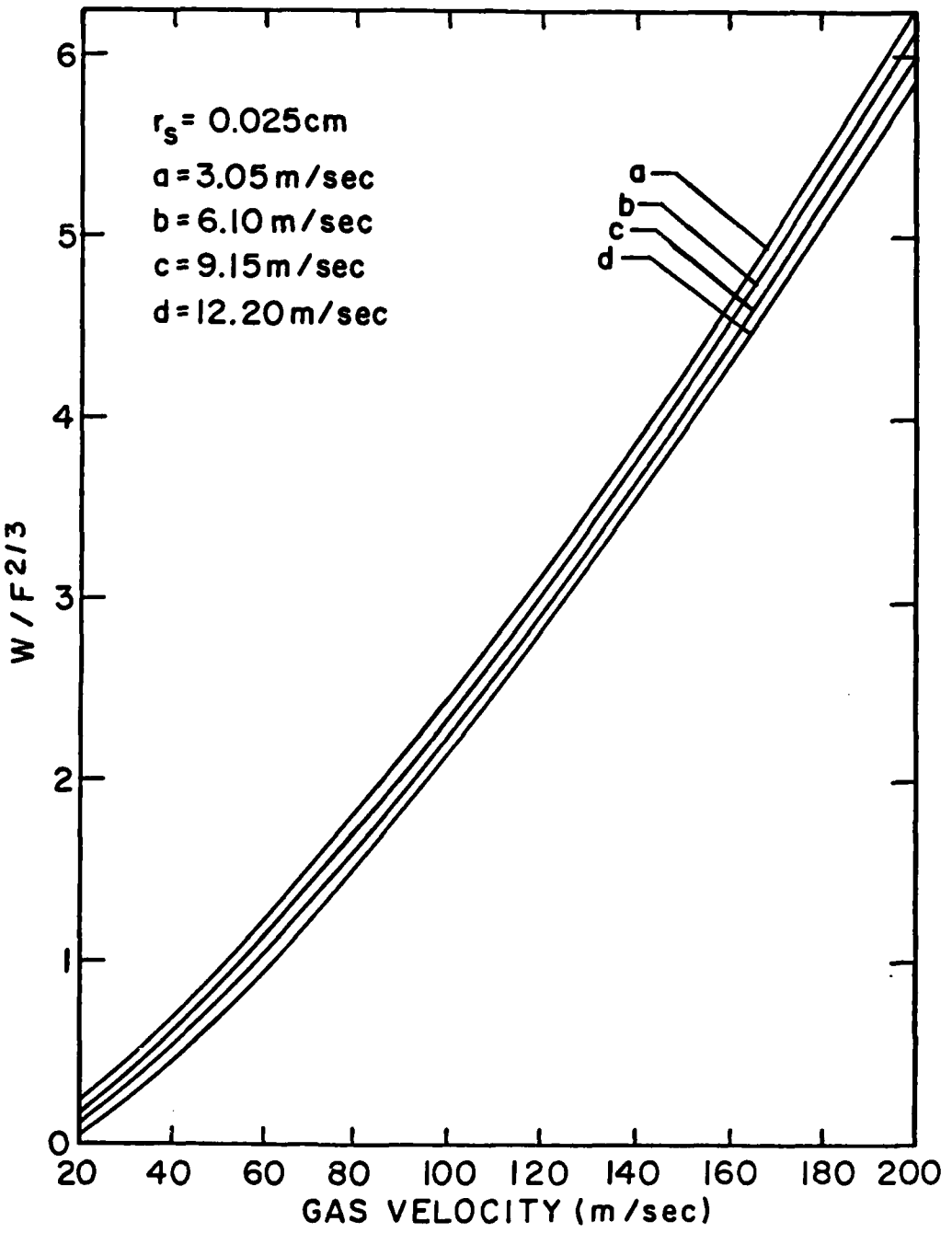

Figure 10. $W/F^{2/3}$ as a Function of Gas Velocity for an Orifice with Radius 0.025 cm

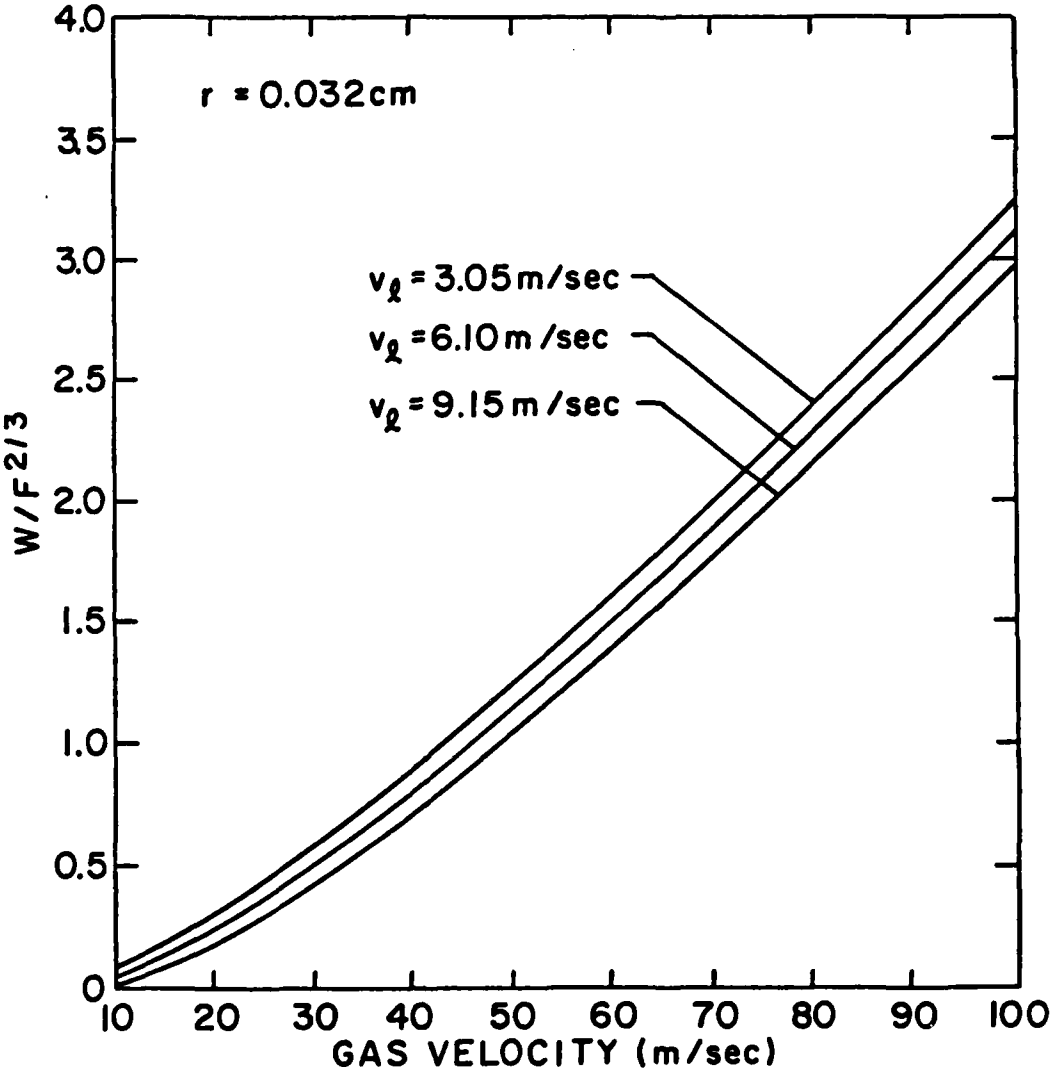

Figure 11. $W/F^{2/3}$ as a Function of Gas Velocity for an Orifice with Radius 0.032 cm

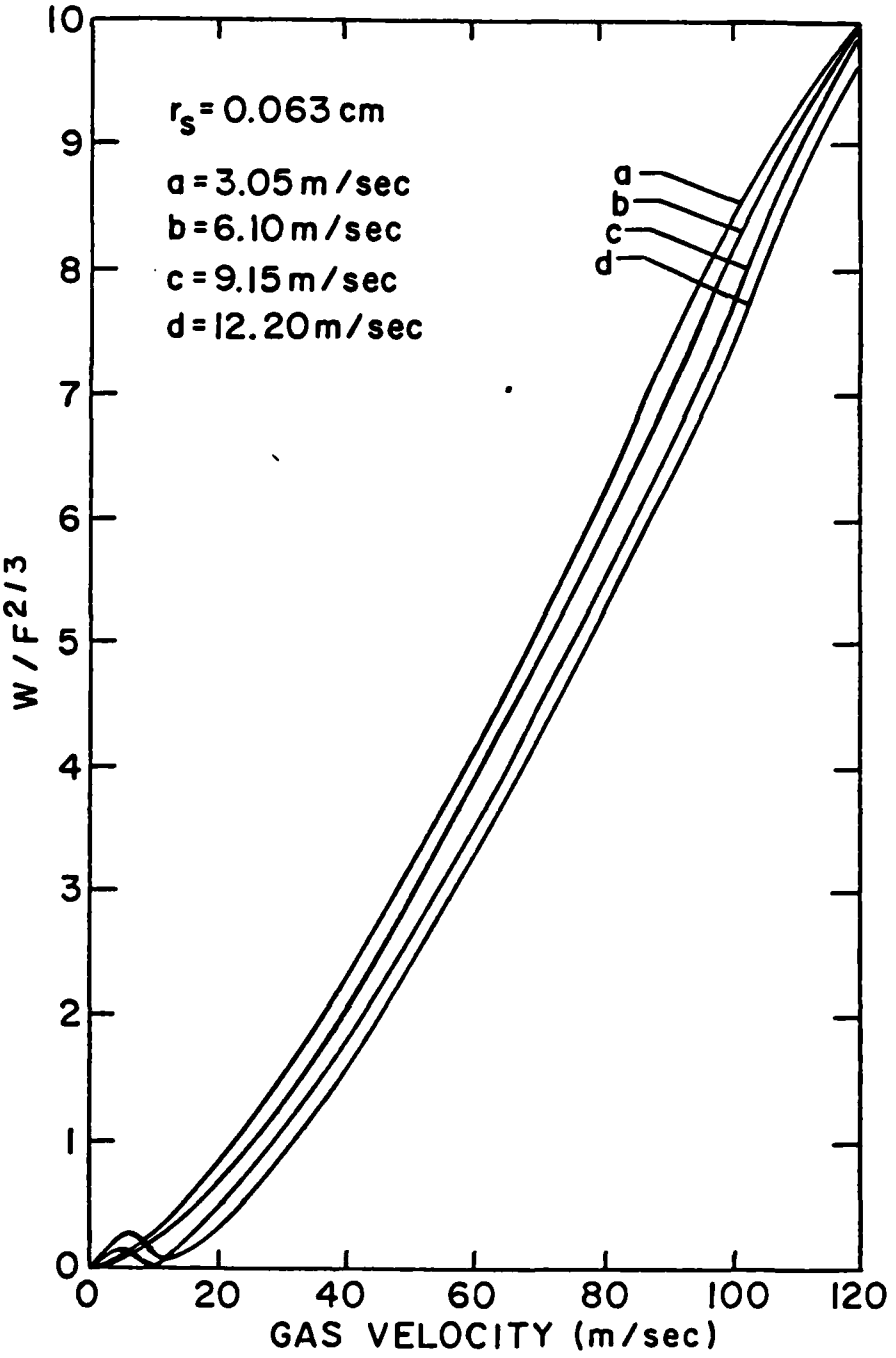

Figure 12. $W/F^{2/3}$ as a Function of Gas Velocity for an Orifice with Radius 0.063 cm

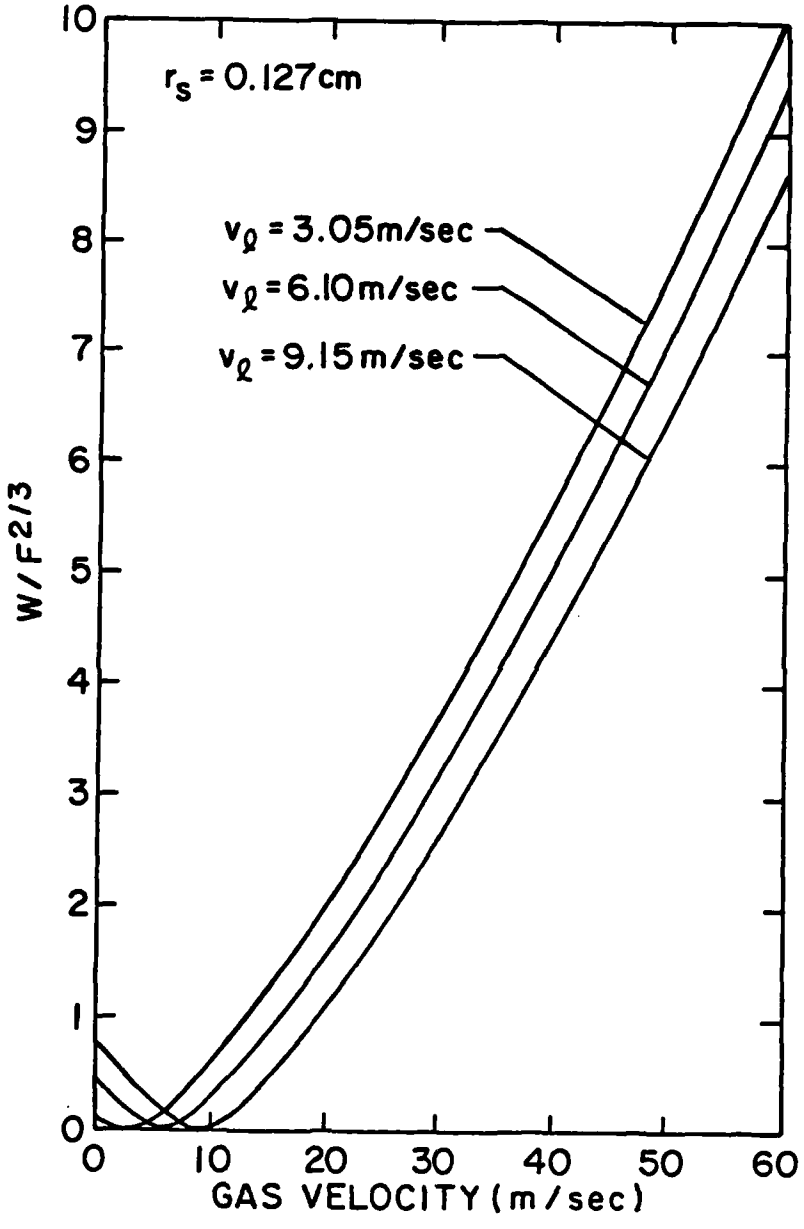

Figure 13. $W/F^{2/3}$ as a Function of Gas Velocity for an Orifice with Radius 0.127 cm

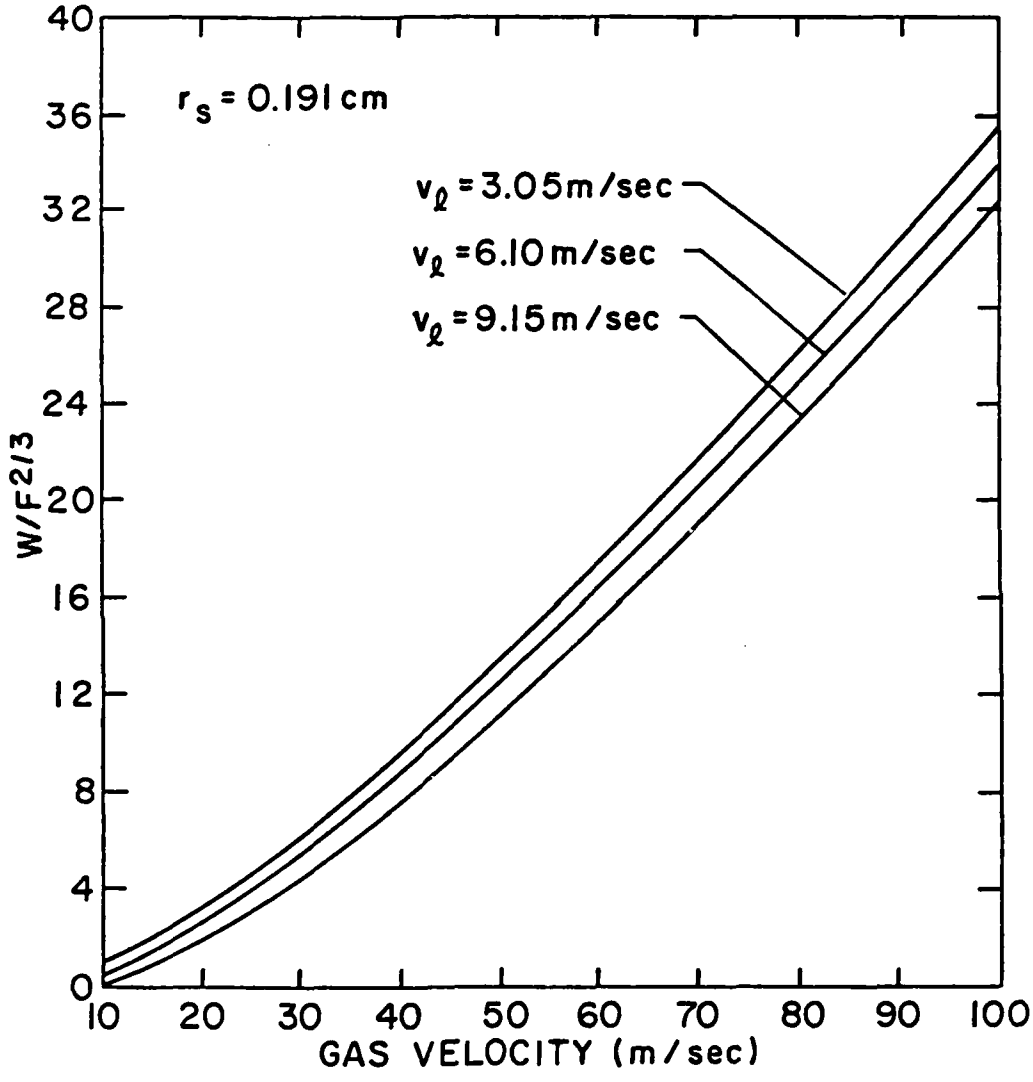

Figure 14. $W/F^{2/3}$ as a Function of Gas Velocity for an Orifice with Radius 0.191 cm

where r_B is the bubble radius. When the Weber number is larger,

$$W > 1.2 \; ; \quad v_\ell/v_g < 1 \quad , \tag{3.8}$$

a gas jet is generated at the orifice and buoyancy forces contribute to the bubble formation process. In this case, Park identifies three situations:

1. $\underline{W/F^{2/3} < 2.0}$

In this so-called transition region, typical bubble radii are given by

$$2.0 < r_B/r_s < 3.75 \quad . \tag{3.9}$$

2. $\underline{2.0 < W/F^{2/3} < 5.0}$

In this region, the average bubble radius is given by

$$r_B/r_s \approx 3.75 \quad . \tag{3.10}$$

3. $\underline{W/F^{2/3} > 5.0}$

Although Park does not discuss bubble formation in moving liquid for this range, he does give results for a stationary liquid. The flow in this range is very complicated, and for

$$v_\ell/v_g < 1 \quad ,$$

the average bubble size should not be very different from the case for

$$v_\ell = 0 \quad .$$

Park's results indicate that the typical bubble size for these flow conditions can be obtained from

$$r_B/r_s = 2.0(W/F^{2/3})^{1/3} \quad . \tag{3.11}$$

By including the factor to account for relative motion between gas and water in the Weber and Froude numbers, this approximate expression for bubble radii will be accurate enough for our purposes.

Bubbles Emitted Into a Turbulent Flow

When gas discharges in a liquid that is not only moving, but is also turbulent, the results are even more complex. Investigations by Kolmogorov [11] and Hinze [8] on bubble break-up show that the maximum bubble size that can exist in a turbulent flow is a function of the turbulence length and velocity scales. A critical Weber number for bubbles in turbulent flows can be defined as

$$W_c = \overline{\rho v^2}\, r_B/\sigma \quad , \tag{3.12}$$

where $\overline{v^2}$ is the spatial average of the square of the velocity differences over a distance equal to twice the bubble radius r_B. The gas-liquid surface tension is σ, while ρ is the liquid density. At higher Reynolds numbers, where energy containing wavenumbers are widely removed from the dissipation wavenumbers, Kolmogorov's Universal Equilibrium Theory is valid and $\overline{v^2}$ is given by

$$\overline{v^2} = 2(2\varepsilon r_B)^{2/3} \quad , \tag{3.13}$$

where ε is the local rate of energy dissipation. This value can be estimated by [29]

$$\varepsilon \sim u^3/L \quad , \tag{3.14}$$

where u and L are the velocity and length scales of the turbulence,

respectively, and the proportionality factor is of order one. With Equations (3.13) and (3.14), Equation (3.12) can be written as

$$r_B = 1/2L^{2/5}(\sigma W_c/u^2\rho)^{3/5} \quad . \qquad (3.15)$$

Park [19] and Sevik and Park [22] recently extended the earlier work of Kolmogorov and Hinze and showed that bubble splitting in turbulent flows is determined by a critical Weber number of 1.3. When the Weber number in any given flow for a particular bubble is greater than 1.3, strong shear forces acting on the bubble will tend to rip it apart. The critical bubble radius at which this tends to occur is plotted in Figure 15 as a function of turbulence length and velocity scales.

Gas Bubble Generation in Various Liquids

One of the ways in which liquids can be separated into classes is on the basis of their ability to either aid or hinder bubble coalescence [25]. These two groupings are usually labeled Class A for those that inhibit bubble coalescence, and Class B for those liquids that aid bubble combinations. Among the liquids in Class A are aqueous solutions of alcohols, ether, concentrated nitric acid, and strong salt solutions. Class B includes such liquids as tap and distilled water, olive oil, dilute salt solutions, and sulfuric acid. All viscous liquids are in Class B. Liquids in Class A tend to maintain a temporary film between two adjacent bubbles, thereby inhibiting coalescence. On the other hand, bubbles in Class B exhibit a strong tendency to combine with one another. Salt solutions change from Class B to Class A when the salt concentration is greater than 10 parts

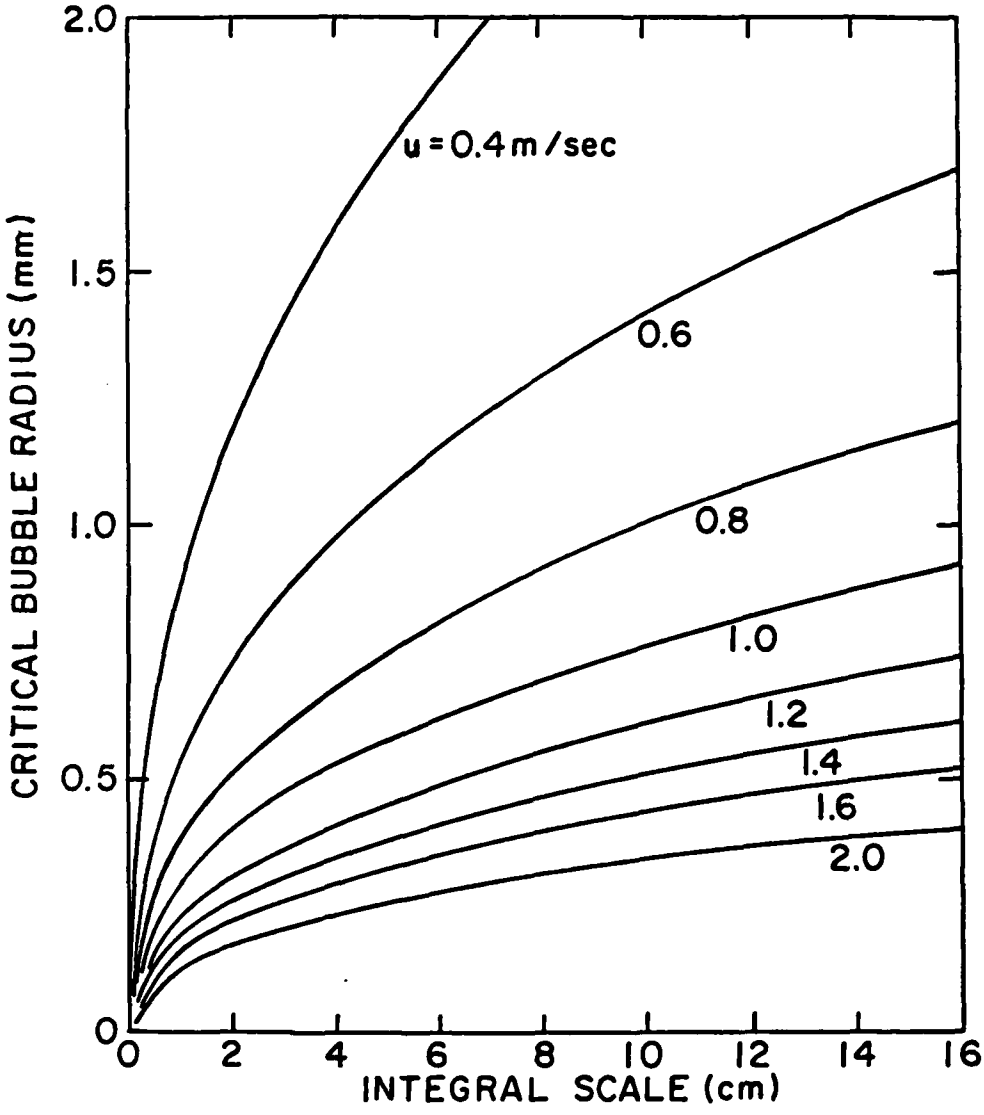

Figure 15. Critical Bubble Radius as a Function of Turbulence Integral Scale for Various Turbulence Velocity Scales

per thousand (ppt) by weight. Since the salt content of sea water is about 32 ppt, it is a Class A solution.

When a bubble is formed with sufficient gas flow at any orifice in pure quiescent water, it may touch and combine with the preceding bubble. This causes the combined bubble to break off at the orifice prematurely, and the next bubble begins to form. When this sequence continues, chain bubbles are formed, rather than single, individual bubbles. In Class A liquids, the emerging bubble would tend to simply push the previously formed bubble out of its path, rather than combine with it. The acoustic behavior of gas bubbles in quiescent pure water is, therefore, not completely analogous to what would be obtained in sea water. When there is relative motion between the orifice and the surrounding liquid, there will be less difference between acoustic behavior in Class A and B liquids. The moving stream sets up shear forces on the emerging bubble, tearing it away from the orifice and sweeping it downstream. In such an environment, there is far less chance for an emerging bubble to combine with previously formed bubbles.

CHAPTER IV

EXPERIMENTAL PROCEDURE

Experimental Facility

The experiments described in this investigation were performed in the Garfield Thomas Water Tunnel at the Applied Research Laboratory of The Pennsylvania State University. The tunnel is a closed-circuit, closed-jet water tunnel without external propeller shafts. It is about 30 meters long and 10 meters high. The cylindrical test section is 122 centimeters in diameter and 4.3 meters long. The speed in the test section is continuously variable up to 25 m/s. The pressure may be reduced to negative gage pressures or raised to several atmospheres positive pressure. The water temperature can be varied over a wide range. The test section is fitted with plexiglass windows along its sides to permit visual and acoustic observations. A large portion of the top of this section is a removable hatch cover allowing access to test objects.

The hydrodynamic circuit of the water tunnel is shown in Figure 16. The cylindrical test section is preceded by a nozzle 6.1 meters long with an area ratio of 9. The contour of the nozzle was chosen to give a uniform jet in the test section and to avoid cavitation at the walls. The test section is followed by a diffuser which decelerates the high-velocity flow before it reaches the pump and turns. This is to prevent high energy losses and possible cavitation at the pump and turns. The diffuser angle is 7 degrees total, i.e., 3-1/2 degrees per side. The transition section between the working section and diffuser

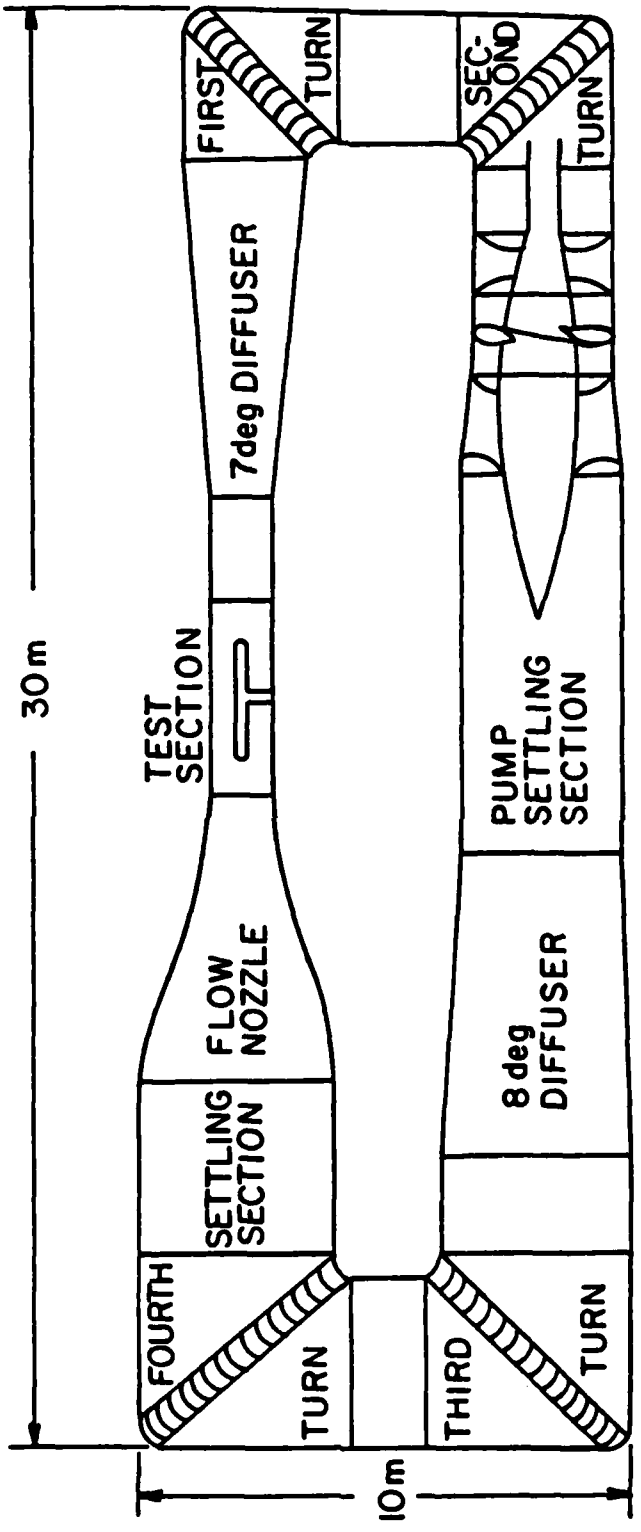

Figure 16. Water Tunnel Hydrodynamic Circuit

was included to prevent the sudden change in flow direction, which would occur with a sharp transition, from initiating cavitation. The first vaned turn has a diameter of 223 centimeters and is composed of 20 airfoil-type guide vanes in a miter turn. The short vertical diffuser between the first and second turns is also of 7 degrees total angle. The turn immediately preceding the pump has 14 guide vanes and a streamlined fairing covering the drive shaft. The diameter at this turn is 249 centimeters.

The pump used to drive the water around the circuit is a propeller-type axial-flow pump having pre- and post-whirl guide vanes and a four-bladed, adjustable-pitch impeller. The impeller has a diameter of 240 centimeters and its pitch is adjustable from -6 degrees (zero net flow) to +22-1/2 degrees. It is driven by a 2000-hp variable-speed induction motor at speeds of 0 to 180 rpm.

The remainder of the circuit consists of: a 274 centimeter diameter straight section; an 8 degree diffuser; 366 centimeter diameter third and fourth turns of 20 vanes each; and a one-diameter-long settling section preceding the nozzle. The settling section is space allowed for turbulence from the turns to decay, and houses a honeycomb and screens which lead to an improvement in the flow.

A turbulent wake was generated under controlled conditions with a cigar-shaped test body mounted in the test section of the water tunnel. An outline of the experimental set-up is given in Figure 17. The test body is 22 centimeters long, 20.3 centimeters in diameter at its thickest point, and tapers gradually to a diameter of 3.8 centimeters at its aft end. A removable circular plate, with typical orifices located as shown in Figure 18, attaches to the aft end of the

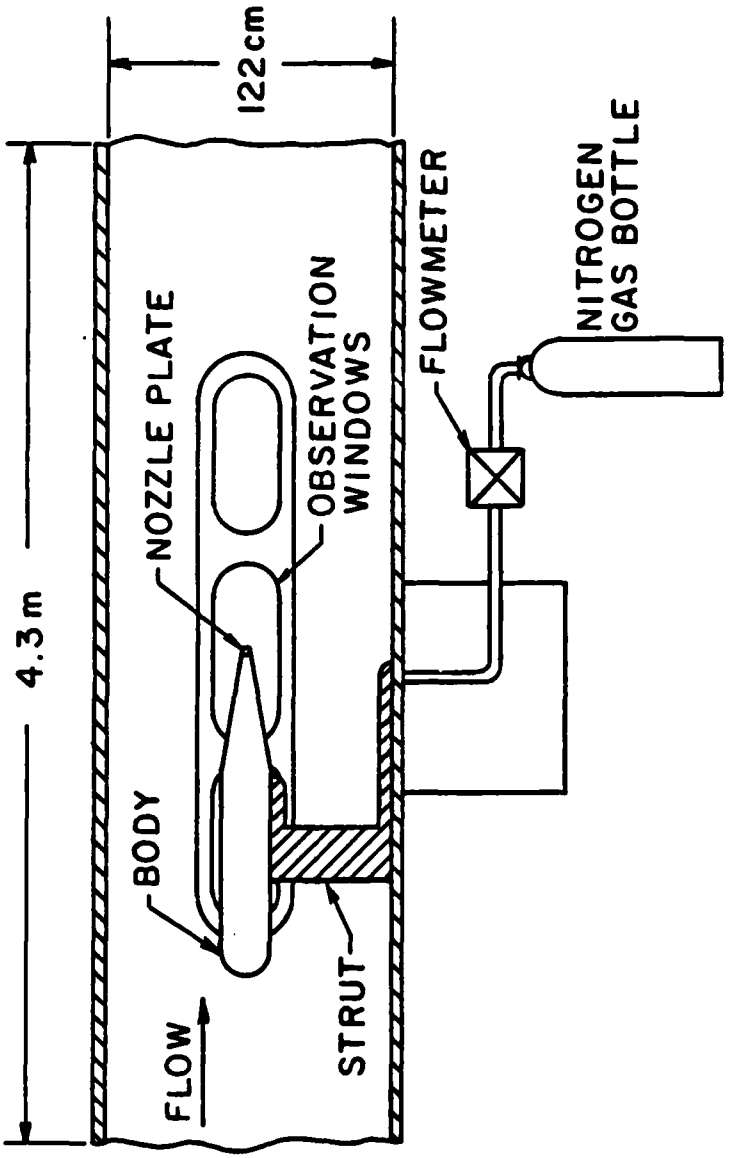

Figure 17. Test Body Used to Generate Wake, Mounted in Test Section of Water Tunnel

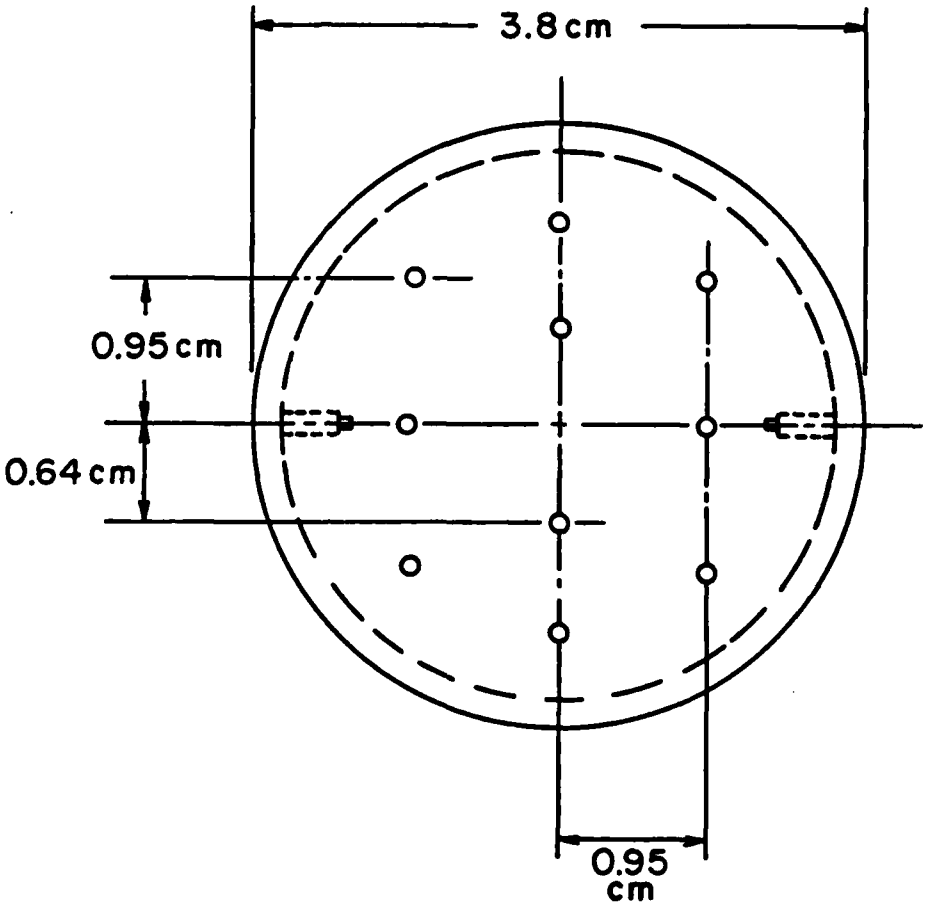

Figure 18. Location of Typical Orifices in Nozzle Plate

body, covering the exhaust pipe. Seven different nozzle plates were used in the series of experiments reported on here. The different nozzle plates are listed in Table I. Gas flow rates per orifice up to 1133 cm^3/sec were used with water speeds up to 9.1 m/sec in the tunnel test section.

As indicated in Figure 17, gas was supplied from a nitrogen tank equipped with a pressure regulator. Three interchangeable flowmeters, manufactured by Gilmont Industries and Fisher Porter, and a pressure gage were mounted outside the test section to monitor the gas flow. A pressure transducer was mounted inside the test body to record the gas pressure before exiting into the turbulent wake. A plastic hose carried the gas from the tank outside the water tunnel through the hollow mounting strut to the nozzle plate at the aft end of the wake generating body.

Noise measurements were made with a directional hydrophone mounted in a large water-filled tank attached to one side of the tunnel test section. A cross-section view of the test section and hydrophone assembly is shown in Figure 19. This instrument was originally designed to serve as a directional hydrophone capable of focusing on individual sound sources located within the tunnel test section. If a sound source were located at a focal point of a prolate spheroid, then a focusing effect could be obtained at the other focal point if an ellipsoidal shell were used to reflect the sound energy.

The reflecting ellipsoidal shell is composed of two thin brass spinnings separated by a reflecting air layer. A hydrophone is then positioned at the ellipsoidal focal point within the shell. The distance between the receiving hydrophone and the center of the tunnel

TABLE I

NOZZLE PLATES USED IN THE GAS BUBBLE NOISE STUDIES

Nozzle No.	Number of Orifices	Orifice Radius (cm)
1	10	0.025
2	10	0.063
3	1	0.191
4	36	0.032
5	4	0.191
6	9	0.127
7	36	0.063

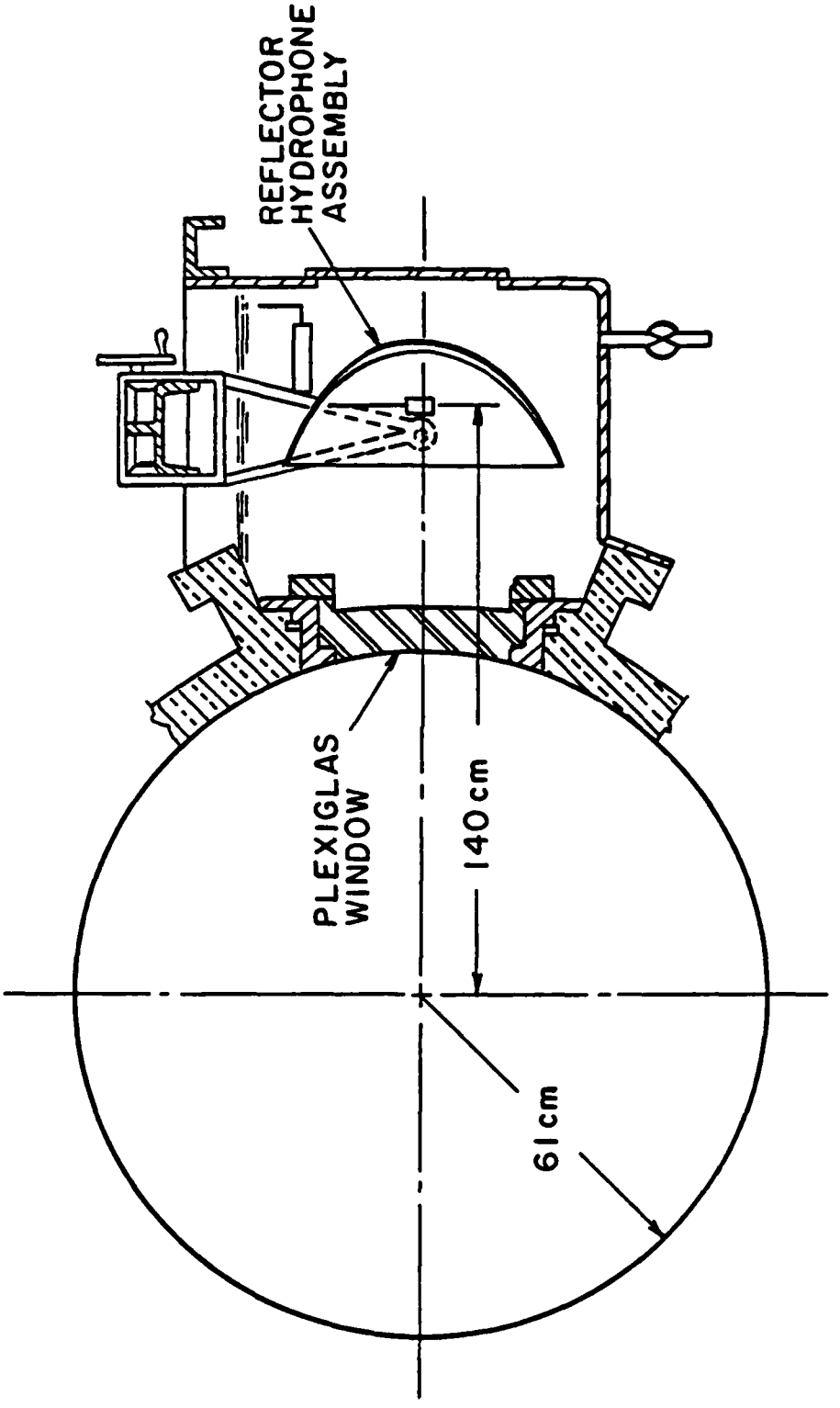

Figure 19. Cross-Sectional View of Water Tunnel Test Section and the Directional Hydrophone Assembly

corresponds to the interfocal distance of the 2:1 ellipsoid used to shape the reflector (140 cm). The sound generated within the tunnel is received by the probe via a path through the acoustically transparent plexiglass windows (its acoustical impedance is approximately that of water). The entire assembly is fastened to a traversing mechanism to enable the receiver to be moved either up- or downstream from the center of the test section.

All noise measurements were made during the first 25 seconds of gas exhaust. Shortly after this time, bubbles complete the water tunnel circuit and contaminate the test area. The presence of gas bubbles in water markedly affects the acoustic properties of water. Therefore, it was necessary to degas the water tunnel after every test. The time for a bubble to complete the circuit for various tunnel velocities is shown in Figure 20.

Calibration

The hydrophone assembly had been calibrated in the free-field [10] and its sensitivity function and directional characteristics determined. However, reflections in the tunnel give rise to sound fields that are different from those generated in the free field, and therefore, the free-field calibration may not be applicable to general sound pressure measurements. In addition, the reverberation in the tunnel will also change the directional characteristics of the hydrophone assembly. It is therefore necessary to recalibrate the assembly in the presence of the streamlined test model mounted in the test section of the water tunnel.

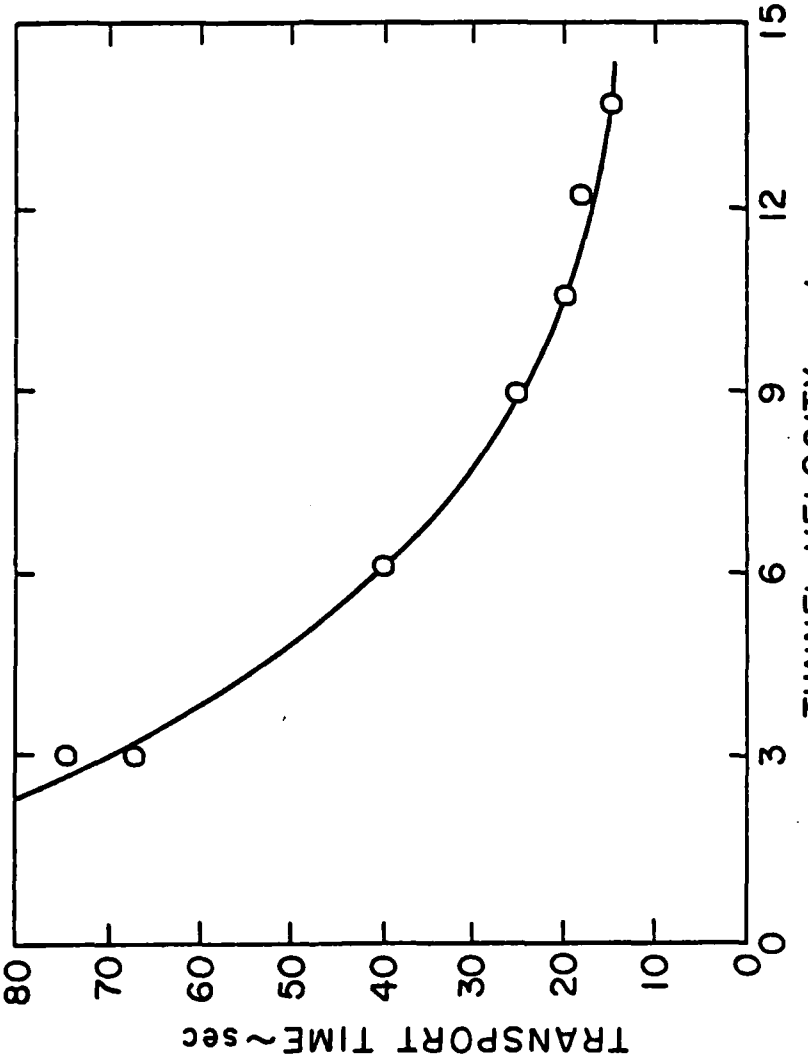

Figure 20. Bubble Transport Time in Water Tunnel as a Function of Tunnel Velocity

The sensitivity of a hydrophone is a matter of determining its transfer function, i.e., the amount of output voltage for a unit microbar of sound pressure acting on its surface as a function of frequency. The method for determining the sensitivity makes use of a sound projector. This sensitivity is usually referenced to one meter and by assuming spherical spreading, making it possible to approximate how much sound pressure is present for a given sound voltage.

The equation for determining the sensitivity is [1]:

$$dB_{sens} = dB_v - dB_{cal} - dB_x + dB_d \quad , \qquad (4.1)$$

where

$$dB_{sens} = \text{sensitivity level re } \frac{1 \text{ volt}}{\mu\text{bar}} \quad , \qquad (4.2)$$

$$dB_v = \text{received output voltage level re 1 volt} \quad , \qquad (4.3)$$

$$dB_{cal} = \text{source calibration level re } \frac{1 \ \mu\text{bar} - 1 \text{ meter}}{1 \text{ volt}} \quad , \qquad (4.4)$$

$$dB_x = \text{source input voltage level re 1 volt} \qquad (4.5)$$

and

$$dB_d = \text{separation distance level re 1 meter} \quad . \qquad (4.6)$$

The free-field measurements were performed in an anechoic tank using a 55-inch separation distance between the projector and the probe. The results are presented in Figures 21 through 23. Figure 21 shows the on-axis open circuit receiving voltage sensitivity with the probe mounted in the reflector. The receiving response of such a simple hydrophone, operated well below its fundamental resonance as this was, would normally be independent of frequency. The odd behavior of this probe cannot be readily explained. Figures 22 and 23 show the

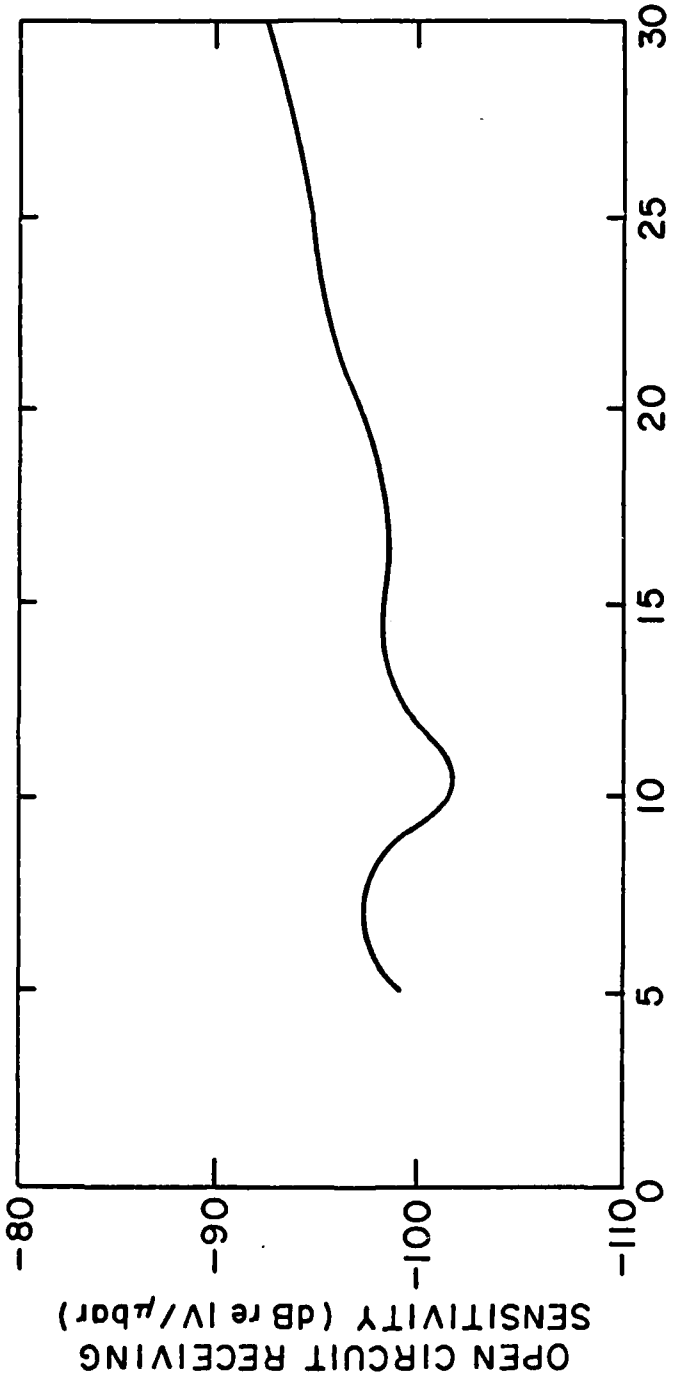

Figure 21. On-Axis Open-Circuit Receiving Voltage Sensitivity of Probe and Probe-Reflector Assembly Measured in Free-Field

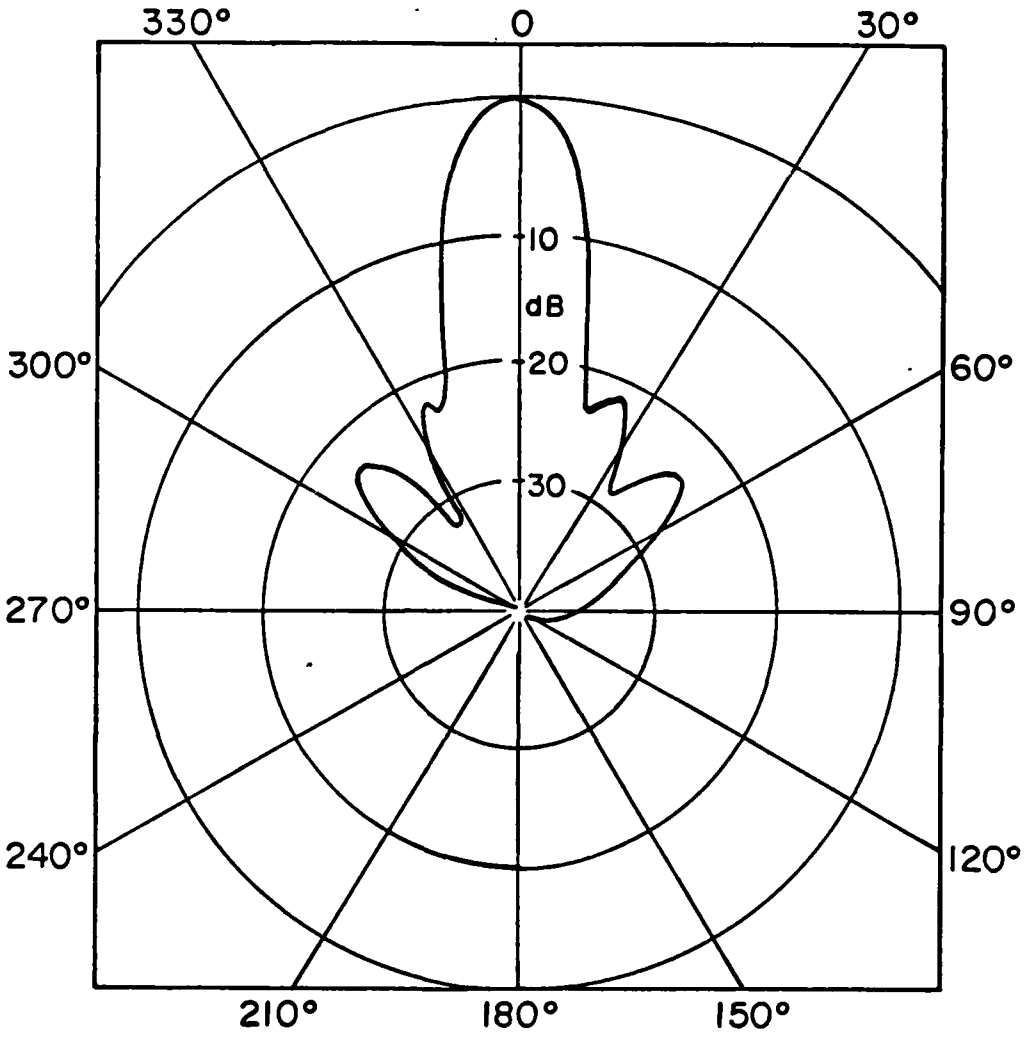

Figure 22. Directivity Function of Probe-Reflector Assembly at 20 kHz as Measured in Free-Field

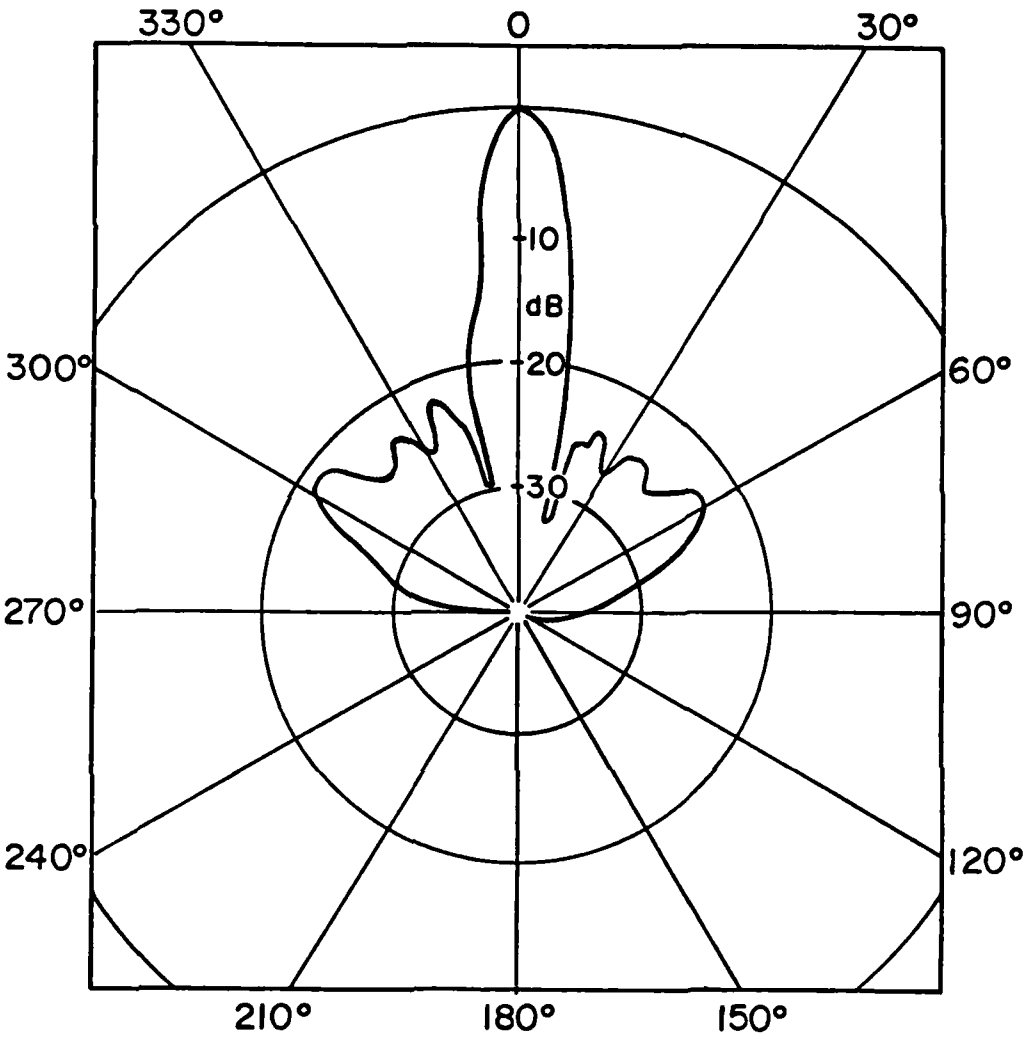

Figure 23. Directivity Function of Probe-Reflector Assembly at 30 kHz as Measured in Free-Field

directivity patterns of the probe-reflector assembly for 20 kHz and 30 kHz, respectively.

Measurements of the sensitivity and directivity patterns of the assembly in a bare tunnel, i.e., with no model present, are presented in Figures 24 through 26. The sensitivity of the reflecting hydrophone was determined by driving the sound source with random noise. The reflecting hydrophone sensitivity as a function of frequency for the sound projector located at the center of the bare tunnel is shown in Figure 24 with the free-field sensitivity function superimposed. The sensitivity curve for the bare tunnel is not very smooth, showing resonance and antiresonance characteristics about a mean line that falls close to the free-field sensitivity. This indicates that the probe is receiving the direct sound generated by the source, but at certain frequencies, the reflection and diffraction effects within the tunnel add either constructively or destructively to the direct sound field causing the fluctuations in the curve. For the frequency range considered, it is assumed that the sound source output is not altered significantly by the reflected sound field since the separation distance between source and walls is greater than or equal to the acoustic wavelength [30].

The directivity functions are measured at discrete frequencies by traversing the receiver and simply measuring the output levels as a function of displacement with the projector fixed. The levels are normalized with the on-axis level. Typical directivity curves for the bare tunnel with the corresponding free-field directivity functions are presented in Figures 25 and 26. From these curves, it is noted that the reflector is not as directional in the tunnel as it is in the free

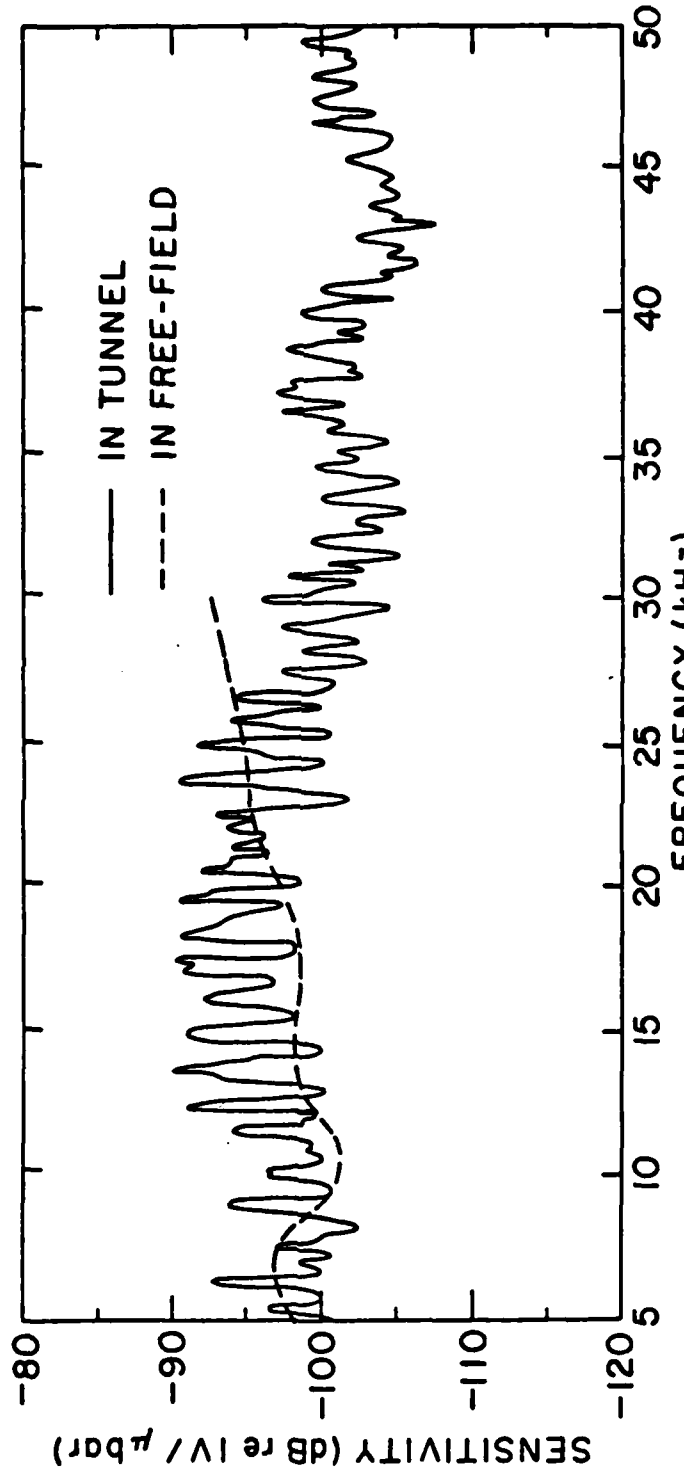

Figure 24. Receiving Voltage Sensitivity of Directional Hydrophone Mounted in a Water-Filled Tank Attached to One Side of 122 cm Diameter Water Tunnel as Measured Without Presence of Test Model

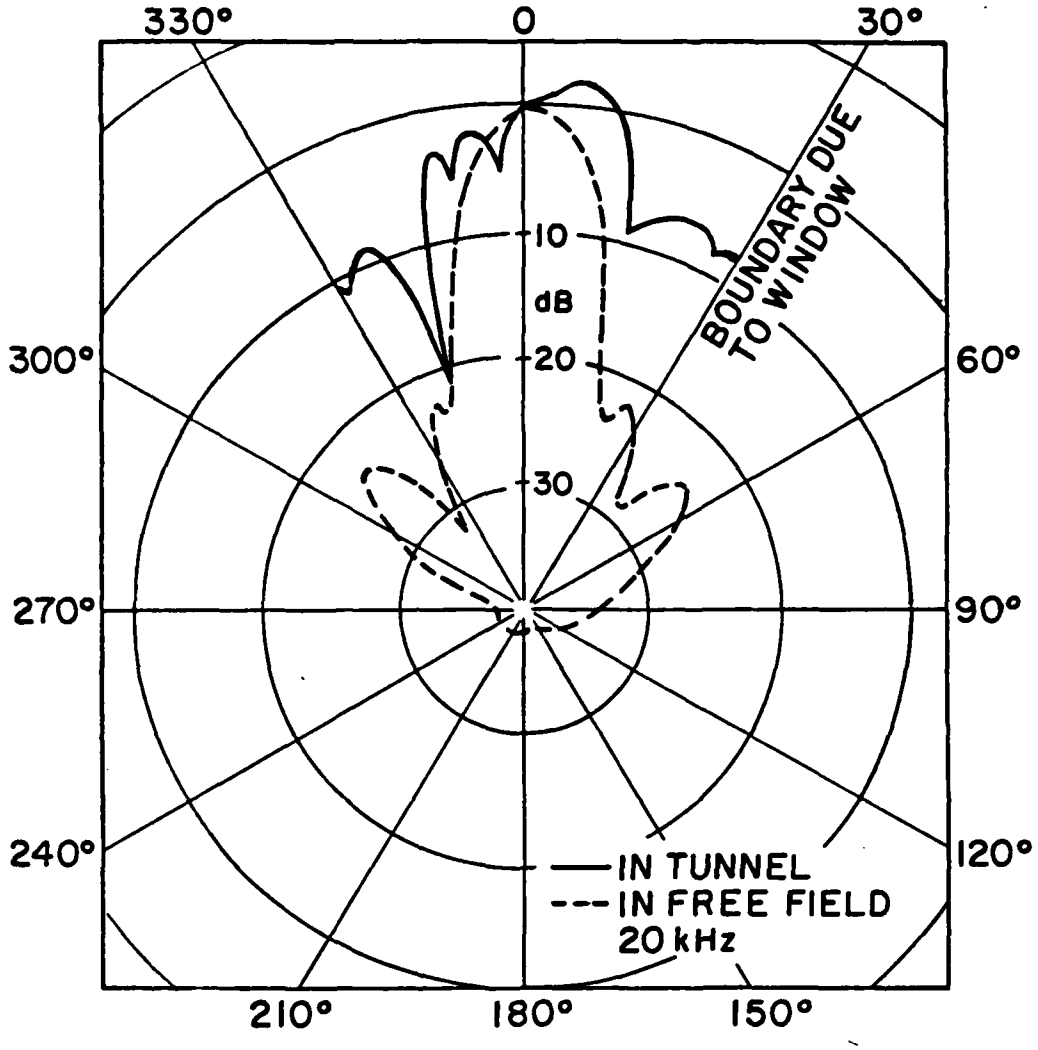

Figure 25. Directivity Function at 20 kHz of Directional Hydrophone Mounted in a Water-Filled Tank Attached to One Side of the 122 cm Diameter Water Tunnel as Measured Without Presence of Test Model

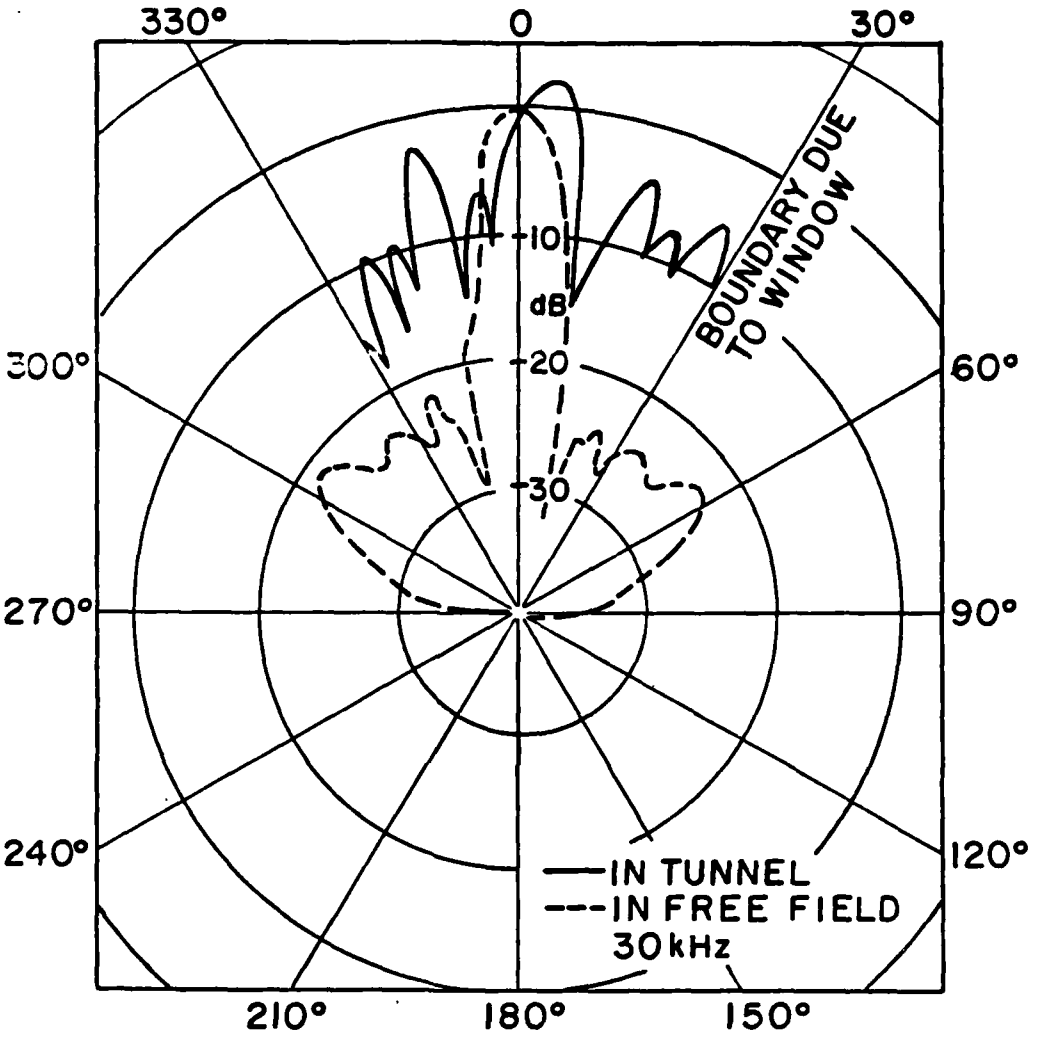

Figure 26. Directivity Function at 30 kHz of Directional Hydrophone Mounted in a Water-Filled Tank Attached to One Side of the 122 cm Diameter Water Tunnel as Measured Without Presence of Test Model

field. Standing waves generated in the tunnel and a diffraction field resulting from sound waves of short wavelength passing through the acoustically transparent window contribute to the difference in the curves. On the directivity curves is marked a sector that corresponds to the boundary due to the window of the test section. Beyond this boundary, no direct acoustic energy is received by the probe, but diffracted energy can pass.

The directivity and sensitivity functions for the model mounted in the test section varied very little from that of the bare tunnel and, consequently, are not presented.

Noise generated by bubble break-up is typically broadband. It is advantageous to perform the spectral analysis of the noise in a wide bandwidth, such as one-third octave. Consequently, it was desirable to obtain a sensitivity curve as a function of one-third-octave frequency bands. This sensitivity was determined by driving the sound source with random noise and analyzing the output voltage from the receiver in one-third-octave frequency bands. Typical sensitivities of the reflecting hydrophone are shown in Figures 27 and 28. All spectral analysis was performed on a Spectral Dynamics Corporation Real Time Analyzer.

During testing, the hydrophone was traversed to several positions to measure radiated noise. Measurements were taken (1) along the streamlined test body, (2) immediately to the rear of the test model, and (3) downstream of the test model. When the hydrophone was focused at a point immediately to the rear of the model, the noise level was considerably higher by a few decibels than at any other point in the test chamber. Therefore, the large majority of the measurements were taken with the hydrophone focused on the rear of the model.

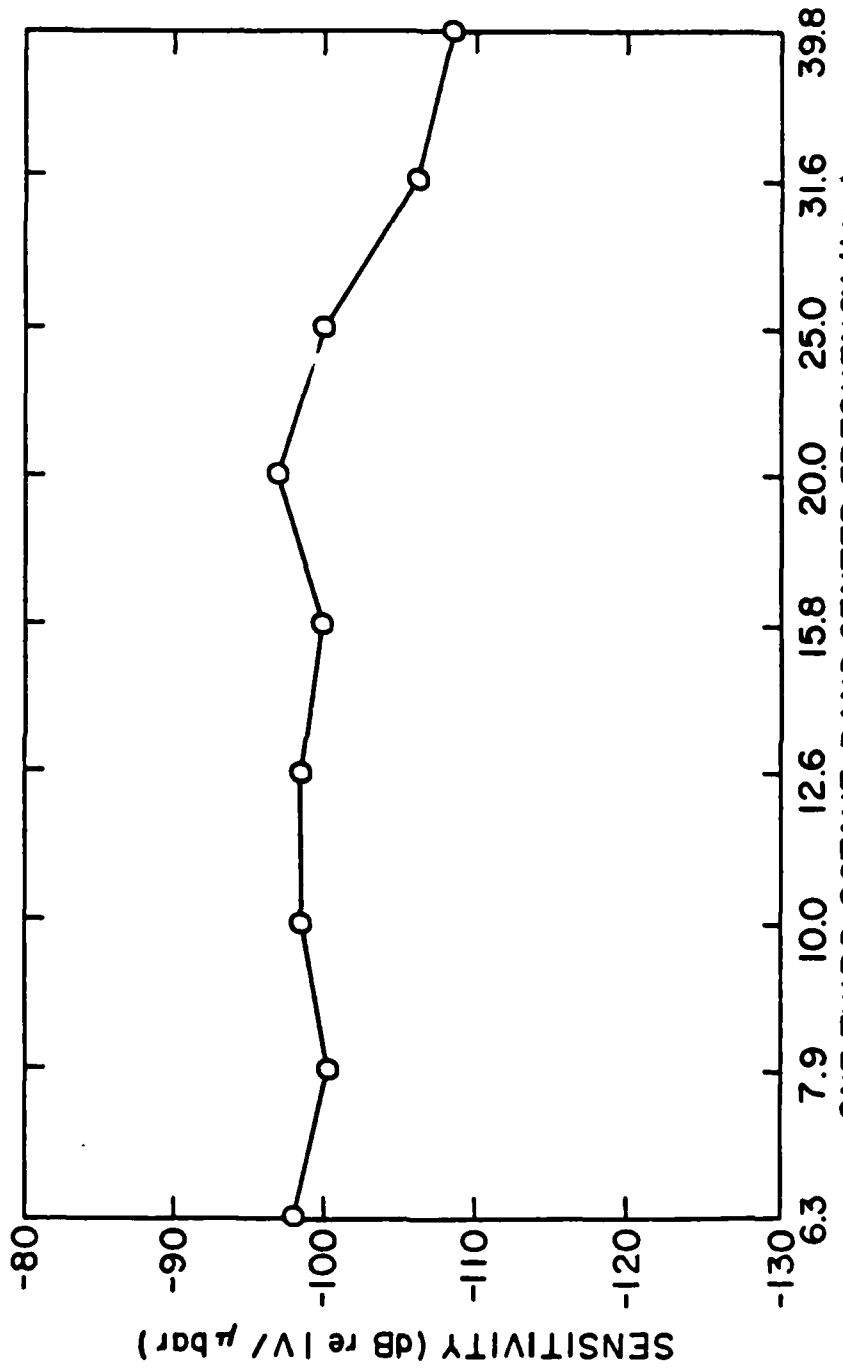

Figure 27. Typical One-Third-Octave Sensitivity for Directional Hydrophone Mounted in Water-Filled Tank Attached to One Side of the 122 cm Diameter Water Tunnel as Measured in Presence of Test Model

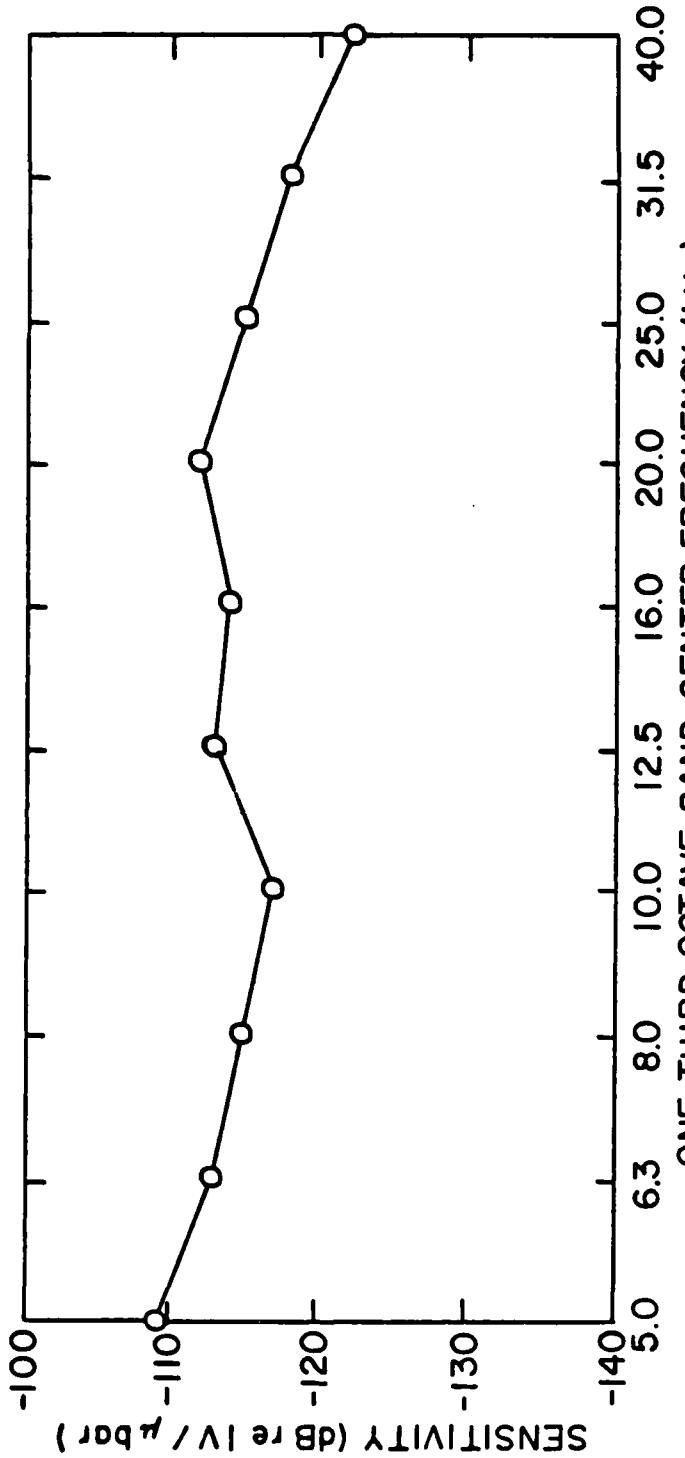

Figure 28. Typical One-Third-Octave Sensitivity for Directional Hydrophone Mounted in a Water-Filled Tank Attached to One Side of the 122 cm Diameter Water Tunnel Measured in Presence of Test Model

In the initial stages of the test program, motion pictures of individual bubbles injected into moving water were taken through the plexiglass windows of the test section. Enlargement of individual frames documented that the size of the bubbles produced was approximately in the range predicted by Park [19]. However, during the actual test sequence, the gas injected through multiple orifices produced many bubbles, making it difficult to isolate individual bubble sizes. Therefore, no meaningful pictures of these bubbles are presented.

CHAPTER V

RESULTS

Preliminary Investigation

In the initial investigation, only Nozzle Plates No. 1 (r_s = 0.025 cm) and No. 2 (r_s = 0.063 cm), along with a single tunnel velocity of 9.1 m/sec, were used. A background one-third-octave sound-pressure level (SPL) was obtained by measuring the noise generated when water flowed past the test body at 9.1 m/sec with no gas discharging through the nozzle plate. These results are plotted in Figures 29 through 32. Unless otherwise noted, all gas flow rates are for each orifice, rather than for the total gas flow rates actually measured. The curves are labeled by the magnitude of the difference between gas and liquid velocities, i.e., $\Delta = |v_g - v_\ell|$. The gas velocity v_g is the ratio of the gas flow rate to the orifice area. The liquid velocity v_ℓ is the tunnel velocity.

With a tunnel speed of 9.1 m/sec and Nozzle Plate No. 2 (r_s = 0.063 cm) covering the exhaust pipe at the rear of the test body, the radiated noise was measured for gas flow rates of 15 cm^3/sec and 37 cm^3/sec. The dot-dash curve in Figure 29 is the one-third-octave SPL when $\dot{Q}$ = 15 cm^3/sec , and the solid curve is for $\dot{Q}$ = 37 cm^3/sec . Weber numbers and the ratio $W/F^{2/3}$ for these flows are given in Table II. Approximate gas velocities at the orifice for $\dot{Q}$ = 15 cm^3/sec and $\dot{Q}$ = 37 cm^3/sec are 12.2 m/sec and 30 m/sec, respectively. The measured SPL's in Figure 29 are what one would expect on the basis of the report by Mühle and Heckl [18]; viz, radiated noise is primarily a

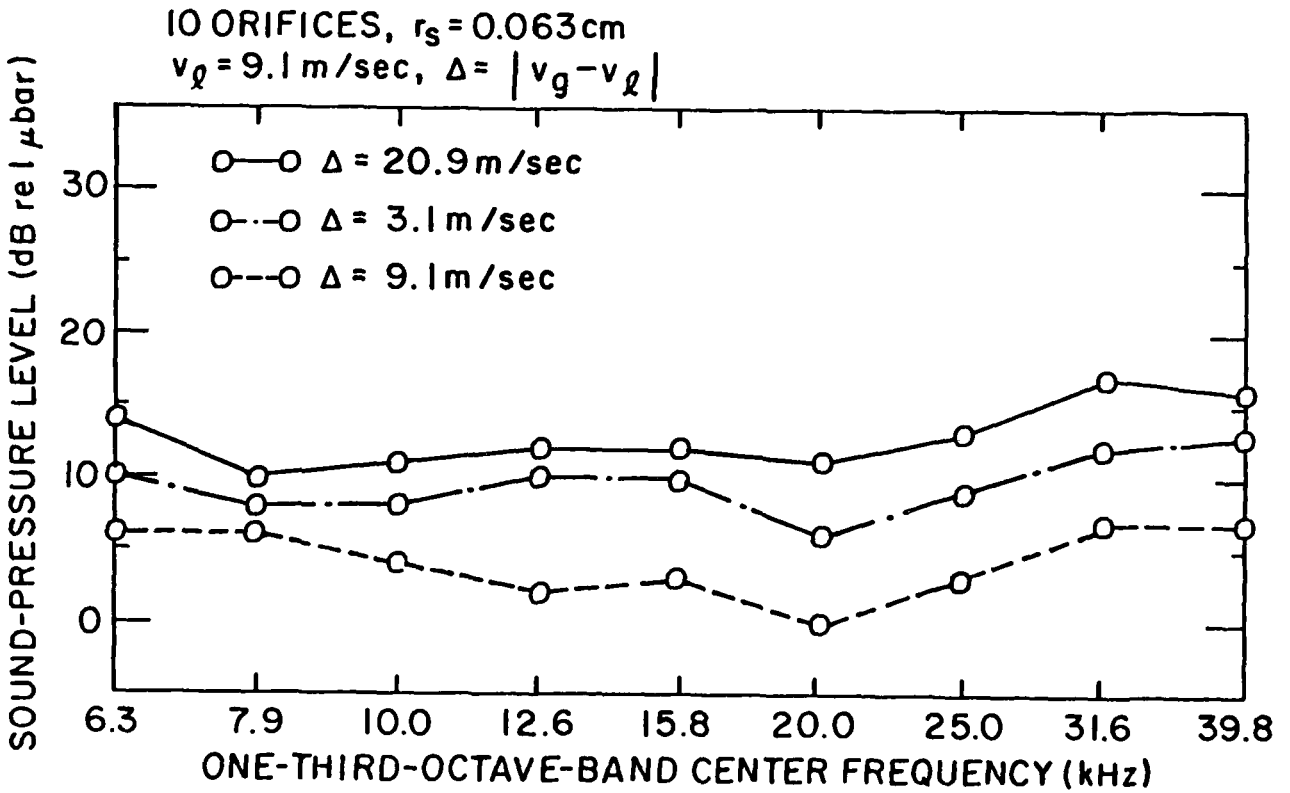

Figure 29. Sound-Pressure Levels in One-Third-Octave Frequency Bands for Gas Flow Through Nozzle Plate No. 2

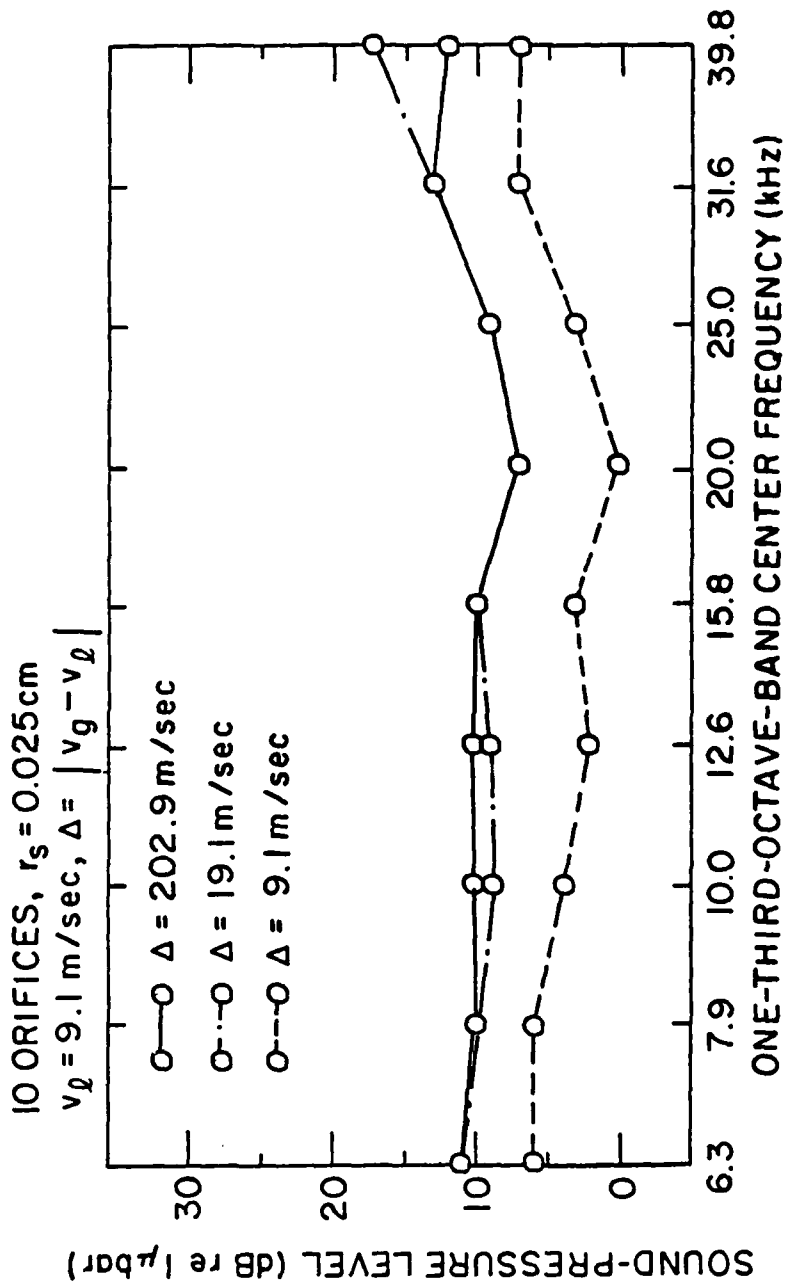

Figure 30. Sound-Pressure Levels in One-Third-Octave Frequency Bands for Gas Flow Through Nozzle Plate No. 1

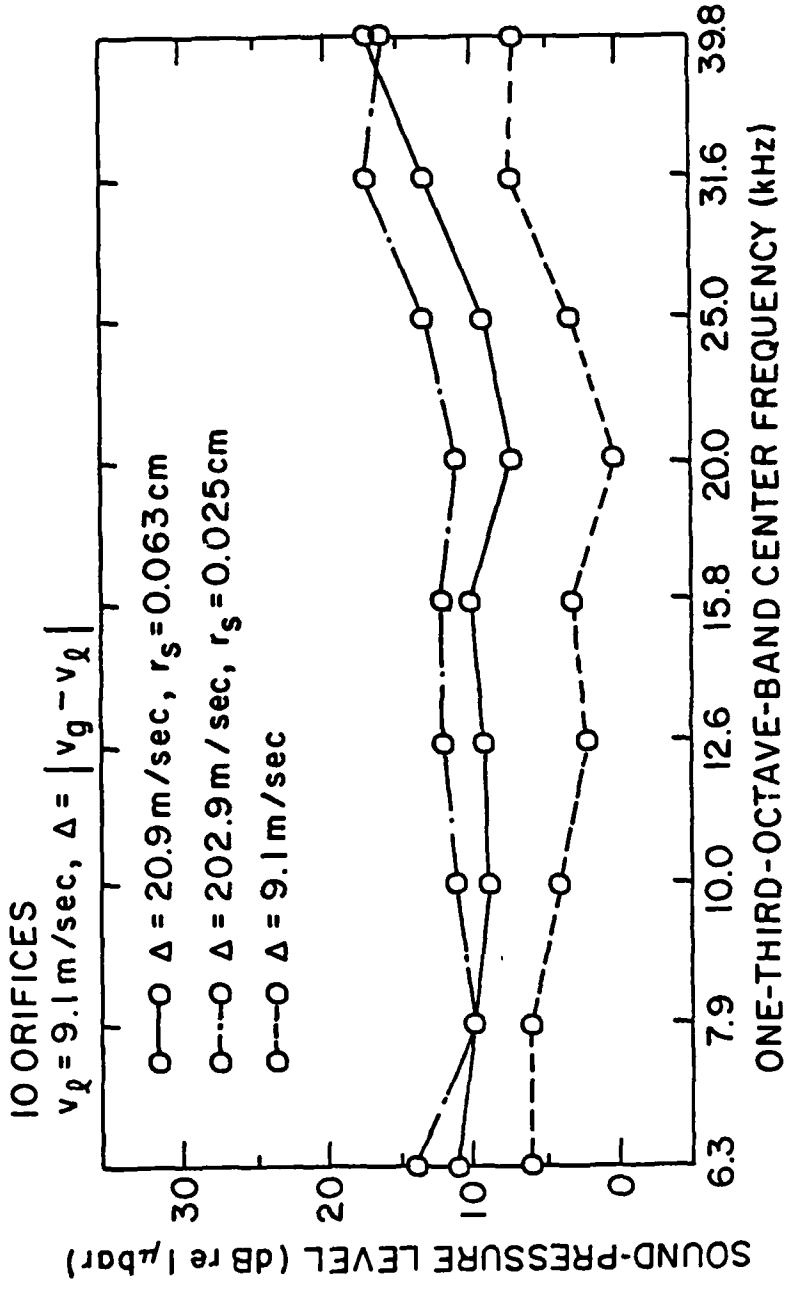

Figure 31. Sound-Pressure Levels in One-Third-Octave Frequency Bands for Gas Flow Through Nozzle Plates No. 1 and No. 2

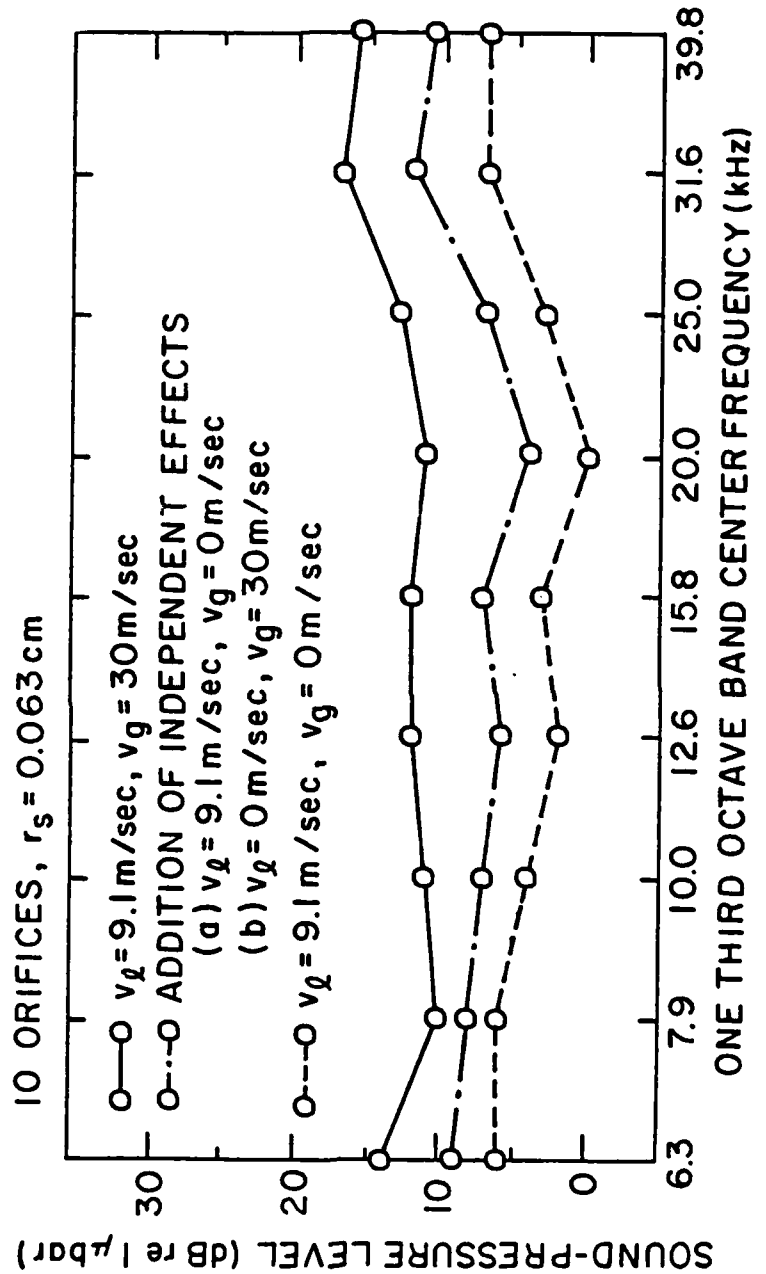

Figure 32. Sound-Pressure Levels in One-Third-Octave Frequency Bands for Gas Flow Through Nozzle Plate No. 2

TABLE II

WEBER NUMBER AND RATIO OF WEBER
TO FROUDE NUMBER FOR GAS FLOW RATES
USED IN PRELIMINARY SERIES OF EXPERIMENTS

$\dot{Q}$ (cm^3/sec	15.7		37		41.7	
Nozzle Plate	1	2	1	2	1	2
W	21	0.12	138	4.4	171	6.2
$W/F^{2/3}$	1.5	0.10	5.4	1.08	6.3	1.3

function of gas flow rates, and the orifice size does not influence the process significantly.

The results shown in Figure 30 are for gas flow rates of 15.7 cm^3/sec and 41.7 cm^3/sec through Nozzle Plate No. 1, where the orifices each have a radius of 0.025 cm. With these gas flow rates, the approximate gas speeds at the orifice are 73 m/sec and 183 m/sec, respectively. For this nozzle plate, a significant increase in gas flow rate does not lead to an increased radiated noise level. Both gas flow rates generate essentially the same radiated noise levels over the entire frequency range used in these measurements. On the basis of these results, we are led to the conclusion that gas flow rate alone does not appear to be the primary noise-generating mechanism.

Results of the one-third-octave measurements of the radiated noise generated by a gas flow rate of 41.7 cm^3/sec discharging through Nozzle Plate No. 1 (r_s = 0.025 cm), and 37 cm^3/sec discharging through Nozzle Plate No. 2 (r_s = 0.063 cm) are given in Figure 31. It is

interesting to note that a significantly higher sound-pressure level is obtained when the lower gas flow rate is exhausted through the nozzle plate made up of larger diameter orifices. Note also that, for the gas flow rates of 37 cm^3/sec and 41.7 cm^3/sec, the gas velocities at the nozzles are 29 m/sec and 212 m/sec, respectively. Since the much higher gas velocity through Nozzle Plate No. 1 is associated with the lower radiated noise level, there does not seem to be a positive correlation between increased gas velocities and increased radiated noise levels. All other parameters being equal, these results appear to indicate that the orifice radius, rather than the gas flow rate, is the dominant parameter in the generation of radiated noise when gas discharges into a turbulent wake.

To isolate whatever influence turbulence has on the generation of noise, the water flow in the tunnel was shut down and gas discharged at a flow rate of 37 cm^3/sec through Nozzle Plate No. 2 (r_s = 0.063 cm) into quiescent water. The radiated noise generated under these conditions includes noise caused by (a) gas flow in the pipe, (b) gas streaming through the orifices, and (c) bubble formation, coalescence, and collapse. By adding these results to those obtained with water flowing past the body without any gas discharging, one has the total noise radiated by gas jets discharging into a turbulent wake, minus any noise caused by interactions between the wake and the jets. This result is given by the dot-dash curve in Figure 32. In the same figure, the solid curve is the measured SPL for the same nozzle plate with water flowing past the body and the gas jets interacting with the turbulent wake. The 6 - 7 dB average difference between these two curves

represents radiated noise caused by the interaction of discharging gas and the turbulent wake.

Volume pulsations of the bubbles due to the turbulence excitation at their resonance frequencies are not a major noise source in the present investigation. A detailed discussion of this noise mechanism is given in the Appendix.

The fluctuating turbulence velocity is estimated as 10% of the mean flow speed and a typical turbulence length scale in the wake, just downstream of the model, is the diameter of the nozzle plate [28]. Exact values of these scales are not crucial to the following analysis, since somewhat larger or smaller scales do not significantly alter the discussion. From Equation (3.15) and Figure 15, the critical bubble radius for the tunnel flow used in these preliminary studies is on the order of 0.065 cm. For the gas and water flow rates used in this investigation, the results obtained by Park [19] indicate that typical bubble radii lie in the range

$$2.0 \leq r_B/r_s \leq 3.75 \quad . \tag{5.1}$$

Typical bubble radii for bubbles exiting from the orifices in Nozzle Plates No. 1 (r_s = 0.025 cm) and No. 2 (r_s = 0.063 cm) are shown in Table III. For Nozzle Plate No. 1 (r_s = 0.025 cm), the critical bubble radius of 0.065 cm lies in the same range as the bubbles produced. Therefore, some of the bubbles formed will tend to break up and split quickly, while others will persist for much longer times. For Nozzle Plate No. 2 (r_s = 0.063 cm), the critical bubble radius is significantly less than the smallest typical bubble radius produced, and all bubbles will have a strong tendency to quickly break up, split or collapse.

Radiated noise generated by these strong sources is generally broad band and similar to cavitation noise [27]. The similar behavior exhibited by the SPL in Figures 29 through 32 strongly suggests that bubble break-up and collapse in the turbulent wake is the dominant mechanism of noise generation by gas jets in the flow ranges used in these preliminary experiments.

TABLE III

TYPICAL RADII FOR BUBBLES GENERATED
BY THE FLOW RATES USED IN THE
PRELIMINARY INVESTIGATION

Orifice Radius (cm)	Typical Bubble Radius (cm)
0.025	$0.050 < r_B < 0.091$
0.063	$0.125 < r_B < 0.235$

More Extensive Investigation

To test the conclusions arrived at in the preliminary phase of our investigation, radiated noise had to be measured under a greater variety of gas and water flow rates. The additional nozzle plates used in these latter investigations have the following orifice radii: No. 3 (r_s = 0.191 cm), No. 4 (r_s = 0.032 cm), No. 5 (r_s = 0.191 cm), No. 6 (r_s = 0.127 cm), and No. 7 (r_s = 0.063 cm). The total area of the orifices in Nozzle Plates No. 5, 6, and 7 was designed to be equal in each nozzle. For a constant gas flow rate, the exit velocity of the gas will, therefore, be the same for each nozzle plate, even though each

has different orifices. This was done to eliminate gas velocity as an uncontrolled parameter in these nozzle plates. In the same way, Nozzle Plates No. 3 and 4 have equal orifice areas which are less than those for Nozzle Plates No. 5, 6, and 7. For any given gas flow rate, therefore, the gas velocity through Nozzle Plates No. 3 and 4 will be higher than the velocity through Nozzle Plates No. 5, 6, and 7.

With Nozzle Plate No. 4 (r_s = 0.032 cm) fastened to the aft end of the test body, gas flow rates of 189 cm^3/sec and 472 cm^3/sec were used and the radiated noise was measured for tunnel water velocities of 3.0 m/sec, 6.1 m/sec, and 9.1 m/sec. These results are plotted in Figures 33 and 34. Weber number and the ratio $W/F^{2/3}$ for these flow rates are listed in Tables IVa and IVb. Approximate gas velocities at the orifice for $\dot{Q}_T$ = 189 cm^3/sec and $\dot{Q}_T$ = 472 cm^3/sec are 16.5 m/sec and 41.5 m/sec, respectively. Figures 33 and 34 are plots of one-third-octave SPL for a single gas flow rate with various tunnel velocities v_ℓ. In Figure 33, the measured SPL's indicate that radiated noise varies as Δ. The upper curve (□) represents a high turbulent velocity, u ~ 0.91 m/sec, the middle curve (Δ) represents an intermediate turbulent velocity, u ~ 0.61 m/sec, the lower curve (o) represents a low turbulent velocity, u ~ 0.30 m/sec, and the bottom curve (—) represents the SPL when gas discharges into quiescent water, u ~ 0 m/sec. In Figure 34, the comparison is the same except for an increase in the gas velocity to 41.5 m/sec. From these curves, it appears that a decrease in the turbulent fluctuating velocity brings a corresponding decrease in the measured overall SPL. The change in SPL brought about by a decreasing turbulence intensity appears to be larger when the gas

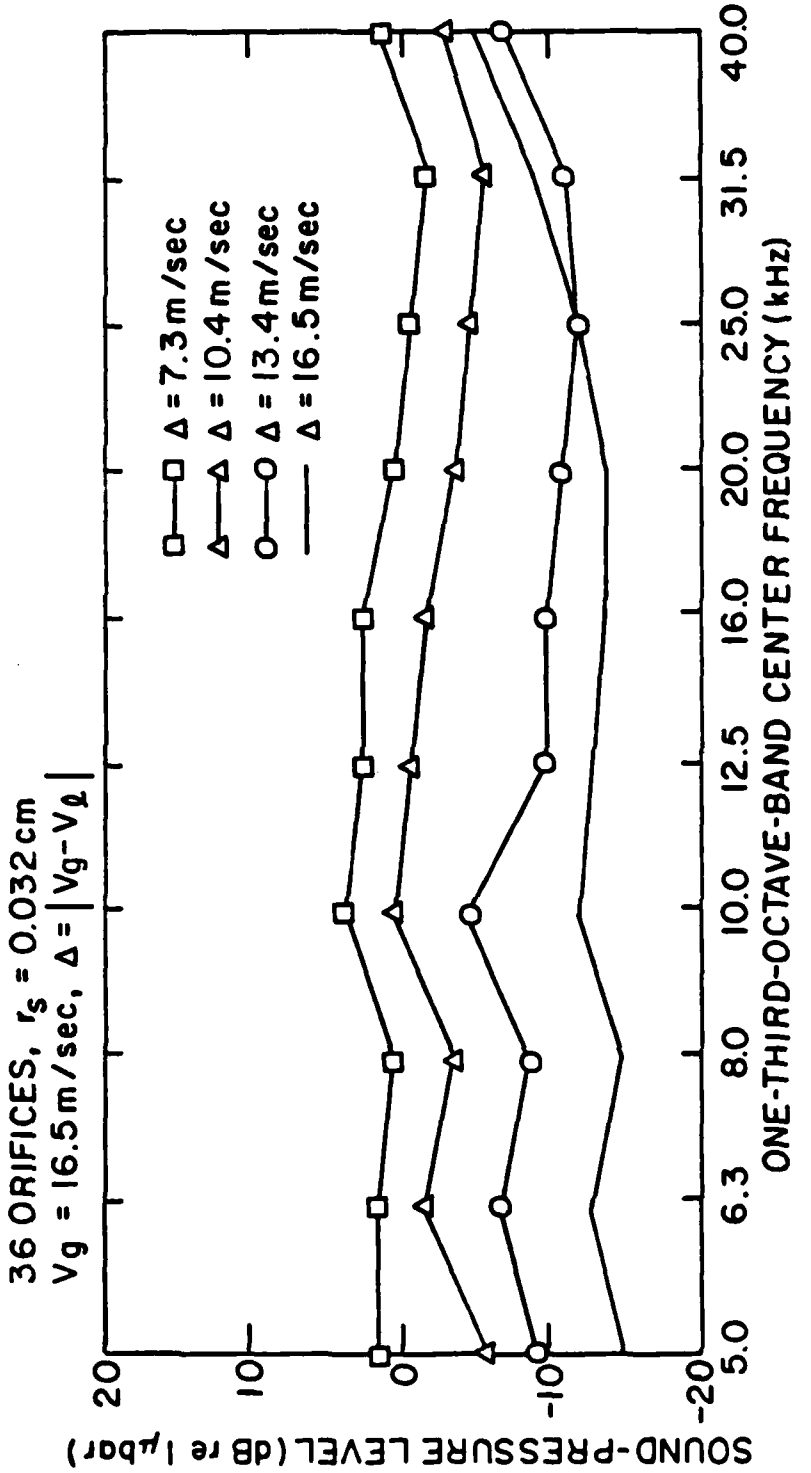

Figure 33. Sound-Pressure Levels in One-Third-Octave Frequency Bands for Gas Flow Through Nozzle Plate No. 4

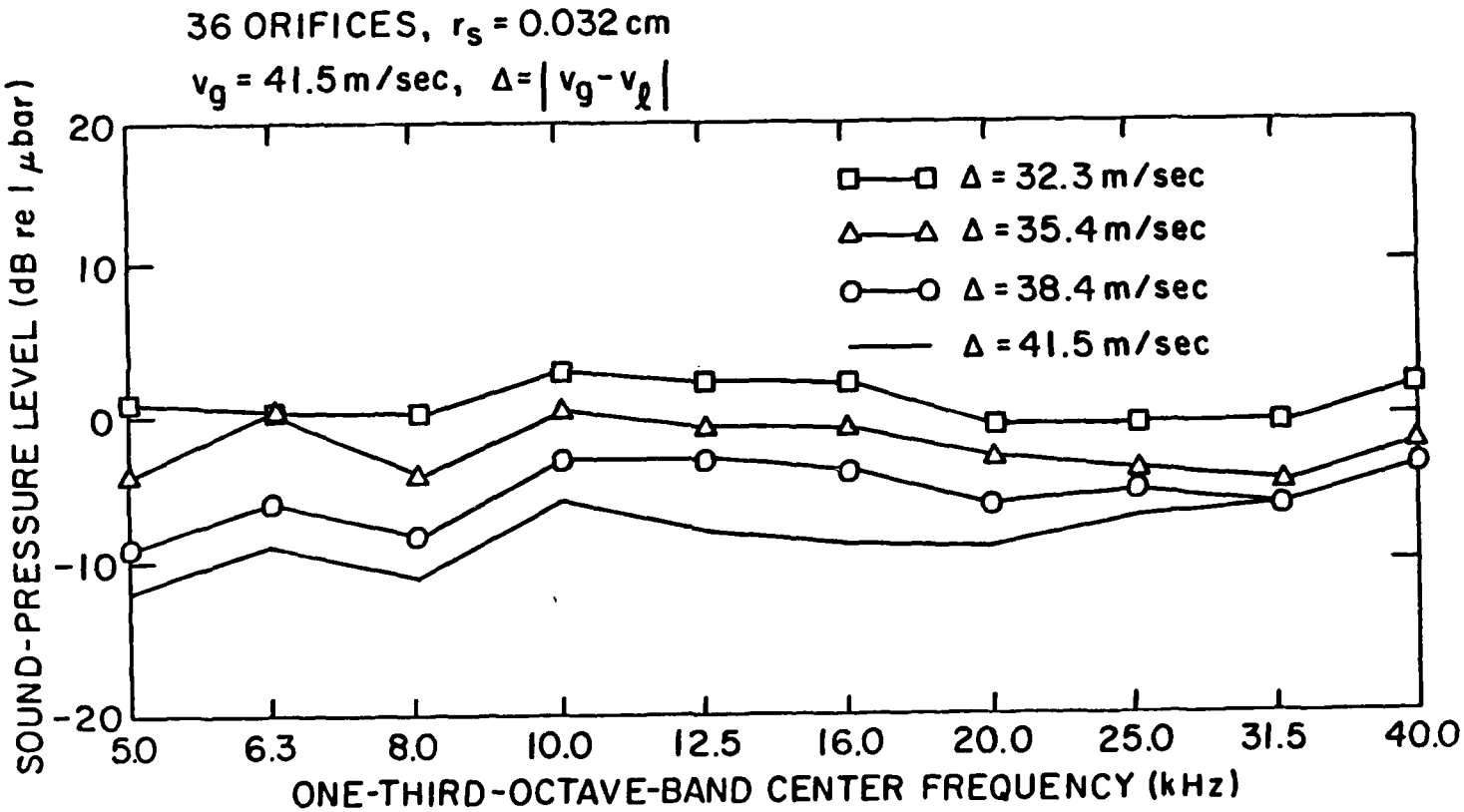

Figure 34. Sound-Pressure Levels in One-Third-Octave Frequency Bands for Gas Flow Through Nozzle Plate No. 4

TABLE IVa

WEBER NUMBER AND RATIO OF WEBER TO FROUDE NUMBER FOR NOZZLE PLATE NO. 3

$\dot{Q}_T$ (cm^3/sec)	189			472		
Turbulence Velocity (m/sec)	0.91	0.62	0.30	0.91	0.61	0.30
W	1.71	3.43	5.74	33.29	39.87	47.04
$W/F^{2/3}$	1.12	1.79	2.52	8.13	9.17	10.24

TABLE IVb

WEBER NUMBER AND RATIO OF WEBER TO FROUDE NUMBER FOR NOZZLE PLATE NO. 4

$\dot{Q}_T$ (cm^3/sec)	189			472		
Turbulence Velocity (m/sec)	0.91	0.61	0.30	0.91	0.61	0.30
W	0.28	0.57	0.96	5.55	6.65	7.84
$W/F^{2/3}$	0.10	0.16	0.23	0.75	0.84	0.94

TABLE IVc

WEBER NUMBER AND RATIO OF WEBER TO FROUDE NUMBER FOR NOZZLE PLATE NO. 5

$\dot{Q}_T$ (cm^3/sec)	189			2501		
Turbulence Velocity (m/sec)	0.91	0.61	0.30	0.91	0.61	0.30
W	0.76	0.11	0.05	66.67	75.85	85.63
$W/F^{2/3}$	0.65	0.18	0.10	12.92	14.08	15.27

TABLE IVd

WEBER NUMBER AND RATIO OF WEBER TO FROUDE NUMBER FOR NOZZLE PLATE NO. 6

$\dot{Q}_T$ (cm^3/sec)	189			2737		
Turbulence Velocity (m/sec)	0.91	0.61	0.30	0.91	0.61	0.30
W	0.51	0.07	0.03	55.09	61.89	69.08
$W/F^{2/3}$	0.38	0.10	0.06	8.68	9.38	10.10

TABLE IVe

WEBER NUMBER AND RATIO OF WEBER TO FROUDE NUMBER FOR NOZZLE PLATE NO. 7

$\dot{Q}_T$ (cm^3/sec)	189			2737		
Turbulence Velocity (m/sec)	0.91	0.61	0.30	0.91	0.61	0.30
W	0.25	0.04	0.02	27.55	30.94	34.54
$W/F^{2/3}$	0.15	0.04	0.02	3.45	3.72	4.01

velocity is smallest (Figure 33), with less change in SPL as the gas velocity is increased (Figure 34).

This interpretation is possible if the size of the exiting bubbles is considered in relation to the critical bubble size. Typical bubble radii for gas bubbles exiting from Nozzle Plate No. 4 (r_s = 0.032 cm) are shown in Table V. From Equation (3.15) and Figure 15, the critical bubble radii for various turbulence velocity scales are calculated and shown in Table VI.

For the higher turbulence velocity scale, the critical bubble radius of 0.065 cm is less than the radius of a typical bubble, which indicates that most of the bubbles formed break up quickly and produce noise. For the intermediate turbulence velocity, the critical bubble radius of 0.100 cm lies within the range of the typical bubble radius, so the bubbles break up less quickly as in the previous case. This is evidenced by a 3 - 4 dB decrease in the SPL as shown in Figure 33, and a 3 dB decrease in the SPL as shown in Figure 34. In the case of the lower turbulence velocity, the critical bubble radius of 0.220 cm is larger than the largest typical bubble radii formed, and consequently, the bubbles have little tendency to break up. In Figure 33, this is depicted by a 10 - 12 dB decrease in the SPL from high turbulence intensity to low turbulence intensity. Compare this with the results in Figure 34, where the decrease in SPL is 6 - 8 dB.

It is interesting to note that the reduction in SPL by decreasing the velocity as shown in Figures 33 and 34 are not equivalent. The typical bubble sizes for the higher gas velocities all tend to be larger than those of the lower gas velocities and thus are more closely allied to the critical bubble radii. Also, when the flow rate is

TABLE V

TYPICAL RADII FOR GAS BUBBLES
EXITING FROM NOZZLE PLATE NO. 4

Turbulence Velocity Scale (m/sec)	Gas Velocity (m/sec)	Typical Bubble Radius (cm)
0.91	16.5	$0.064 < r_B < 0.095$
0.61	16.5	$0.064 < r_B < 0.095$
0.30	16.5	$0.064 < r_B < 0.095$
0.91	41.5	$0.064 < r_B < 0.119$
0.61	41.5	$0.064 < r_B < 0.119$
0.30	41.5	$0.064 < r_B < 0.119$

TABLE VI

CRITICAL BUBBLE RADII FOR
THREE TURBULENCE VELOCITY SCALES

Turbulence Velocity Scale (m/sec)	Critical Bubble Radius (cm)
0.91	0.065
0.61	0.100
0.30	0.220

increased, the gas jet diameter as calculated from Equation (3.3) increases. For a gas flow rate of 472 cm^3/sec through Nozzle Plate No. 4 (r_s = 0.032 cm), the gas jets tend to no longer behave as individual jets, but merge with adjacent jets and become a noise source. Therefore, the SPL will not decrease as much as when the gas jets themselves do not interact. The gas jet diameters for all orifice sizes and flow rates are calculated from Equation (3.3) and listed in Table VII.

The results of injecting gas through Nozzles Plates No. 5, 6, 7, and 3 with varying tunnel velocities are shown in Figures 35 through 42. Typical bubble radii for gas bubbles exiting from Nozzle Plates No. 5, 6, 7, and 3 are shown in Tables VII, IX, X, and XI, respectively.

For gas flow through Nozzle Plate No. 5 (r_s = 0.191 cm), Figures 35 and 36 show a decrease in the SPL as the turbulence velocity is reduced. The reduction is less pronounced for the higher gas velocity. This is what is expected when comparing the critical bubble radii from Table VI with the typical bubble radii from Table VIII. As turbulence intensity is decreased, the difference δ between a typical bubble radius and the critical bubble radius is decreased. Values of δ for Nozzle Plate No. 5 are shown in Table XII. Larger values of δ, the difference between the size of the bubbles formed and the maximum allowable size, seem to indicate more violent bubble break-up and, correspondingly, more noise. For the higher gas velocity, δ decreases as turbulence intensity decreases, but not by as great an amount as in the case of the lower gas velocity. This would seem to indicate a lowering of the SPL as turbulence decreases, but the values of SPL for

TABLE VIIa

GAS JET DIAMETER FOR NOZZLE PLATE NO. 4

$\dot{Q}_T$ (cm^3/sec)	189			472		
Tunnel Velocity (m/sec)	9.15	6.10	3.05	9.15	6.10	3.05
Jet Diameter (cm)	0.08	0.10	0.15	0.13	0.15	0.23

TABLE VIIb

GAS JET DIAMETER FOR NOZZLE PLATE NO. 5

$\dot{Q}_T$ (cm^3/sec)	189			2501		
Tunnel Velocity (m/sec)	9.15	6.10	3.05	9.15	6.10	3.05
Jet Diameter (cm)	0.25	0.30	0.43	0.94	1.14	1.63

TABLE VIIc

GAS JET DIAMETER FOR NOZZLE PLATE NO. 6

$\dot{Q}_T$ (cm^3/sec)	189			2737		
Tunnel Velocity (m/sec)	9.15	6.10	3.05	9.15	6.10	3.05
Jet Diameter (cm)	0.18	0.20	0.30	0.66	0.79	1.12

TABLE VIId

GAS JET DIAMETER FOR NOZZLE PLATE NO. 7

$\dot{Q}_T$ (cm^3/sec)	189			2737		
Tunnel Velocity (m/sec)	9.15	6.10	3.05	9.15	6.10	3.05
Jet Diameter (cm)	0.08	0.10	0.15	0.33	0.41	0.56

TABLE VIII

TYPICAL RADII FOR GAS BUBBLES
EXITING FROM NOZZLE PLATE NO. 5

Turbulence Velocity Scale (m/sec)	Gas Velocity (m/sec)	Typical Bubble Radii (cm)
0.91	4.3	$0.382 < r_B < 0.573$
0.61	4.3	$0.382 < r_B < 0.573$
0.30	4.3	$0.382 < r_B < 0.573$
0.91	54.9	0.893
0.61	54.9	0.918
0.30	54.9	0.945

TABLE IX

TYPICAL RADII FOR GAS BUBBLES
EXITING FROM NOZZLE PLATE NO. 6

Turbulence Velocity Scale (m/sec)	Gas Velocity (m/sec)	Typical Bubble Radii (cm)
0.91	4.3	$0.254 < r_B < 0.381$
0.61	4.3	$0.254 < r_B < 0.381$
0.30	4.3	$0.254 < r_B < 0.381$
0.91	59.1	0.522
0.61	59.1	0.536
0.30	59.1	0.522

TABLE X

TYPICAL RADII FOR GAS BUBBLES
EXITING FROM NOZZLE PLATE NO. 7

Turbulence Velocity Scale (m/sec)	Gas Velocity (m/sec)	Typical Bubble Radii (cm)
0.91	4.3	$0.127 < r_B < 0.191$
0.61	4.3	$0.127 < r_B < 0.191$
0.30	4.3	$0.127 < r_B < 0.191$
0.91	59.1	0.238
0.61	59.1	0.238
0.30	59.1	0.238

TABLE XI

TYPICAL RADII FOR GAS BUBBLES
EXITING FROM NOZZLE PLATE NO. 3

Turbulence Velocity Scale (m/sec)	Gas Velocity (m/sec)	Typical Bubble Radii (cm)
0.91	16.5	$0.381 < r_B < 0.714$
0.61	16.5	$0.381 < r_B < 0.714$
0.30	16.5	0.714
0.91	41.5	0.766
0.61	41.5	0.798
0.30	41.5	0.827

TABLE XII

DIFFERENCE BETWEEN CRITICAL BUBBLE RADII
AND TYPICAL BUBBLE RADII
EXITING FROM NOZZLE PLATE NO. 5

Turbulence Velocity Scale (m/sec)	Gas Velocity (m/sec)	Difference (δ) (cm)
0.91	4.3	$0.317 < \delta < 0.508$
0.61	4.3	$0.282 < \delta < 0.473$
0.30	4.3	$0.162 < \delta < 0.353$
0.91	54.9	0.828
0.61	54.9	0.818
0.30	54.9	0.725

higher gas velocities would be more closely allied as turbulence decreases, as shown in Figures 35 and 36.

It is expected that this trend is followed when analyzing gas flow through Nozzle Plates No. 6, 7, and 3. Results similar to those described above were obtained for these nozzle plates and are shown in Figures 37 through 42.

For the range of gas velocities mentioned thus far, the mechanism for the generation of noise appears to be related to the critical bubble radius. All things being equal, lower turbulence velocities provide larger critical bubble radii. Any one size bubble will not break up as readily at these lower velocities and will, accordingly, generate less noise.

When gas velocities increase significantly, as noted in the previous figures, there is less of a pronounced drop in the SPL as the turbulence velocity decreases. Higher gas velocities emerging from an orifice as a jet tend to be noisy in themselves. It is interesting to examine the effects of increasing gas velocity and so determine its role in the generation of noise. These results are shown in Figures 43 through 47, which are plots of the relative SPL versus tunnel velocity for various nozzle plates. The SPL in these curves were obtained by running the tape-recorded noise measurements through a 5 - 50 kHz band-pass filter and into a Thermo System RMS meter. It is interesting to note in Figures 43 through 47 the decrease in the relative SPL as the tunnel velocity is decreased. As the gas velocity is increased, the decrease in the relative SPL is less pronounced as the tunnel velocity decreases. These results are a composite of the previous discussion on the effect turbulence velocity has on the SPL. In

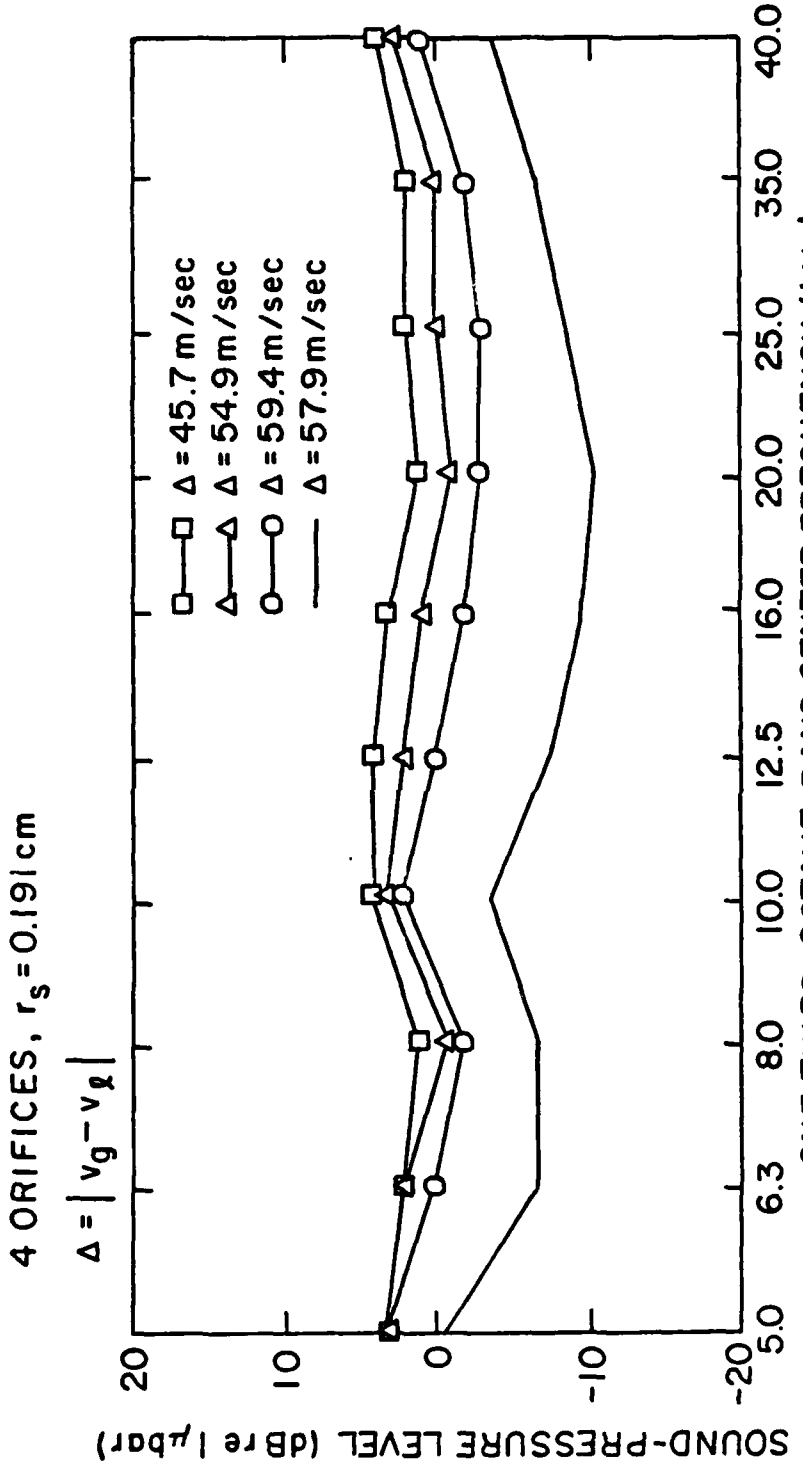

Figure 35. Sound-Pressure Levels in One-Third-Octave Frequency Bands for Gas Flow Through Nozzle Plate No. 5

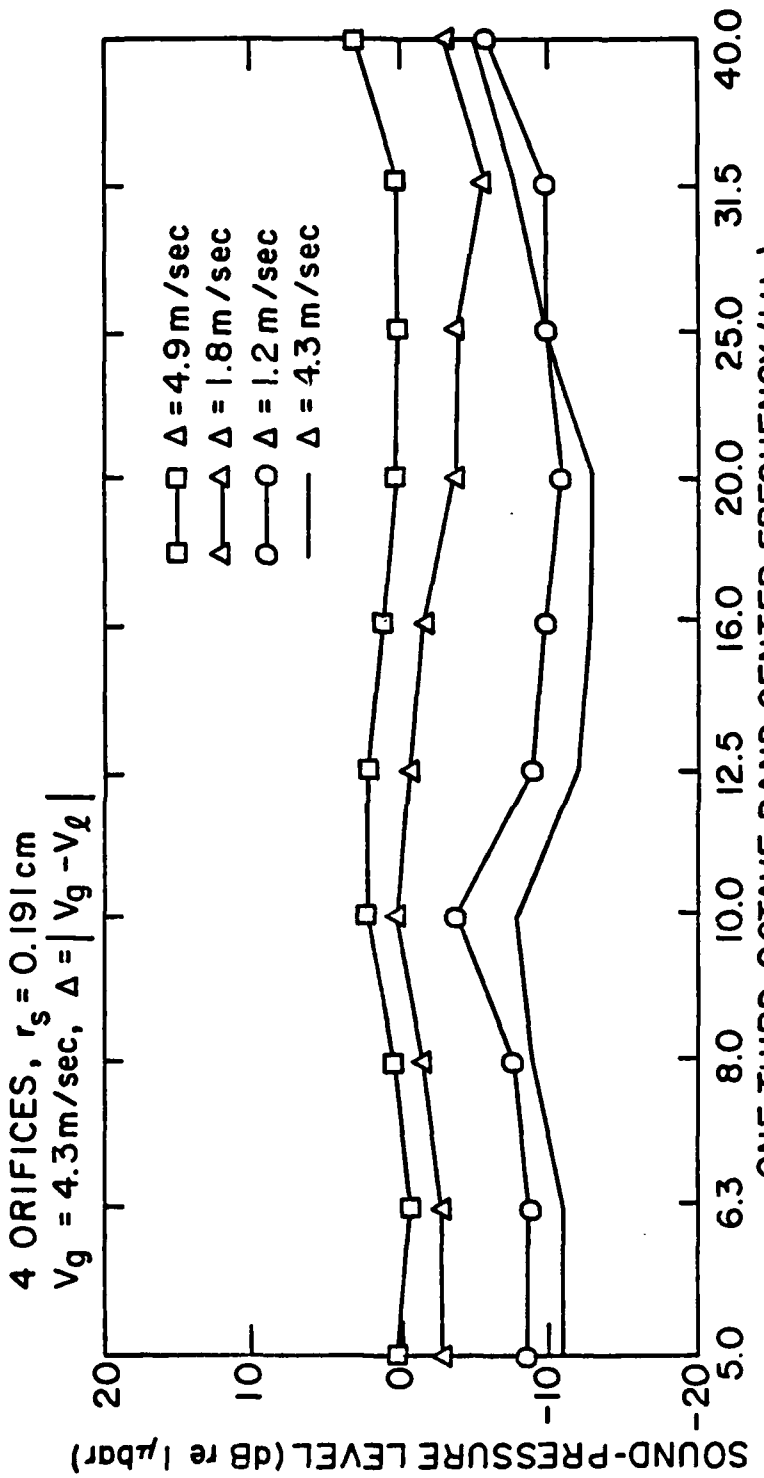

Figure 36. Sound-Pressure Levels in One-Third-Octave Frequency Bands for Gas Flow Through Nozzle Plate No. 5

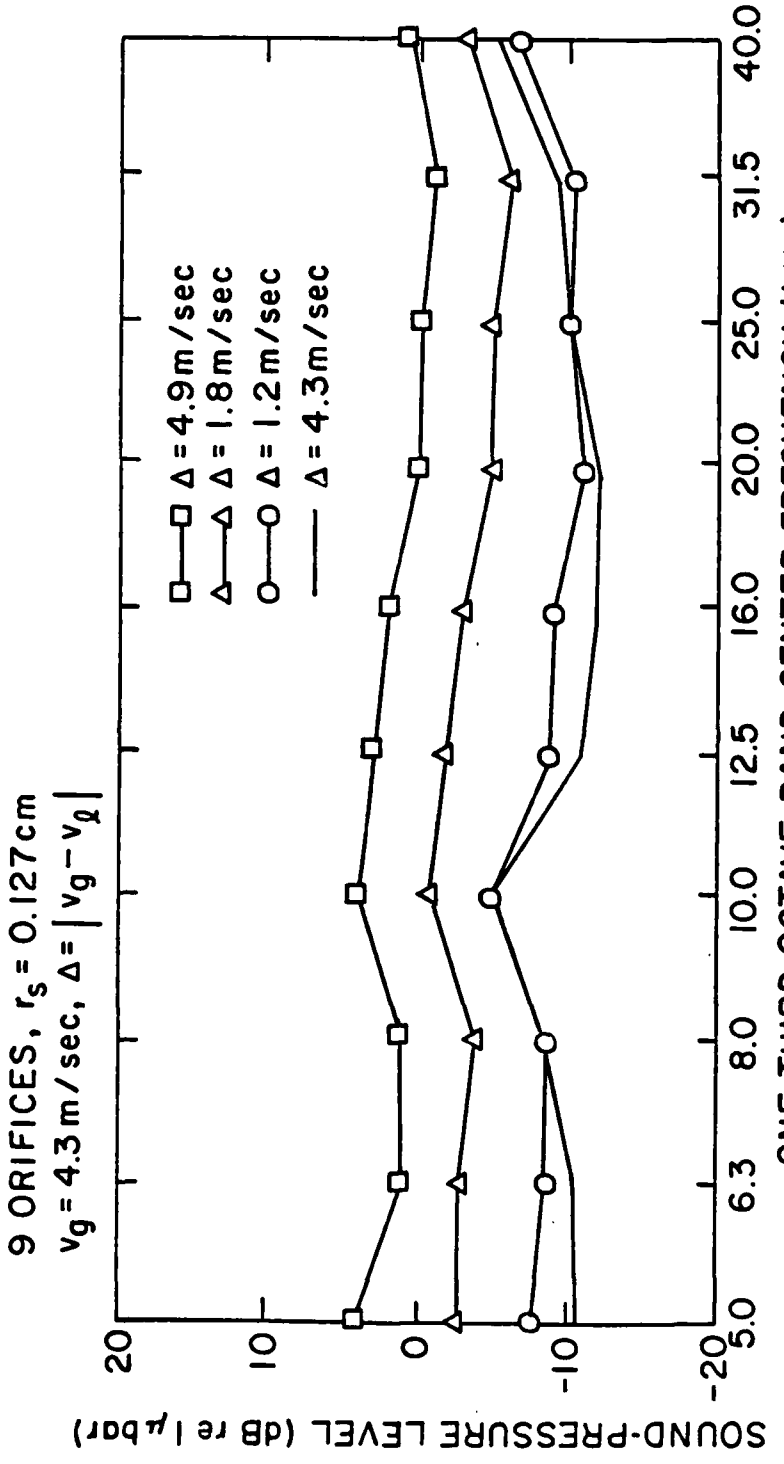

Figure 37. Sound-Pressure Levels in One-Third-Octave Frequency Bands for Gas Flow Through Nozzle Plate No. 6

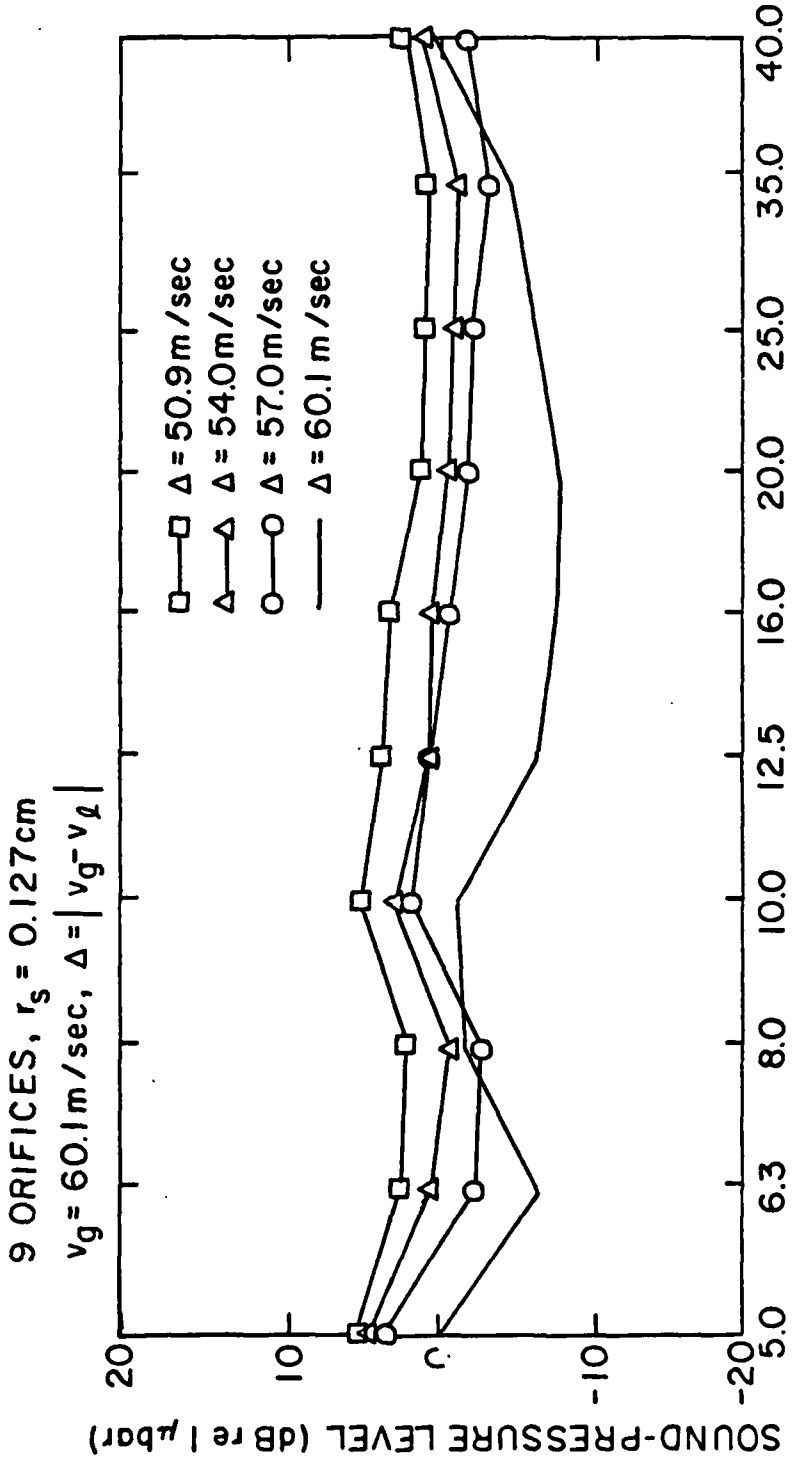

Figure 38. Sound-Pressure Levels in One-Third-Octave Frequency Bands for Gas Flow Through Nozzle Plate No. 6

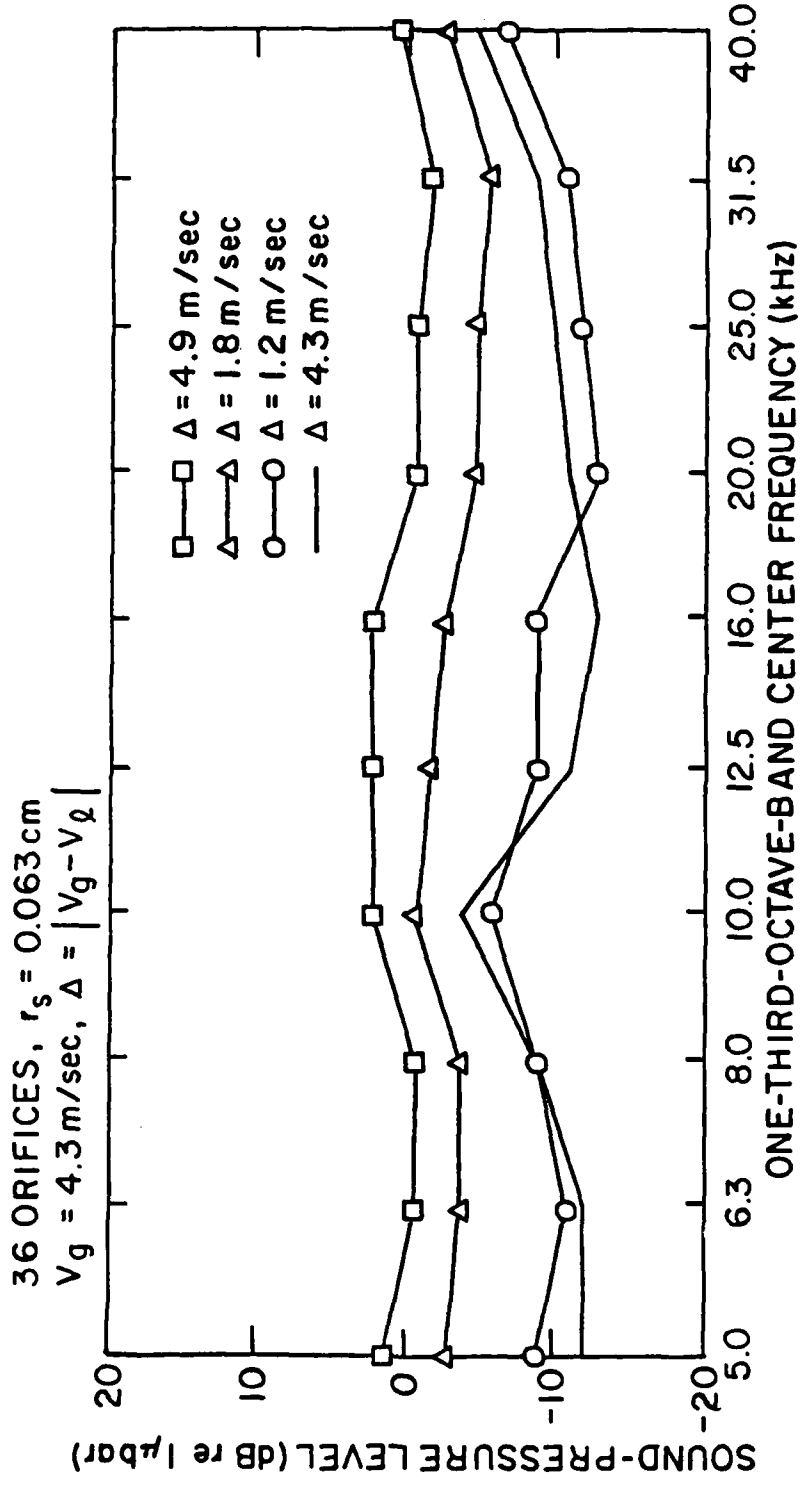

Figure 39. Sound-Pressure Levels in One-Third-Octave Frequency Bands for Gas Flow Through Nozzle Plate No. 7

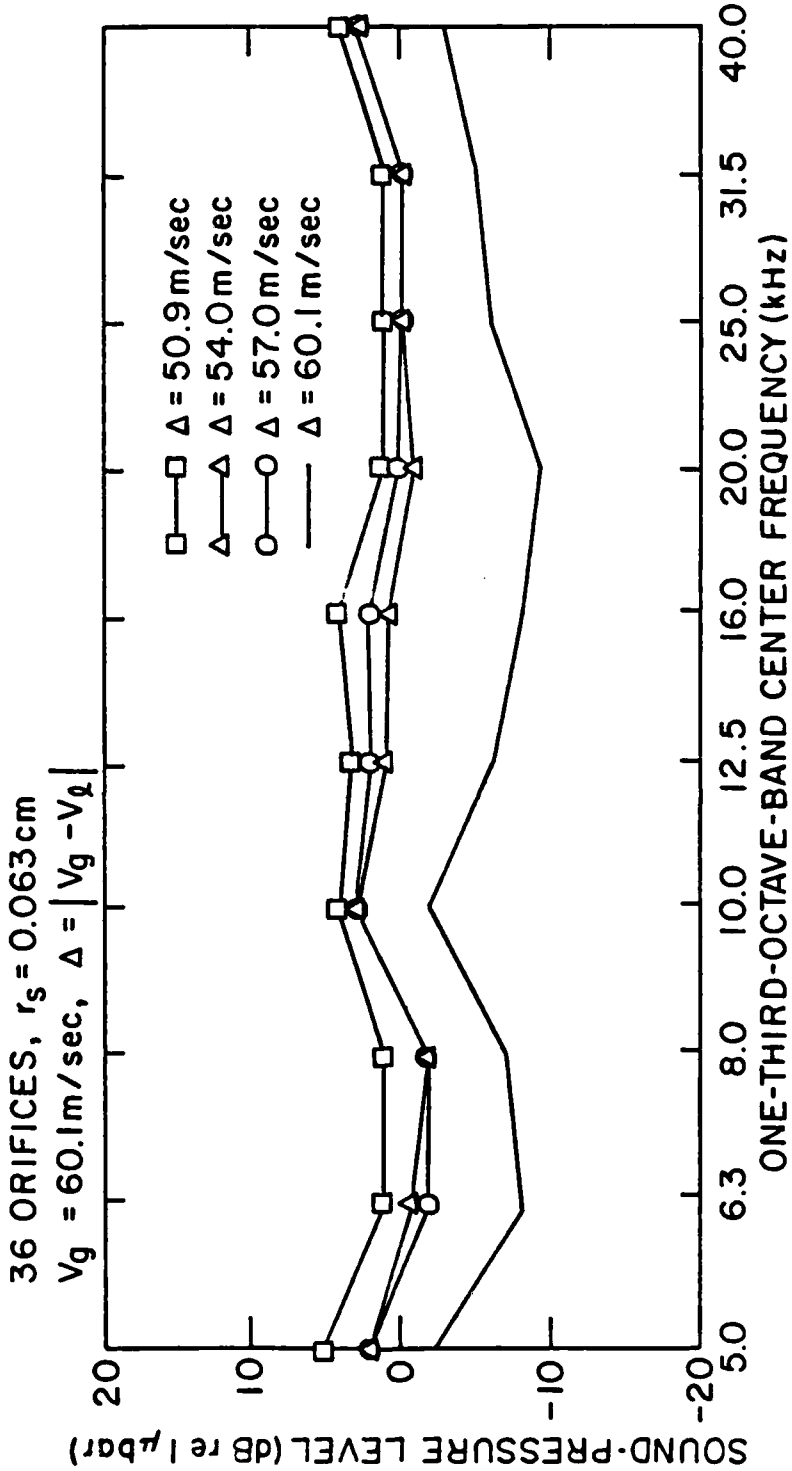

Figure 40. Sound-Pressure Levels for One-Third-Octave Frequency Bands for Gas Flow Through Nozzle Plate No. 7

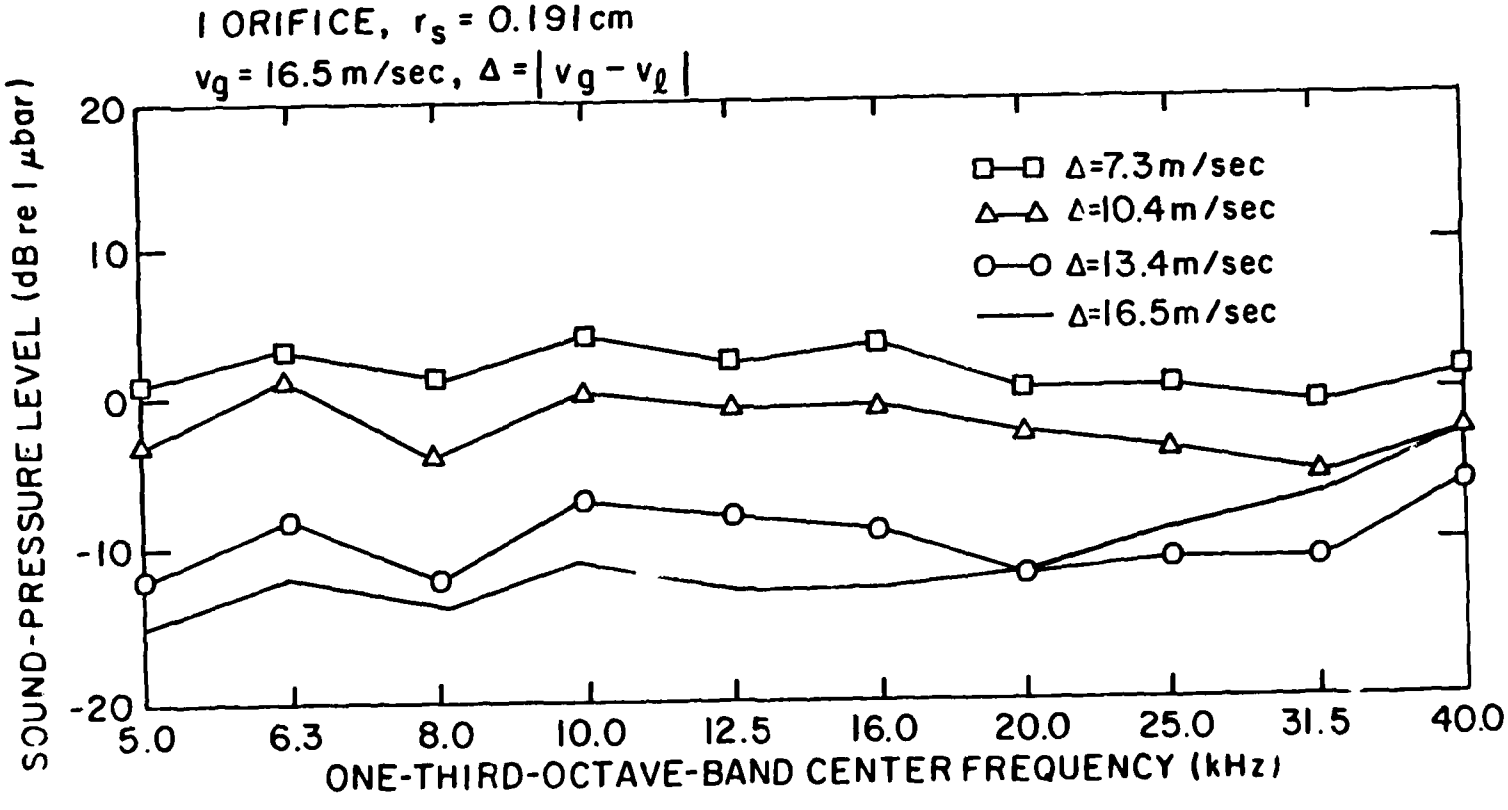

Figure 41. Sound-Pressure Levels in One-Third-Octave Frequency Bands for Gas Flow Through Nozzle Plate No. 3

AD-A106 223 PENNSYLVANIA STATE UNIV UNIVERSITY PARK APPLIED RESE--ETC F/G 20/1
NOISE GENERATION BY GAS JETS IN A TURBULENT WAKE.(U)
APR 81 J J GAVIGAN N00024-79-C-6043
UNCLASSIFIED ARL/PSU/TM-81-99 NL

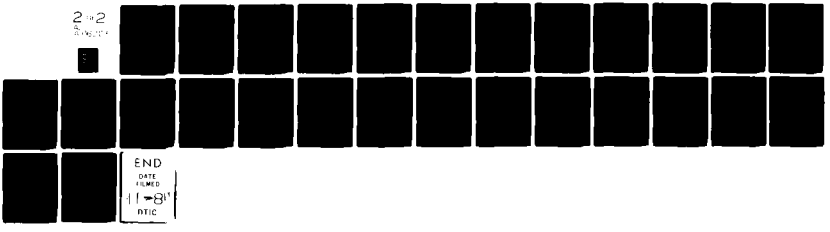

END
DATE FILMED
11-81
DTIC

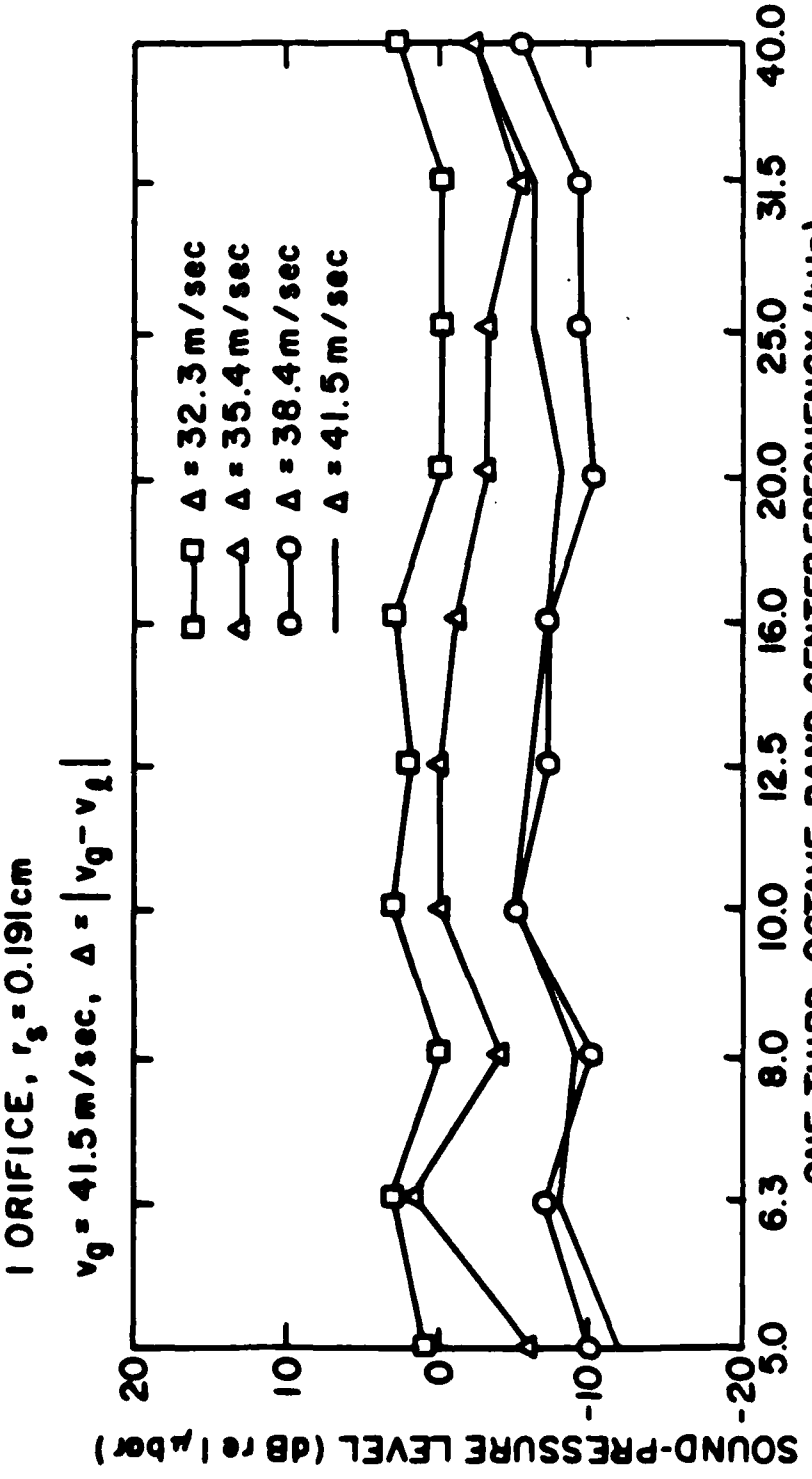

Figure 42. Sound-Pressure Levels in One-Third-Octave Frequency Bands for Gas Flow Through Nozzle Plate No. 3

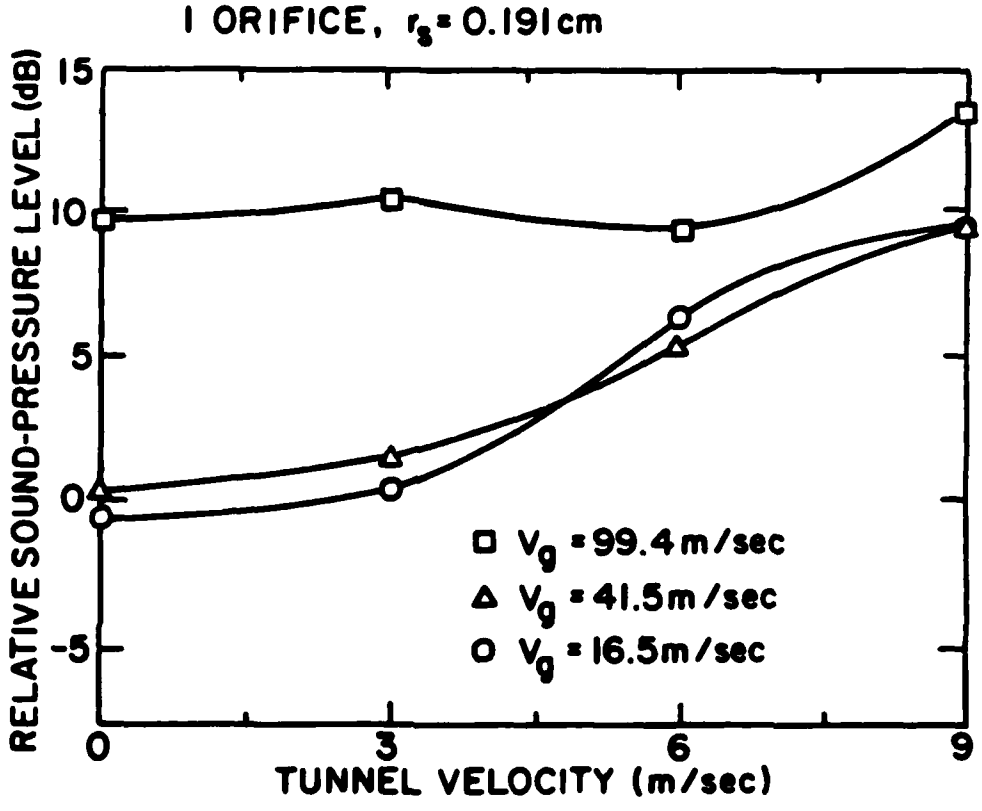

Figure 43. Relative Sound-Pressure Levels as a Function of Tunnel Velocity for Gas Flow Through Nozzle Plate No. 3

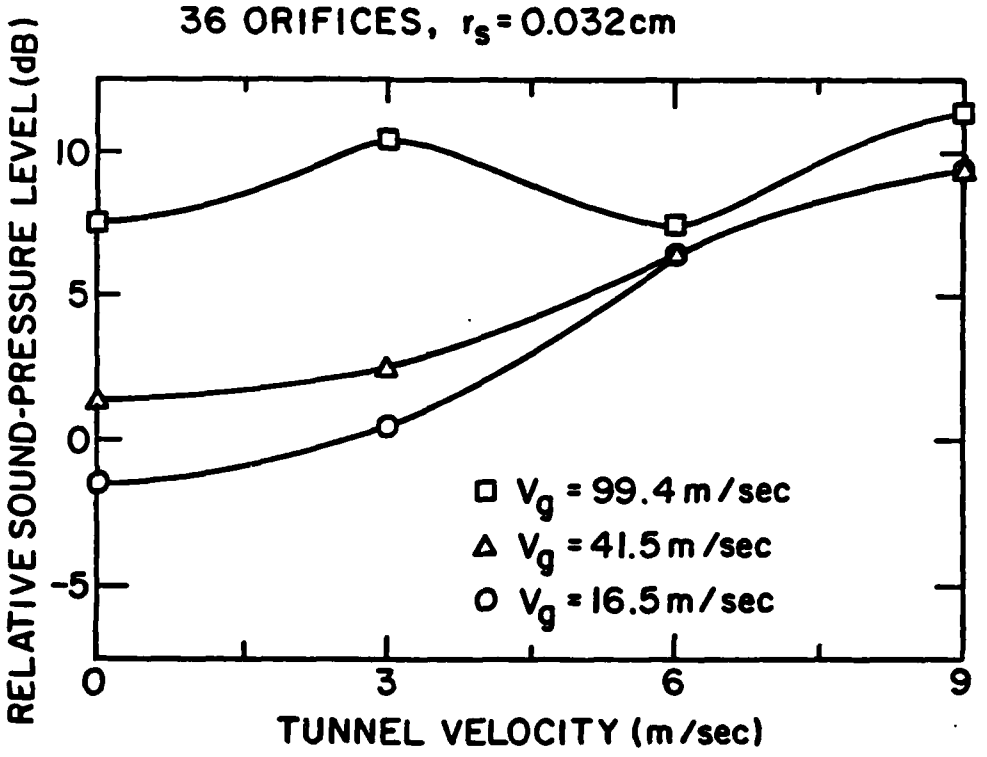

Figure 44. Relative Sound-Pressure Levels as a Function of Tunnel Velocity for Gas Flow Through Nozzle Plate No. 4

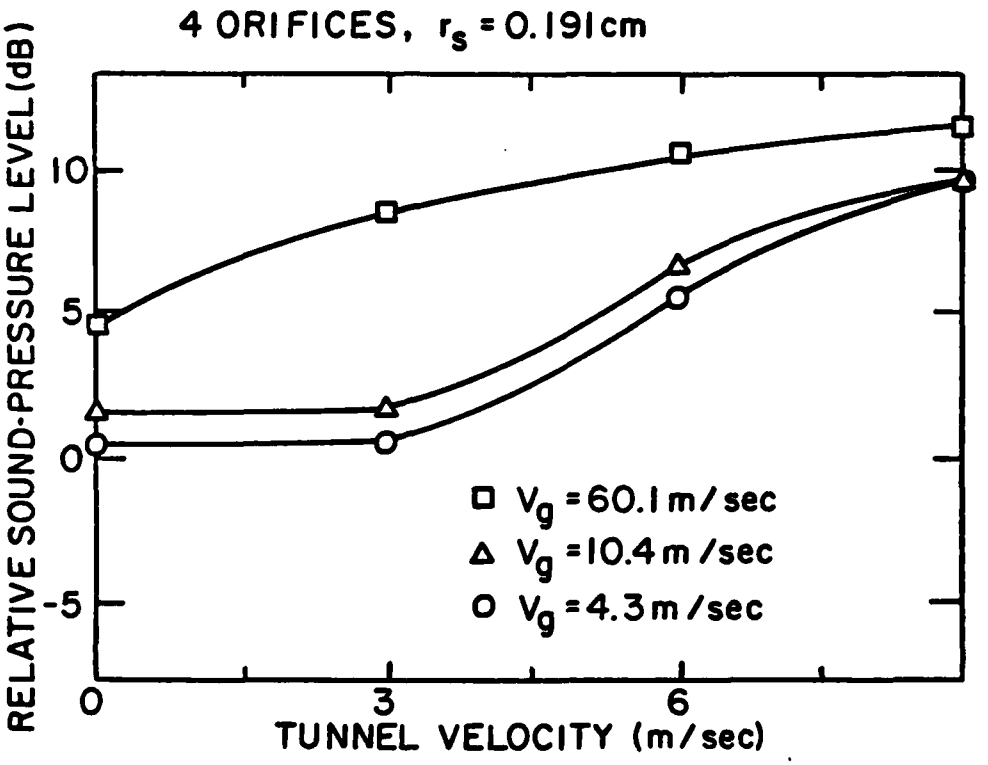

Figure 45. Relative Sound-Pressure Levels as a Function of Tunnel Velocity for Gas Flow Through Nozzle Plate No. 5

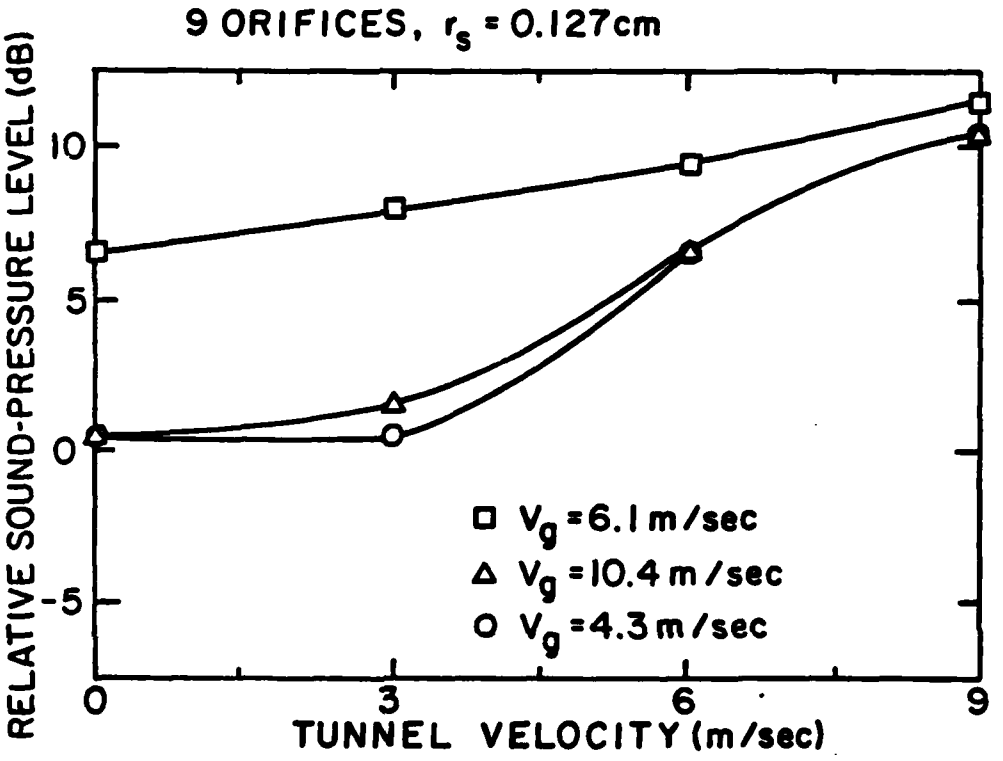

Figure 46. Relative Sound-Pressure Levels as a Function of Tunnel Velocity for Gas Flow Through Nozzle Plate No. 6

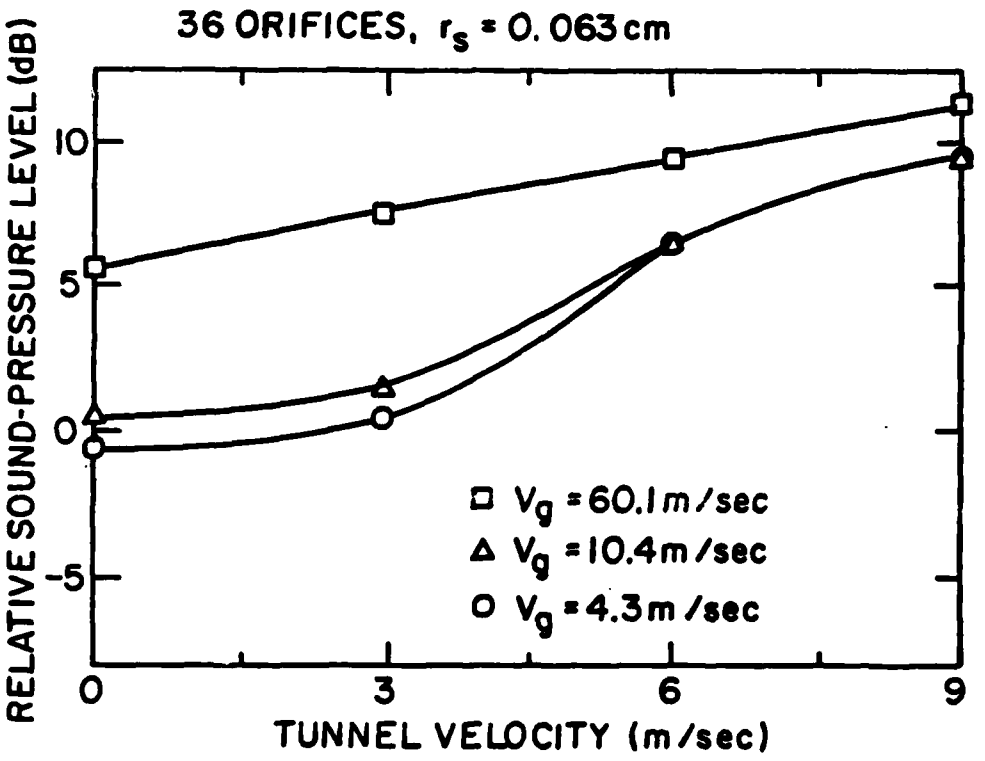

Figure 47. Relative Sound-Pressure Levels as a Function of Tunnel Velocity for Gas Flow Through Nozzle Plate No. 7

Figures 43 and 44, note that, for gas velocities of 16.5 m/sec and 41.5 m/sec, the measured SPL decreases as tunnel velocity decreases, as one would expect on the basis of the previous discussion. However, when the gas velocity is increased to 99.4 m/sec, the SPL is not reduced at the lowest turbulence velocity. Instead, after the SPL is decreased when the turbulence velocity is reduced from 0.91 to 0.61 m/sec, the noise level is increased as the turbulence velocity is further reduced. A possible explanation is that the high gas velocity streaming through the orifices contributes considerably to the amount of noise generated. When gas is discharged into quiescent water with an extremely high velocity, noise is generated by a combination of the bubble formation, coalescence, and break-up, and the gas streaming through the orifice (jet noise). When a low turbulence intensity is introduced (0.3 m/sec), a slight increase in SPL is obtained because of increased bubble break-up due to turbulence. As the turbulence intensity is increased to an intermediate level (0.61 m/sec), the jet noise effect does not appear to be relatively as great a factor. With an increasing tunnel velocity, the jet noise appears to be propagated downstream and is not picked up by the side-mounted hydrophone. When the turbulence intensity is highest (0.91 m/sec), the jet noise contributes very little to the measured noise, while bubble break-up due to turbulence is, relatively, a much larger factor.

It is useful to isolate whatever influence a varying turbulence velocity has on noise generation. As in the preliminary investigation, water flow in the tunnel was shut down and gas discharged at high and low flow rates. The radiated noise generated under these conditions includes noise generated by (a) gas flow in the pipe, (b) gas streaming

through the orifices, (c) bubble formation, coalescence, and collapse, and (d) multiple jets. By adding these results to those obtained with water flowing past the body without gas discharging, the total noise radiated by gas jets discharging into a turbulent wake is given, minus any noise caused by interactions between the wake and jets. In the figures presented in the following discussions, this result will be given by the middle curve (Δ). The upper curve (□) in these same figures represents measured SPL for the same nozzle plate with water flowing past the body and gas jets interacting with the turbulent wake. In each case, the difference between the upper and middle curves represents the radiated noise generated by bubble-turbulence interactions.

The results of discharging gas through Nozzle Plate No. 5 (r_s = 0.191 cm) at the rate of 189 cm^3/sec for tunnel velocities of 9.15 m/sec and 3.05 m/sec are shown in Figures 48 and 49, respectively. The approximate gas velocity is 4.3 m/sec. In Figure 48, a 10 - 12 dB average difference exists between the upper (□) and middle (Δ) curves, whereas in Figure 49, a 2 - 4 dB difference is obtained. As mentioned previously, the difference between the upper (□) and middle (Δ) curves represents radiated noise generated by bubble-turbulence interaction. The turbulence velocity for a tunnel speed of 9.15 m/sec is $u \sim 0.91$ m/sec, while the turbulence velocity for a tunnel speed of 3.05 m/sec is $u \sim 0.30$ m/sec. From Table VI, the critical bubble radius for conditions shown in Figure 48 is 0.065 cm, while the critical bubble radius for conditions in Figure 49 is 0.220 cm. From Table VIII, the typical bubble radius for both conditions lies in the range

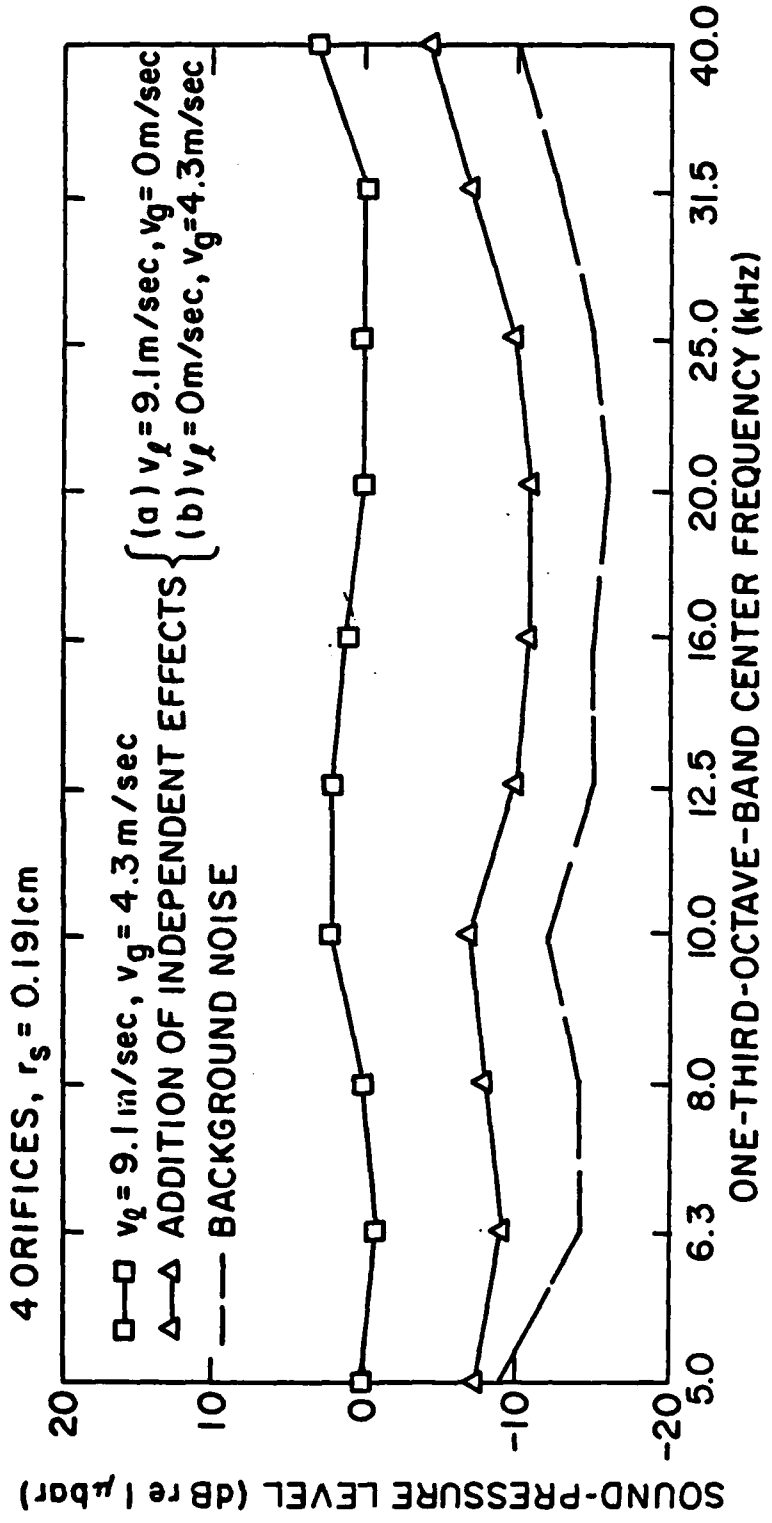

Figure 48. Sound-Pressure Levels in One-Third-Octave Frequency Bands for Gas Flow Through Nozzle Plate No. 5

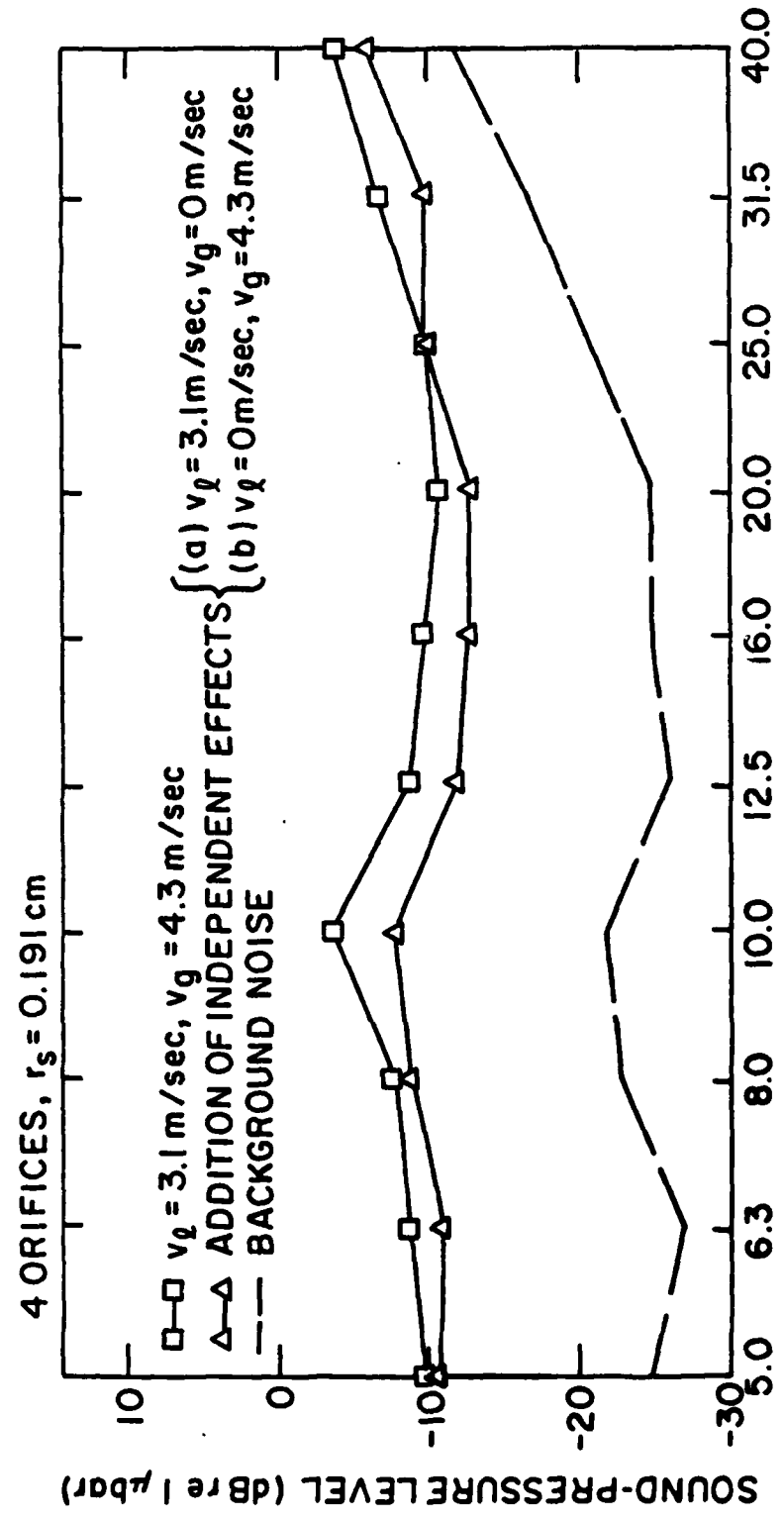

Figure 49. Sound-Pressure Levels in One-Third-Octave Frequency Bands for Gas Flow Through Nozzle Plate No. 5

$$0.382 \text{ cm} < r_B < 0.573 \text{ cm} \quad . \tag{5.2}$$

The difference δ between the critical bubble radius and a typical bubble radius for Nozzle Plate No. 5 is shown in Table XII. The larger the difference δ, the stronger the tendency for the bubble to split up, and accordingly, a greater amount of noise is generated. There is no influence due to multiple jets for this flow condition.

The gas discharge flow rate was increased to 2500 cm^3/sec and these results are shown in Figures 50 and 51 for tunnel velocities of 9.15 m/sec and 3.05 m/sec, respectively. The approximate gas velocity is 54.9 m/sec. In Figure 50, there is a 10 - 12 dB average difference between the upper and middle curves, whereas in Figure 51, this difference is only 7 dB. The general trend established in Figures 48 and 49 is also present in Figures 50 and 51, i.e., higher turbulence velocities reduce the size of the critical bubble radius, and consequently, is the dominant mechanism for sound radius. From Table VIII, for gas velocity of 54.9 m/sec and a turbulent velocity of 0.91 m/sec, the typical bubble radius is

$$r_B \approx 0.893 \text{ cm} \quad , \tag{5.3}$$

while for a turbulent velocity of 0.3 m/sec, the typical bubble radius is

$$r_B \approx 0.945 \text{ cm} \quad . \tag{5.4}$$

From Table VI, the critical bubble radius for conditions described above are 0.065 cm and 0.220 cm, respectively. From Figures 50 and 51, the turbulence effect appears to be significant in both cases. This appears to be the case since the size of the bubbles formed in

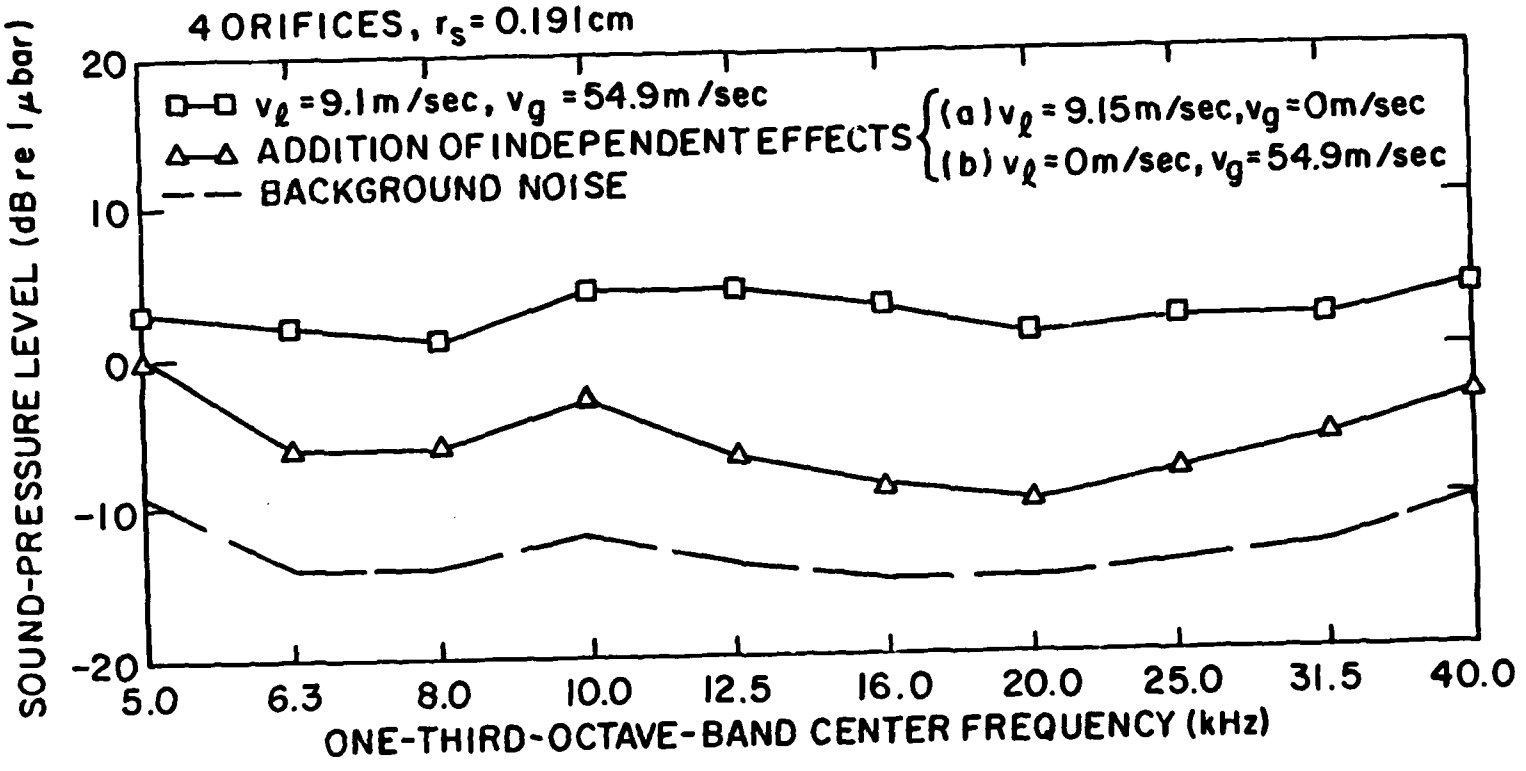

Figure 50. Sound-Pressure Levels in One-Third-Octave Frequency Bands for Gas Flow Through Nozzle Plate No. 5

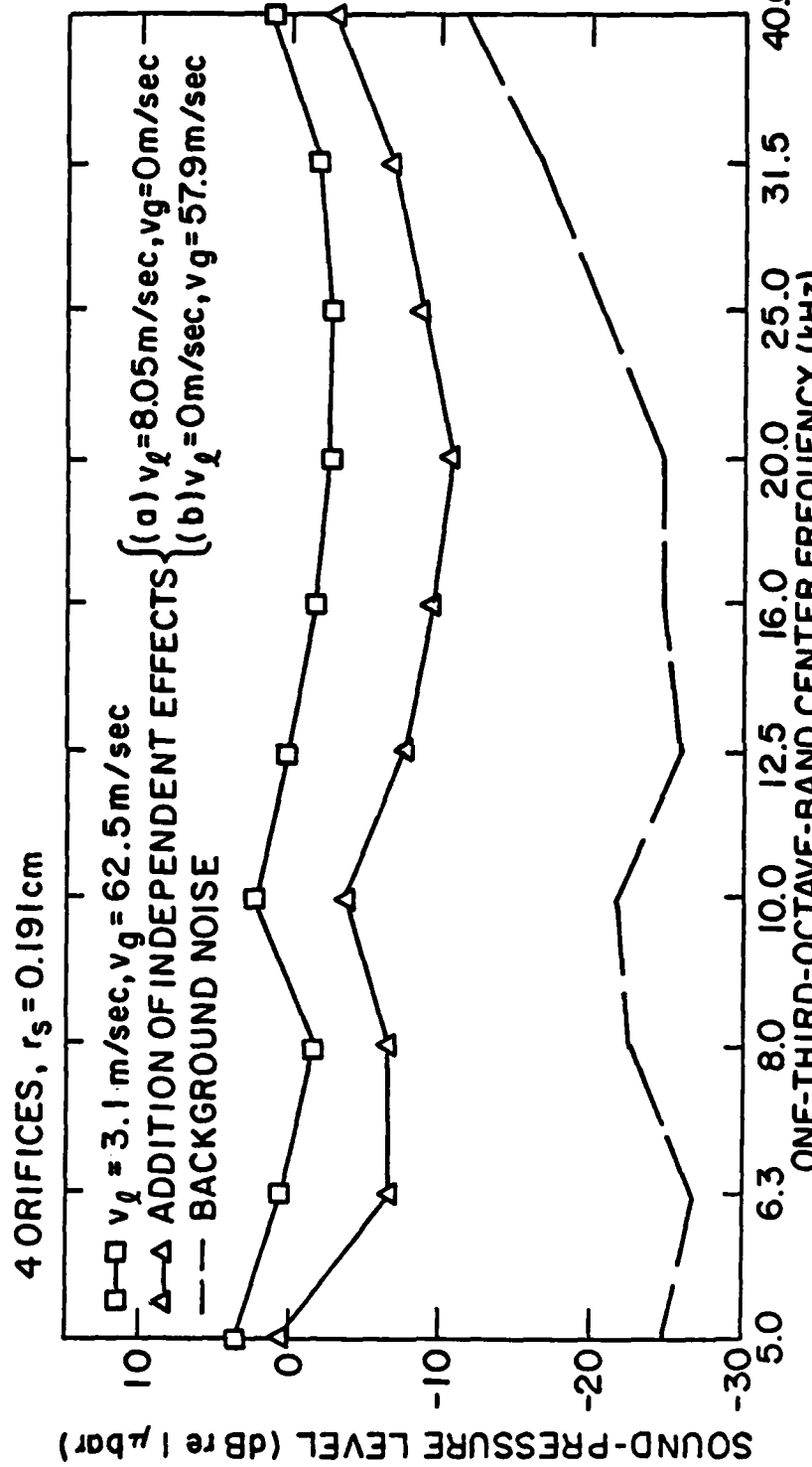

Figure 51. Sound-Pressure Levels in One-Third-Octave Frequency Bands for Gas Flow Through Nozzle Plate No. 5

both instances are considerably larger than the critical bubble size. In addition, there appears to be a slightly larger effect of turbulence displayed in Figure 50 than in Figure 51. This is due to the slightly larger difference δ (see Table XII) between the typical bubble radius and the critical bubble radius for the conditions displayed in Figure 50, as compared to those in Figure 51. Consequently, the bubble break-up will be more violent when δ is larger, and accordingly, more noise will be generated.

For completeness, there should also be an analysis of the effect of changing the gas velocity while keeping the turbulence velocity constant. For the case of a high turbulence velocity, with low and high gas velocities, observe Figures 48 and 50. The effect of increasing the gas velocity is to increase the typical size bubble. Since the critical bubble radius remains the same, our results indicate that the radiated sound will increase as the velocity increases, which it does by a 2-dB average. One might expect that the effect of turbulence would increase likewise, which is manifested in the difference between the upper ($\square$) and middle (Δ) curves. However, the average difference for both figures is 10 - 12 dB, which indicates that as velocity increases, the noise due to the increased gas streaming through the orifices increases, which, in turn, raises the level of the middle (Δ) curve.

For the case of a low turbulence velocity with both low and high gas velocities, see Figures 49 and 51. Again, the radiated noise is increased as the velocity increases, by a 6-dB average. Figure 51 shows an increase in the effect of turbulence on radiated sound as the velocity of the gas increases.

CHAPTER VI

SUMMARY AND CONCLUSIONS

In many marine applications, it is necessary to evaluate the level of noise radiated by the flow of gas through a submerged orifice into a turbulent liquid. Depending upon the magnitude of the gas flow rate, either individual bubbles are formed at the orifice, or a jet of gas is established and bubbles are formed near the tip of the jet rather than at the orifice. Sound is generated by volume fluctuations of individual bubbles as well as by those associated with the collapse of the jet and subsequent formation of bubbles. The objectives of the present work are to provide quantitative information under controlled conditions of the acoustic radiation generated by the interaction of this two-phase mixture and turbulence.

When gas is ejected through a submerged orifice into surrounding liquid, bubbles are generated at all but very high gas flow rates. Factors which determine the size of these bubbles are the gravitational, inertial, and interfacial forces. These forces can conveniently be expressed as the non-dimensional Weber and Froude numbers. For well defined ranges of these numbers, gas jets rather than bubbles are formed at the orifice and bubbles are then produced downstream near the tip of the jet. In this latter case, the ratio of bubble to orifice diameter varies from 3 to 10, depending on the respective Weber and Froude numbers.

If the ambient liquid into which gas is injected is in motion, four flow regimes can be identified. In all regimes, however, the ratio of bubble to orifice diameter varies only within very narrow limits, viz., from about 2 to 3.75. Parameters governing bubble formation and the corresponding typical bubble size are listed on pages and .

When gas discharges into a turbulent liquid, the pressure forces caused by velocity changes over distances of the order of the bubble diameter are important. These dynamic pressure forces, together with interfacial tension, constitute the dominant forces.

Noise generated by gas jets exhausting into turbulent wakes was measured under controlled conditions in the 1.22 m diameter test section of a water tunnel. These measurements were made in the frequency range 5 - 50 kHz with a directional hydrophone mounted in a water-filled tank attached to one side of the tunnel test section. Plexiglas windows in the test section provided good acoustical paths between the noise sources and hydrophone. A turbulent wake was generated by water flowing past a strut-mounted hydrodynamic body at speeds of either 9.1 m/sec, 6.1 m/sec, or 3.1 m/sec. Nitrogen gas was discharged at a number of different flow rates through various nozzle plates attached to the aft end of the wake-generating body. These flow rates are listed in Tables II and IV, and the nozzle plates in Table I.

The investigation was separated into the following two phases:

Phase I

Gas was discharged through two different nozzle plates, each having the same number of orifices. Those in Nozzle No. 1 all have radii of 0.025 cm, while those in Nozzle No. 2 have radii of 0.063 cm. This allowed equal quantities of gas to be ejected through each nozzle, but at different exit speeds. The various gas flow rates and corresponding non-dimensional parameters for these nozzle plates are listed in Table II. Typical radii of bubbles generated by gas flow through these nozzle plates, calculated from values of W and $W/F^{2/3}$, are listed in Table III. Values of W for these experiments ranged from 0.02 to 15.7. Radiated noise generated by gas discharging into the turbulent wake for a number of different experimental situations was measured in one-third-octave bands. These results are plotted in Figures 29 to 32. An analysis of these results implies that gas flow rates alone do not determine the level of generated noise. In addition, there is no positive correlation between increased gas velocity and increased radiated noise level. These observations indicate that orifice radius, rather than gas flow rate or velocity, is the determining parameter for the level of noise generated by gas discharging into a turbulent wake.

If the radii of bubbles formed at a submerged orifice exceed a value known as the critical bubble radius, they will have a strong tendency to quickly break up, split, or collapse. Because of the finite range of bubble radii that can be expected from a particular orifice, some gas flow rates can generate bubbles whose radii bracket the critical radius. In this case, that fraction of bubbles with radii

greater than the critical value will tend to break up, while the rest will tend to persist for much longer times. If the results in Figures 29 to 32 are examined with the critical bubble radius in mind, interesting conclusions can be drawn. Figure 29 shows the measured levels for gas discharging through the same nozzle plate but at different speeds. As might be expected, higher gas speeds through the same orifices generate higher sound levels. Results of an almost identical experiment are shown in Figure 30. The principal difference between this set of measurements and those summarized in Figure 29 is that the orifice radii used for the measurements in Figure 30 are less than half as great as those used for the measurements in Figure 29. As the curves in Figure 30 show, gas flow rate no longer determines radiated noise levels.

Turbulence length and velocity scale strongly influence the critical bubble size. By examining Figure 15 and noting the parameters in Figures 29 - 32, one finds that the majority of bubbles generated with the smaller nozzle orifices lie below the critical bubble size. In other words, the ratio of turbulence length scale to orifice radius is a much more important parameter for radiated noise than gas flow rate. The results in Figure 31 further strengthens this conclusion. It can be seen from these results that a ten-fold increase in gas speed through the orifices yields, nevertheless, a lower sound level than the lower gas speed exhausting through the larger orifices. All of the results in Figures 29 - 31 suggest that the dominant parameter influencing the level of radiated noise is the ratio of turbulence length scale to orifice radius. Figure 32 illustrates the effect of

turbulence on noise levels. The dot-dash curve was obtained by adding the measured levels obtained without water (i.e., there is no turbulent wake) to the background noise levels obtained with water flow but without gas flow. The upper solid curve is the radiated sound level for gas exhausting through the same nozzle plate with water flowing at 9.1 m/sec. The 4 - 7 dB difference in sound levels is, therefore, due to the action of turbulence on the bubbles.

Phase II

In this phase of the study, gas was exhausted through nozzle plates having equal total orifice areas. This eliminated gas velocity as a variable when gas was discharged through nozzle plates having different orifice radii. One of the objectives in this phase was to examine what effects varying the water velocity (and hence, the turbulence velocity scale) has on radiated sound. The various gas flow rates and corresponding values of W and $W/F^{2/3}$ for the nozzle plates used in this phase are given in Table IV. Typical bubble radii corresponding to these flow parameters and the various nozzle plates are listed in Tables V, VIII, IX, X, and XI. One-third-octave-band radiated noise measurements obtained by discharging gas at various velocities through these nozzle plates into turbulent wakes at three different water speeds are given in Figures 33 - 42. From an examination of these results, it is clear that radiated noise levels from gas discharge decrease as water speeds (turbulence intensity levels) decrease.

When all of the experimental results are considered, it is apparent that the prime source of radiated noise when gas is discharged

through orifices into turbulent water is the break up and collapse of the bubbles. Contributions to the radiated noise spectrum from oscillations of bubbles at their resonant and higher frequencies were investigated. The results, presented in the Appendix, indicate that such oscillations are not a major contributor to the radiated noise generated by gas jets discharging into turbulent water.

The main conclusion of this investigation is that bubble break up and collapse in the turbulent wake is the dominant source of noise generated when gas jets are discharged into the wake. The ratio of turbulence length scale to orifice radius is the most important parameter in determining radiated noise, whereas gas flow rates affect noise levels only in a secondary manner. For the ranges of parameters used in this study, lower radiated noise levels were obtained when smaller orifice radii were employed, all other parameters being equal. There must, however, be a lower limit beyond which noise levels would increase if orifice radii were further reduced. For example, if a fine mesh screen were placed over a large orifice, gas streaming through the screen might generate considerable edge noise, and the value of reducing bubble size below the critical level would be diminished. This and the accompanying problem of varying the turbulence length scale should be investigated in a future extension of this work.

APPENDIX

It is possible for bubbles to radiate acoustic energy in both narrow and broad bands. If the radii of typical bubbles in a turbulent flow with integral scale L satisfy the inequality $r_B/L \ll 1$, acoustic energy can also be radiated at the turbulence frequency u/L, where u is the fluctuating turbulence velocity. Recent calculations [5] have shown that bubbles can cause the nearfield turbulence energy to radiate to the farfield, thereby increasing the sound power output of the flow by the factor $(C_o/C_m)^4$, where C_o and C_m are sound speeds in the pure liquid and bubbly mixture, respectively. If the fluctuating turbulence velocity is estimated as 10% of the mean flow speed and the turbulence length scale as the aft diameter of the test body [29], the turbulence frequency is of order

$$u/L \simeq 24 \text{ Hz} \quad .$$

This very low frequency is much below the range of our measurements.

If a turbulent flow could excite a bubble at its resonance frequency f_o, given by Equation (2.1), the resulting volume pulsations would not be forced as they are at the turbulence frequency. The radiating sound would, therefore, be generated very efficiently. Although much of the energy contained in any turbulent flow lies near frequencies of order u/L, some energy is available over a wide frequency range. The turbulent eddies required to drive a bubble at its resonance frequency must have typical length scales L' of order

$$L' \sim u/f_o \quad . \qquad \text{(A.1)}$$

From Equation (2.1), the radius of a bubble with resonance frequency f_o can be approximated by

$$r_o \sim 325/f_o \quad , \qquad (A.2)$$

where r_o is in centimeters, and f_o is in hertz. In the experiments, the largest fluctuating turbulence velocity is of order 0.9 m/sec. If Equations (A.1) and (A.2) are compared with this value for u, then $r_o > L'$ and the pressure field driving the bubble would very rapidly over the bubble surface. To produce a symmetric volume oscillation of the bubble, the driving pressure field must be in phase over the bubble surface (for a discussion of turbulence excitation of bubbles, see Ref. [5]). It appears that volume pulsations of bubbles at their resonance frequencies are not a major noise source in the present investigation.

Also of interest is the sound pressure radiated by a bubble at the natural frequency of its higher modes. For the natural frequency of the n^{th} order mode, Lamb's [14] expression is

$$f_n = \left[(n^2 - 1)(n + 2)\sigma/\rho r_B\right]^{1/2} / 2\pi r_B \quad . \qquad (A.3)$$

There is no natural frequency for the $n = 1$ mode, since to restoring force is associated with a free bubble in translational oscillation. When the bubble oscillates at the n^{th} order natural frequency, the sound pressure amplitude at a large distance from the bubble as given by Strasberg [27] is

$$P_n = N_n(\sigma/r_B)(\sigma/r_B\rho c^2)^{n/2}(r_n/d)S_n \quad , \qquad (A.4)$$

where

$$N_n = 2^n\, n!\,(n-1)(n^2-1)^{n/2}(n+2)^{1+n/2}\,/(2n)! \quad . \quad (A.5)$$

S_n is the spherical harmonic of order n describing the variation of the bubble surface with angle, d is the distance from the center of the bubble, and r_n is the amplitude of oscillation associated with the n^{th} order.

Calculated values of sound pressure for several modes are listed in Table XIII for $r_B = 0.050$ cm at an amplitude of oscillation $r_n = 1/4\ r_B$.

The values in the table indicate that appreciable sound is radiated only when the bubble is in volume pulsation. Indeed, sound pressures associated with the shape modes are negligible. Since a relatively large amplitude of oscillation was assumed for the calculations, it does not seem that shape oscillations would ever result in significant sound pressures. The size of the bubble for which calculations are made is the smallest radius bubble generated in any of the experiments. Any larger bubble would produce significantly lower values for the radiated sound pressure. The value of d selected corresponds to the distance from the center of the tunnel to the receiving hydrophone.

TABLE XIII

SOUND PRESSURE AND FREQUENCY OF A BUBBLE OSCILLATING IN VARIOUS MODES IN WATER FOR $r_n = 1/4\ r_B$ AND $P_o = 1$ ATMOSPHERE

r_B cm	n	f_n Hz	P_n at d = 140 cm μbar
0.050	0	6570	3.80×10^{2}
	2	422	1.35×10^{-7}
	3	771	3.65×10^{-10}
	4	1156	7.67×10^{-13}

REFERENCES

1. Bobber, R. J. Underwater Electroacoustics Measurements. Washington, DC: U. S. Government Printing Office, 1970, p. 19.

2. Bragg, W. The World of Sound. London: Bell, 1920.

2. Card, D. C., Sims, G. E., and Chant, R. E. "Ultrasonic Velocity of Sound and Void Fraction in a Bubbly Mixture," ASME Paper 71-FE-26, 1971, pp. 1-5.

4. Carstensen, E. L., and Foldy, L. L. "Propagation of Sound Through a Liquid Containing Bubbles," J. Acoust. Soc. Am., Vol. 19, 1947, pp. 481-501.

5. Crighton, D. G., and Ffowcs Williams, J. E. "Sound Generation by Turbulent Two-Phase Flow," J. Fluid Mech., Vol. 36, 1969, pp. 585-603.

6. Davidson, J. F., and Shüler, B. O. G. "Bubble Formation at an Orifice in a Viscous Liquid," Trans. Inst. Chem. Engrs. (London), Vol. 38, 1960, pp. 144-154.

7. Davidson, L., and Amick, E., Jr. "Formation of Gas Bubbles at Horizontal Orifices," J. Amer. Inst. Chem. Engr., Vol. 2, No. 3, 1956, pp. 337-342.

8. Hinze, O. "Fundamentals of the Hydrodynamic Mechanisms of Splitting in Dispersion Processes," J. Amer. Inst. Chem. Engr., Vol. 1, 1955, pp. 289-295.

9. King, W. F., III "Sound Propagation in Wakes," J. Acoust. Soc. Am., Vol. 54, 1973, pp. 735-745.

10. King, W. F., III Private communication (1974).

11. Kolmogorov, A. N. "On the Disintegration of Drops in a Turbulent Flow," Doklady Akad. Nauk, Vol. 66, 1949, pp. 825-829.

12. van Krevelen, D. W., and Hoftijzer, P. J. "Studies of Gas-Bubble Formation," Chem. Eng. Prog., Vol. 46, No. 1, 1950, pp. 29-35.

13. Laird, D. T., and Kendig, P. M. "Attenuation of Sound in Water Containing Air Bubbles," J. Acoust. Soc. Am., Vol. 24, 1952, pp. 29-32.

14. Lamb, H. Hydrodynamics. New York: Dover Press, 1932.

15. Meyer, E., and Skudrzyk, E. J. "Uber die Akustischen Eigenschaften von Gasblasenschleieren in Wasser," Acust., Vol. 3, 1953, pp. 434-440.

16. Meyer, E., and Tamm, K. "Eigenschwingung und Dämpfung von Gasblasen in Flussigkeiten," Akust Z., Vol. 4, 1939, pp. 145-152.

17. Minnaert, M. "On the Musical Air Bubbles and the Sounds of Running Water," Phil. Mag., Vol. 16, 1933, pp. 235-248.

18. Mühle, C., and Heckl, M. "Sound Radiation by Submerged Exhaust," Müller Bolt Beranek & Newman GMBH Report 2605, 1971, Translated from the German, available as NAVSHIPS Translation No. 1321, 1972.

19. Park, S. H. "The Formation and Break-Up of Drops and Bubbles by Turbulent Fluid Flow," PhD Thesis, The Pennsylvania State University, 1971.

20. Pattle, R. E. "The Aeration of Liquids. II. Factors in the Production of Small Bubbles," Trans. Inst. Chem. Engrs. (London), Vol. 28, 1950, p. 27.

21. Robinson, G. E. "Noise Generation During Bubble Growth in a Nucleate Boiling System," PhD Thesis, The Pennsylvania State University, 1970.

22. Sevik, M., and Park, S. H. "The Splitting of Drops and Bubbles by Turbulent Fluid Flow," J. Basic Eng., Trans. ASME, Paper No. 72-WA/FE-32, 1972, pp. 1-8.

23. Silberman, E. "Production of Bubbles by the Disintegration of Gas Jets in Liquid," Proc. of the Fifth Midwestern Conference of Fluid Mechanics, University of Michigan, April 1957.

24. Smith, P. W., Jr. "Noise of a Gas Jet in a Liquid," Bolt Beranek and Newman Report 897, Cambridge, MA, 1961.

25. Soo, S. L. Fluid Dynamics of Multiphase Systems. Waltham, MA: Blaisdell Publishing Co., 1967, Chapter 3.

26. Spitzer, L., Jr. "Acoustical Properties of Gas Bubbles in a Liquid," Naval Ship Research and Development Center, Report No. 6.1-sr20-918, 1943.

27. Strasberg, M. "Gas Bubbles as Sources of Sound in Liquids," J. Acoust. Soc. Am., Vol. 28, 1956, pp. 20-26.

28. Tennekes, H. Private communication (1974).

29. Tennekes, H., and Lumley, J. L. A First Course in Turbulence. Cambridge, MA: MIT Press, 1972, p. 20.

30. Waterhouse, R. V. "Output of a Sound Source in a Reverberation Chamber and Other Reflecting Environments," J. Acoust. Soc. Am., Vol. 30, No. 1, 1958, pp. 4-13.

31. Welle, F., Verheugen, A. J., Haagh, V. J. M. N., and Bogaardt, M. "A Study of the Application of Acoustical Methods for Determining Void Fractions in Boiling Water Systems," European Atomic Energy Community, Report EUR2336e, 1966.

DISTRIBUTION LIST FOR TM 81-99

Commander (NSEA 0342)
Naval Sea Systems Command
Department of the Navy
Washington, DC 20362

Copies 1 and 2

Commander (NSEA 9961)
Naval Sea Systems Command
Department of the Navy
Washington, DC 20362

Copies 3 and 4

Defense Technical Information Center
5010 Duke Street
Cameron Station
Alexandria, VA 22314

Copies 5 through 10


DA
FILM